Qualcomm Atheros, Inc.

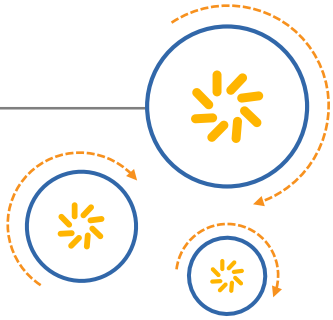

Acer N15W8 802.11ad RF Exposure Assessment

80-YA685-1 Rev. C

June 9, 2016

Qualcomm Atheros, Inc.
1700 Technology Drive
San Jose, CA 95110
U.S.A.

Revision history

Revision	Date	Description
A	April 2016	Initial release
B	May 2016	Revised per FCC response on 05/09/2016
C	June 2016	Revised per FCC response on 06/06/2016

Contents

Tables

List of Figures

1 Document Scope

This report is generated for the class II permissive change application against FCC ID: PPD-QCA9008-TBD1. As shown in Figure 1-1, the 2.4/5GHz WLAN antennas are 220 mm and 290 mm distance away from the 802.11ad antenna. Therefore, the RF exposure assessment for simultaneous transmission is not needed.

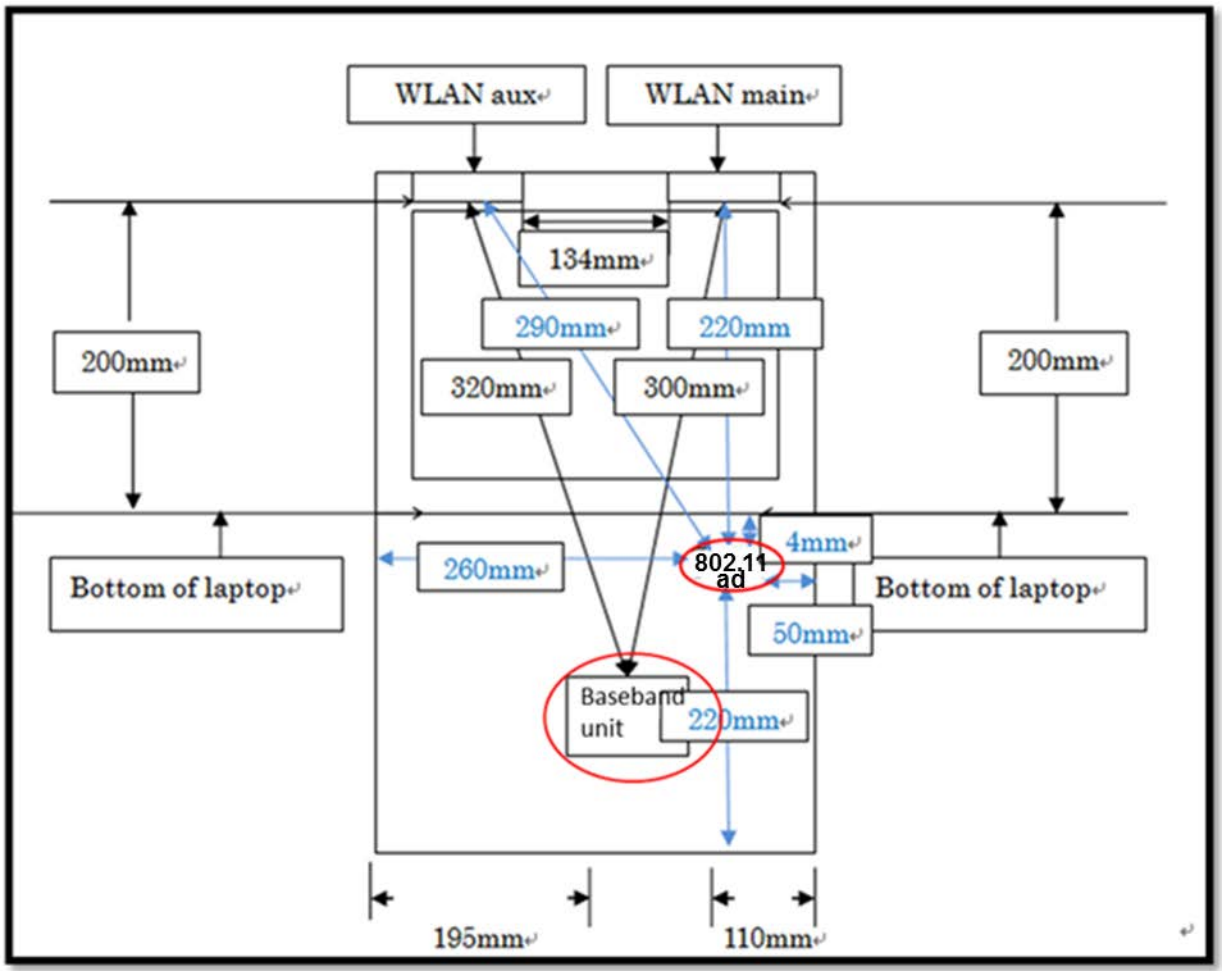

Figure 1-1: WLAN and 802.11ad antenna placement

The QCA9008-TBD1 802.11a/b/g/ac/ad + BT module was installed in N15W8 Acer platform. It consists of two separate modules, i.e., the 802.11ad module and baseband unit, as circled in red in Figure 1-1. The base band unit contains the 802.11a/b/g/ac/BT as well as provides power/control

signals/IF to the 802.11ad module. The 802.11ad module consists 60GHz RF and antenna array elements on a printed circuit board (PCB), which is referred to as the "QCA9008-TBD1 802.11ad module" or simply "802.11ad module" in this report. The 802.11ad module is mounted at the hinge where the closest distance between the 802.11ad module and the body of an end user will be in the near field. This report is submitted to demonstrate the RF exposure from 802.11ad radio in compliance with FCC rule parts §2.1093 and §15.255(g).

A given combination of amplitude and phase of array elements is referred to as an "antenna configuration". There are many antenna configurations available in Acer N15W8 application. The confidential document Appendix A describes the design details on antenna schematics as well as how to adjust antenna configuration depending on transmission environment in order to steer the antenna beam for establishing a good communication link having the best signal to noise ratio.

We used a "validated simulation approach" to evaluate all the available antenna configurations, in order to determine the top three worst cases. Subsequently, using a "validated test methodology", the three selected worst-cases were measured. Then, based on the measured phase and amplitude of E-fields at adequate separation distance(s), near-field back transformation using Plane Wave Spectrum (PWS) described in Appendix D was applied to obtain the power density distribution and strength at the exposure plane (closest contact point with the human body) to determine the RF exposure compliance.

The highest EIRP case was also determined using simulation, and it was then tested in UL lab to confirm that the highest EIRP level is equal to or below the value reported in the initial grant. The EIRP test result is provided in a separate UL report.

The definition of near field and far field boundary is as follows:

$$R = \frac{2 \times D^2}{\lambda}$$

where R is the distance from observation point to radiating source; D is the maximum dimension of the radiating source; λ is wavelength. QCA9008-TBD1 802.11ad module is integrated onto a 17.5 x 7.9 x 2 mm^3 of the printed circuit board. Therefore, the near-field and far-field range is determined as:

Near field range: $R \leq 122.5$ mm

Far field range: $R > 122.5$ mm

It should be noted that in this report, all the measurements and simulations conducted on QCA9008-TBD1 802.11ad module for assessment of power density were performed in the near-field, unless explicitly stated, say for example, far field antenna pattern and waveguide probe calibration in the far field.

In this report:

- Chapter 2 gives the product description.
- Chapter 3 determines the worst-case antenna configurations using simulation.
- Chapter 4 provides the measurement results for worst-case antenna configurations.
- Chapter 5 proves the validity of the measurement and simulation approaches.
- Chapter 6 concludes the compliance.

2 Product Description

The 802.11ad RF and antennas of QCA9008-TBD1 module operating in the 60GHz band is installed at the hinge inside N15W8 Acer laptop (shown in Figure 2-1), which receives the baseband signals from the baseband unit. The relative location of the 802.11ad module is shown in Figure 2-2. This 802.11ad module supports all mandatory channels in IEEE 802.11ad (namely channels 1 to 3), and is in compliance with 802.11ad standard.

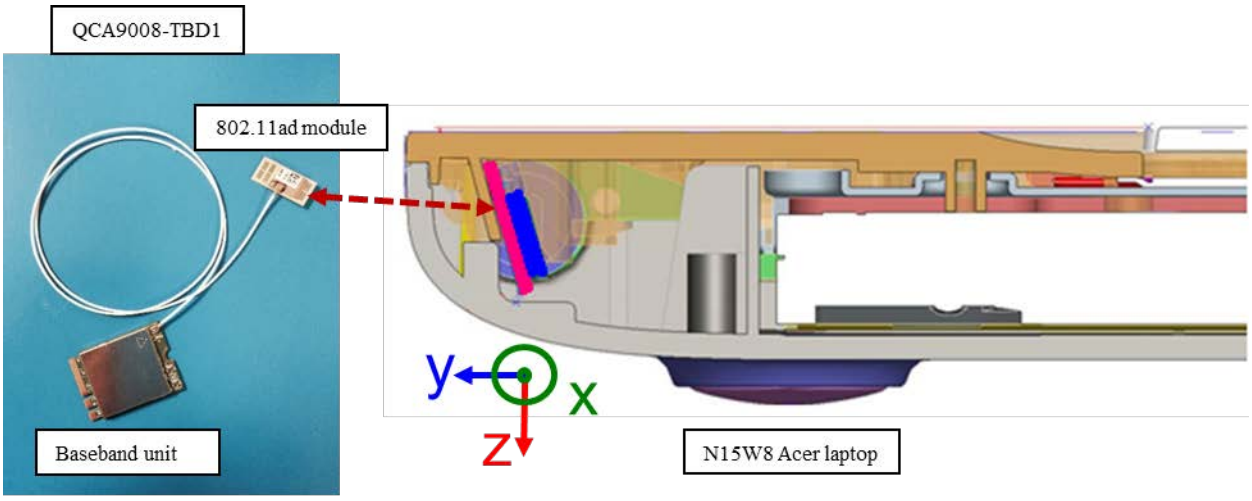

Figure 2-1: N15W8 Acer laptop with QCA9008-TBD1 802.11ad module

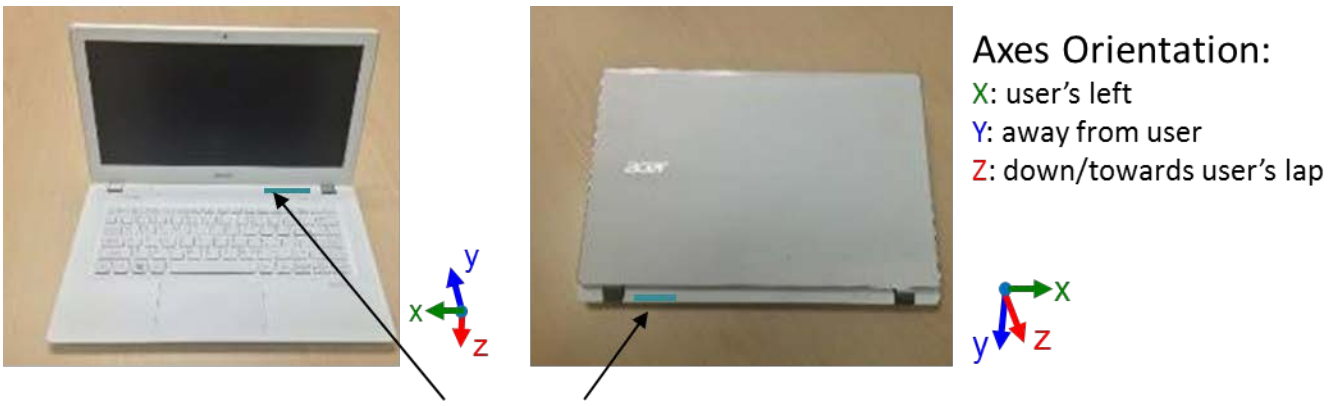

Figure 2-2: Location of QCA9008-TBD1 802.11ad module

The actual installation is shown in Figure 2-3, which shows the left top corner of back housing and zoomed-in picture of that corner showing the 802.11ad module location to the right of the hinge when looking at the bottom of Acer. The pictures of the QCA9008-TBD1 802.11ad module are shown in Figure 2-4, which show the shield containing the RF components and the antenna array elements on the PCB. Here, the front view is looking from the top edge of the laptop with the laptop's bottom surface sitting on the table.

For easier identification of the 802.11ad module orientation relative to the laptop, we have shown the coordinate system on all figures with the positive Z-axis protruding out of the laptop's bottom surface.

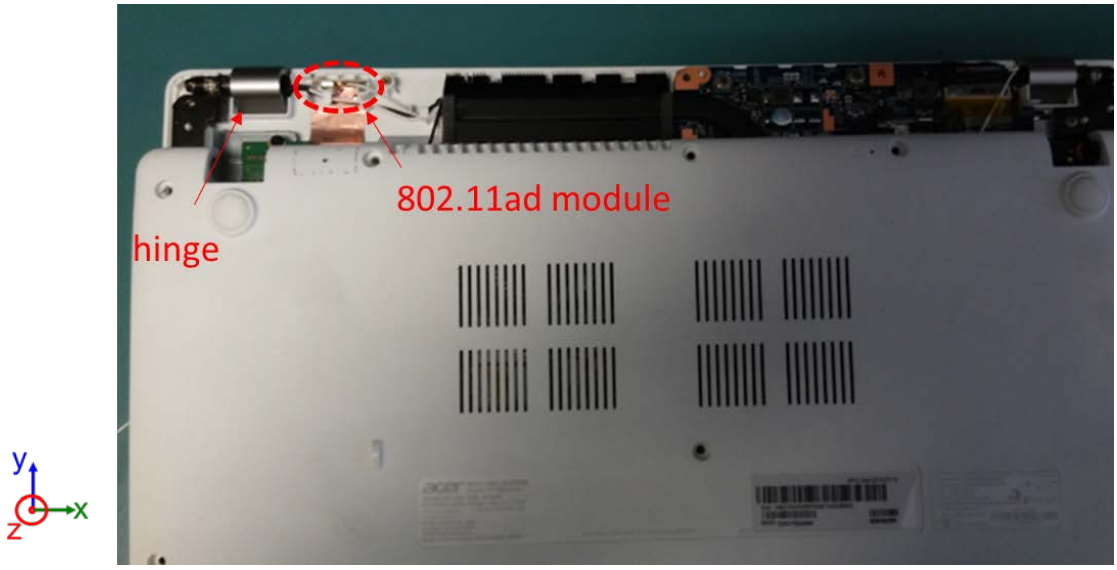

(a)

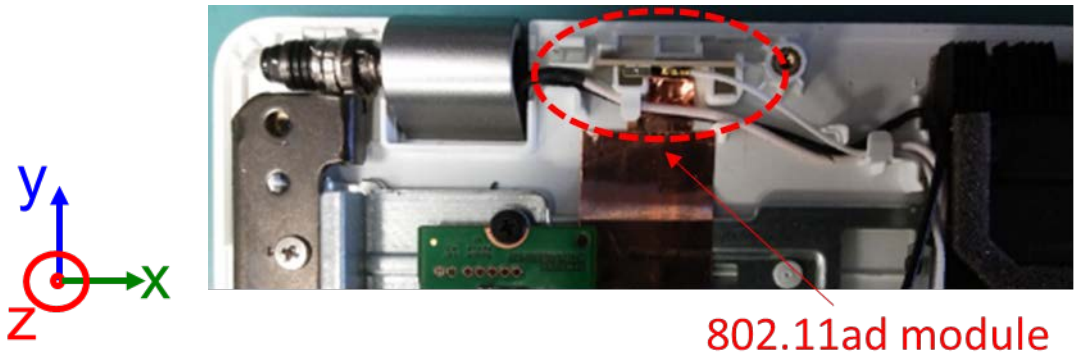

(b)

Figure 2-3: Actual installation of QCA9008-TBD1 802.11ad module in Acer N15W8: (a) location of the module; (b) zoomed-in view

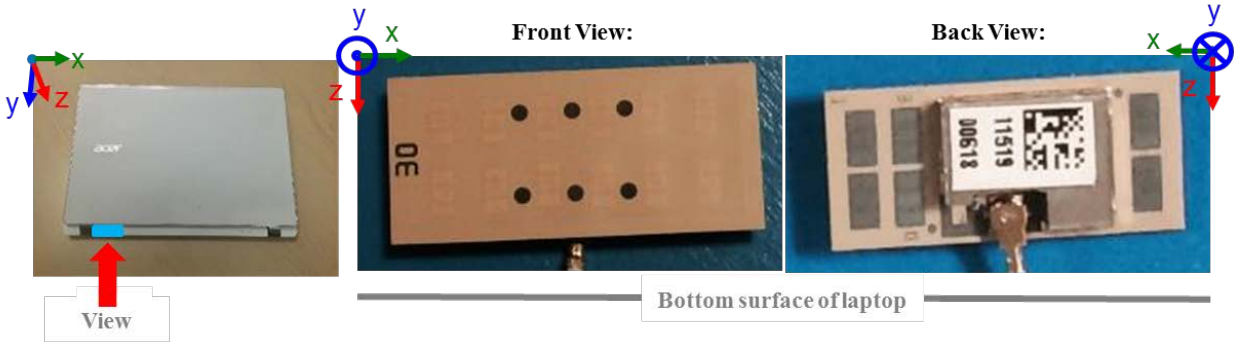

Figure 2-4: QCA9008-TBD1 802.11ad module

3 Worst Case Determination Using Simulation

The QCA9008-TBD1 802.11ad module is installed inside Acer N15W8, and depending on transmission environment, it can activate an optimal antenna configuration to establish a good communication link. It is extremely time consuming to measure all the antenna configurations. To be more practical, the Ansys Electromagnetics suite 17.0.0 was used to evaluate all the possible antenna configurations. Due to the lack of information on the material properties of Acer housing and surroundings, and the limitation of computation resources, the simulation was performed under free space condition. The goal of the simulation is to perform the relative comparison and determine the top three worst-case antenna configurations having the highest power density value, and then perform the measurement on the identified worst cases to demonstrate the compliance.

In general, we expect the worst-case antenna configurations to have the following

1. More active elements closer to the exposure plane
2. More active elements grouped together
3. More active elements relatively farther away from the Acer housing/surroundings resulting in minimal detuning (more transmitted power)

This is because these characteristics will contribute towards higher and focused power flowing through the exposure plane with or without Acer housing, and thereby result in higher power density value.

3.1 Simulation modelling

Figure 3-1 shows where QCA9008-TBD1 802.11ad module is located inside Acer N15W8. Since the user could place the laptop in the lap, i.e., closest possible distance to the 802.11ad module, the bottom surface is treated as the exposure plane.

The 802.11ad module was completely modelled, which includes layers, ground, shields, antenna array elements, vias, as well as all the traces (including from output PA to antenna feed). The modelling detail, including the PCB layout, is provided in the confidential document Appendix A.

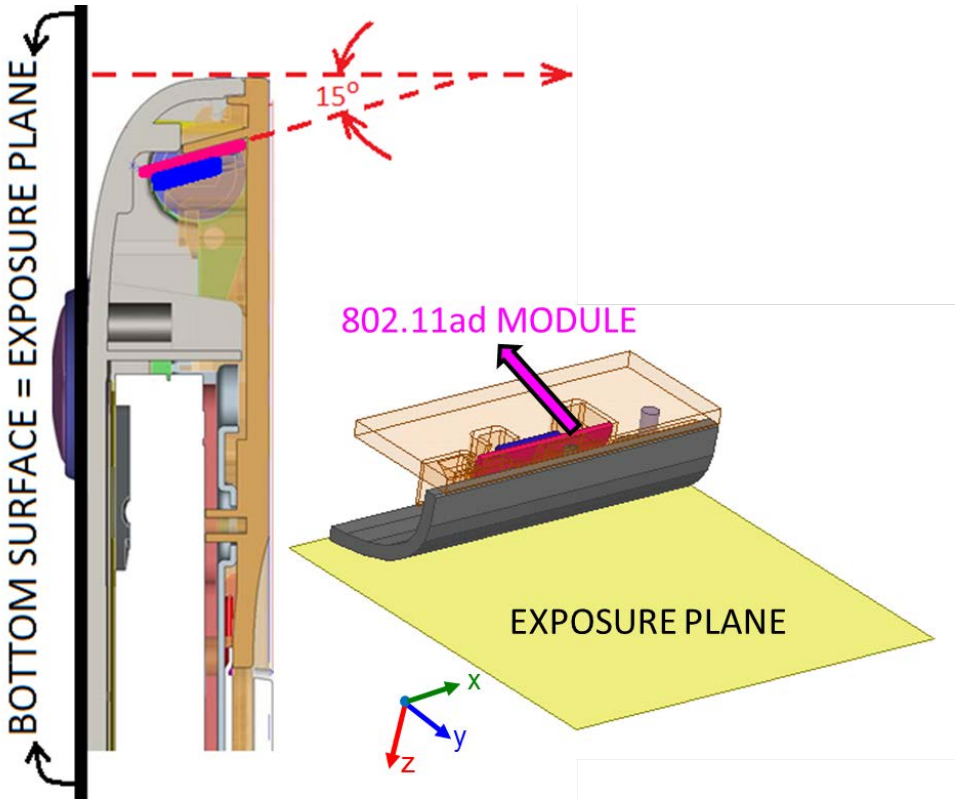

Figure 3-1: QCA9008-TBD1 802.11ad module placed inside Acer N15W8

3.2 Simulation setup

FEM simulations were performed to assess the power density of the QCA9008-TBD1 802.11ad module in free-space using ANSYS Electromagnetics suite 17.0.0. In these simulations, the Acer's laptop housing the 802.11ad module (contained in the red outline in Figure 3-2(a)) was not simulated since the material properties of the Acer housing and other components of the laptop are not available at mmWave frequencies. The laptop model was simulated as free-space to determine the relative orientation of the 802.11ad module with respect to the exposure plane shown in Figure 3-2(b), where the power density was determined to identify the worst-case antenna configurations. In Figure 3-2(b), only the 802.11ad module shown in blue and pink (blue represents the shield containing the RF components, pink represents the PCB containing the antenna array elements, layers, vias, and connecting traces) were modelled. The remaining cut out of the housing of Acer's laptop shown in grey along with laptop components are simulated as free-space.

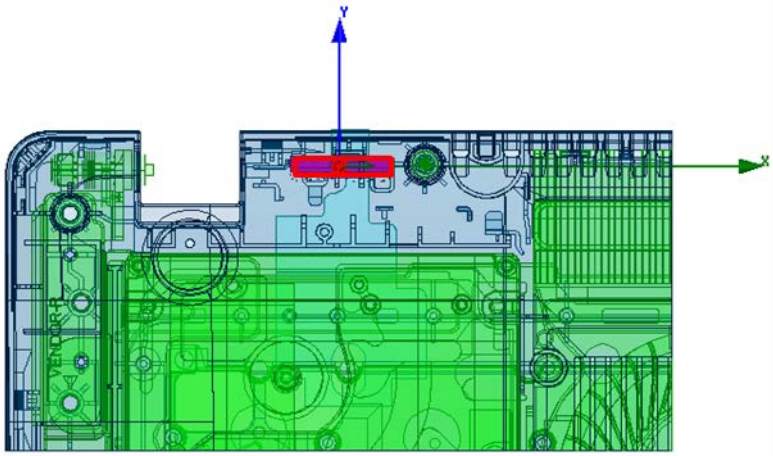

(a)

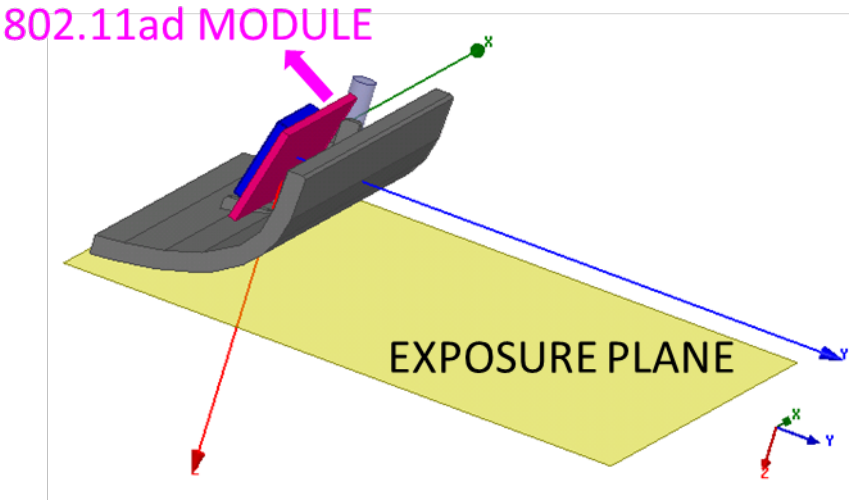

(b)

Figure 3-2: (a) N15W8 Acer laptop CAD model showing the relative location of QCA9008-TBD1 802.11ad module (red box), (b) QCA9008-TBD1 802.11ad module's orientation with respect to the exposure plane (grey: laptop bottom, pink: the 802.11ad module's PCB, blue: shield containing RF components of 802.11ad module. The 802.11ad module's PCB is at ~75^0 angle with respect to the exposure plane).

In the simulation set up, we selected the auto initial mesh, defined "lambda refinement" (i.e., Ansys Electromagnetics suite 17.0.0 refines the initial mesh based on the material-dependent wavelength) and used 30% maximum refinement per pass as our adaptive option. The system (Ansys Electromagnetics suite 17.0.0) computes the error, and the iterative process (solve – error analysis – adaptive refinement) repeats until the convergence criteria are satisfied. In Ansys Electromagnetics suite 17.0.0, as long as the convergence is reached, the converged results are accurate. We verified the convergence by changing the convergence criteria, maximum magnitude delta S, from 5% to 3%, the influence was less than 0.5%. This influence is included in our uncertainty budget (Appendix B). Figure 3-3 shows the mesh used over front surface (see Figure 2-4) of the QCA9008-TBD1 802.11ad module, and the convergence error (i.e., maximum magnitude delta S) in all our simulation was less than 3%.

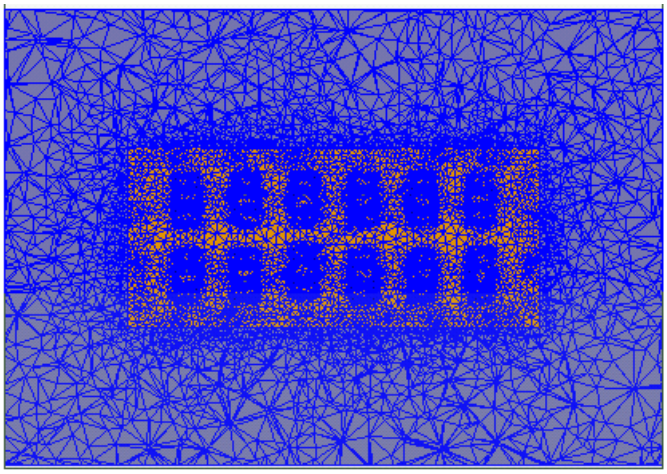

Figure 3-3: Simulation mesh setup used in QCA9008-TBD1 802.11ad module modelling

The 2nd order absorbing boundary condition (ABC) was used as radiation boundary for all simulations in this report. This radiation boundary simulates an electrically open surface that allows waves to radiate infinitely far into space. The system absorbs the wave via the 2nd order radiation boundary, essentially ballooning the boundary infinitely far away from the structure and into space. The radiation boundaries may also be placed relatively close to a structure and can be of arbitrary shape.

Typically, as per ANSYS recommendation for their simulation tool, the radiation boundary plane has to be located at least a quarter wavelength from strongly radiating structure, or at least a 10th of wavelength from weakly radiating structure. In this RF exposure report, we used at least 1 wavelength from all the direction of the 802.11ad module (in the main beam direction, about 6 wavelengths was applied, as shown in Figure 3-4) to ensure the convergence. We have further guaranteed that this spacing is sufficient by moving the boundaries closer towards the module by 30% to see the influence on simulated power density. This influence was < 0.05dB confirming that the space between module and computational boundary is sufficient. This influence on power density was also included in the simulation uncertainty budget in Appendix B. As stated earlier, only the 802.11ad module (shown in pink color for PCB and blue for shield behind PCB in Figure 3-4) is modeled in the simulation, the remaining cutout of Acer laptop's housing (shown as wire model in Figure 3-4) is simulated as free-space.

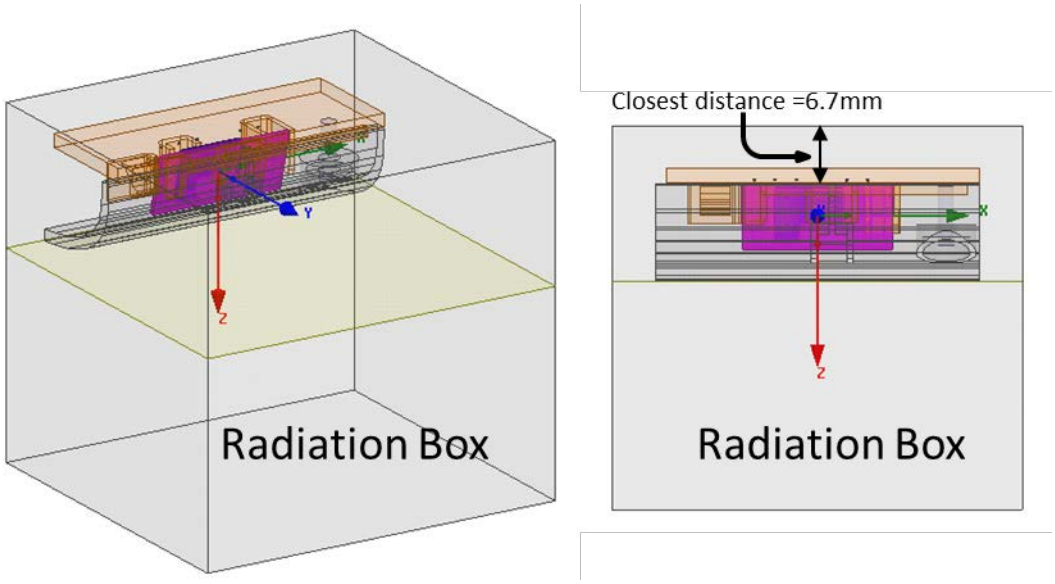

Figure 3-4: Radiation boundary setup (note the 802.11ad module is highlighted in pink)

The total simulation uncertainty was analyzed and is described in Appendix B.

3.3 Simulation results

The objective of the simulation is to compare the power density levels among antenna configurations to determine the three worst-case antenna configurations having the highest peak 1 cm^2-averaged power density in the exposure plane. Then, power density is measured for these worst-case antenna configurations at a finite separation distance, and back transform the measured power density to the exposure plane for compliance evaluation, as explained further in Section 4.

Per consultation with FCC in the evaluation guidance KDB inquiry, for the circumstances with this filing only, the power density in free-space was estimated by extracting the Poynting vector normal to and at the bottom surface (exposure plane) of the laptop at a frequency of 60.5 GHz for each antenna configuration for comparison. Here, the simulation data for normal component of power density, PD_{normal}, was extracted at 1.0 mm resolution in the exposure plane. 1 cm^2 spatial averaging was obtained by moving 1cm x 1cm square window, every 1.0 mm step size in the exposure plane. Figure 3-5 shows the normalized peak PD_{normal} in the exposure plane for all available antenna configurations after applying 1 cm^2 area spatial averaging.

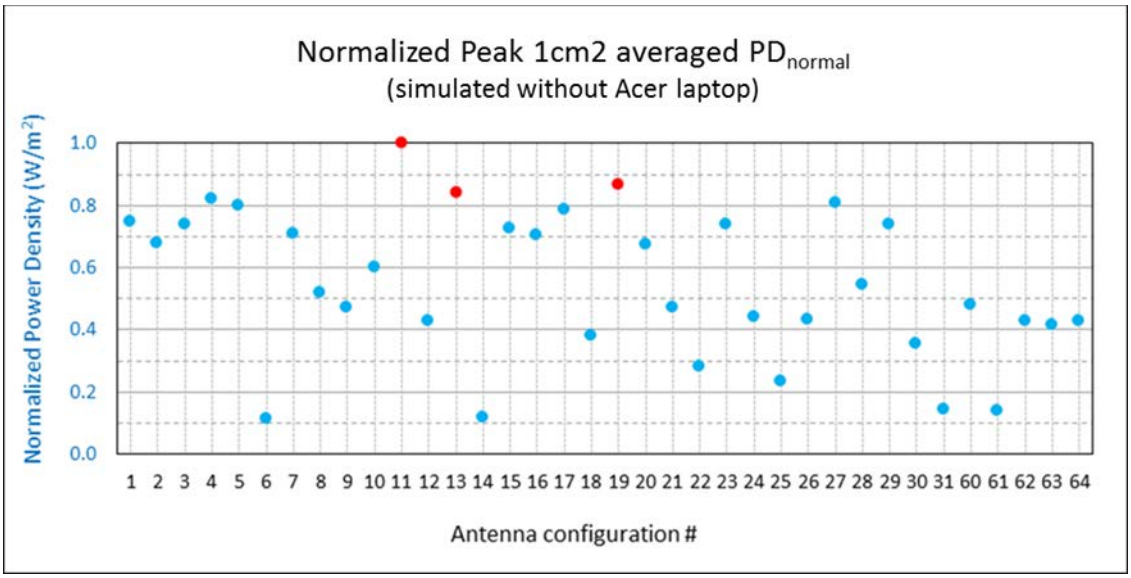

Figure 3-5: Normalized peak 1cm^2-averaged PD_{normal} levels

Appendix C has the complete simulation results of power density distributions for all antenna configurations. The antenna configurations #11, #13 and #19 were identified as the worst-case antenna configurations having the highest power density in the exposure plane. These identified worse-case antenna configurations all contain more number of active elements grouped together and closer to the exposure plane when compared with other antenna configurations. The normalized power density distributions at 60.5GHz for these three worst cases are provided in Figure 3-6.

Each antenna configuration is fixed for all the channels (i.e. 802.11ad channels 1~3). The optimization is typically done at mid-channel as shown in the EIRP measurement in the original filing (copied below).

Table 3-1: EIRP values copied from the original filing

Channel	Frequency (GHz)	EIRP (dBm)
1	58.5	23.5
2	60.5	29.8
3	62.5	28.0

The antenna gain of each antenna configuration in the Acer case is the same or equivalent across the operating frequency band. Table 3-2 shows the antenna gains for the three worse-case antenna configurations for low, mid, and high channel. It is clear that the evaluation made at mid-channel (i.e., 60.5 GHz) only is sufficient.

Table 3-2: Antenna gains for configuration #11, 13 and 19

Channel	Frequency (GHz)	G (dBi)		
		Antenna configuration 11	Antenna configuration 13	Antenna configuration 19
1	58.5	4.4	6.6	4.5
2	60.5	6.4	8.7	4.4
3	62.5	5.4	8.7	4.2

a. **Antenna configuration #11: normalized 1cm^2-averaged power density**

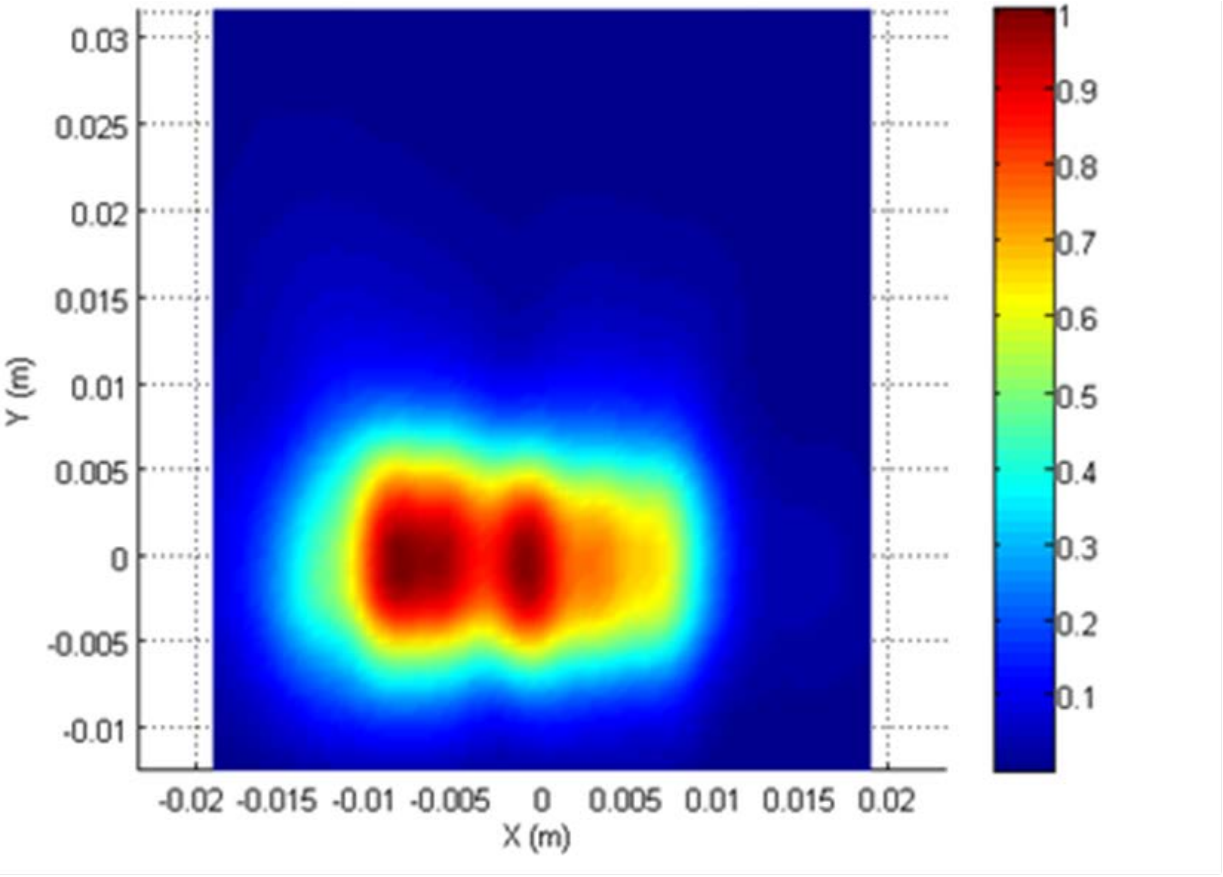

b. **Antenna configuration #13: normalized 1cm^2-averaged power density**

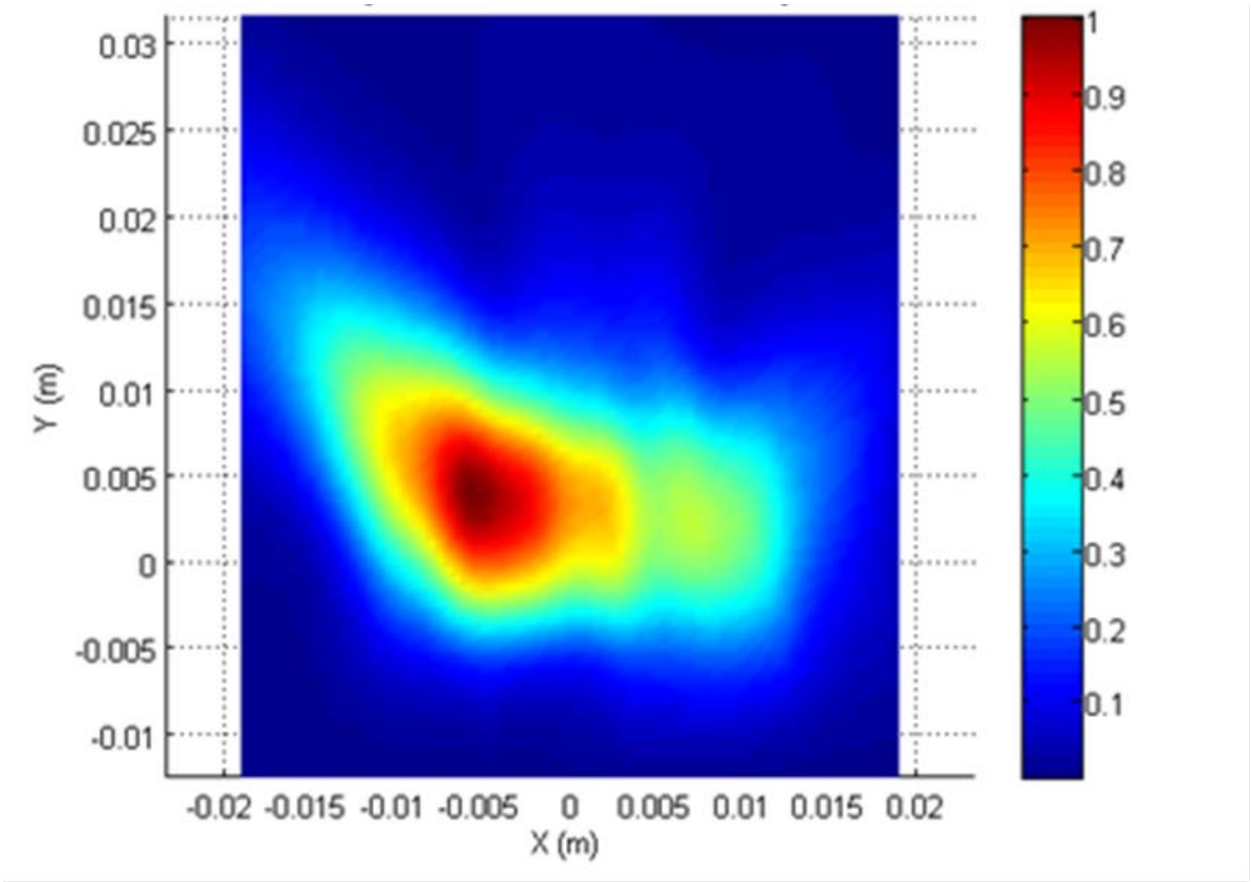

c. **Antenna configuration #19: normalized 1cm^2-averaged power density**

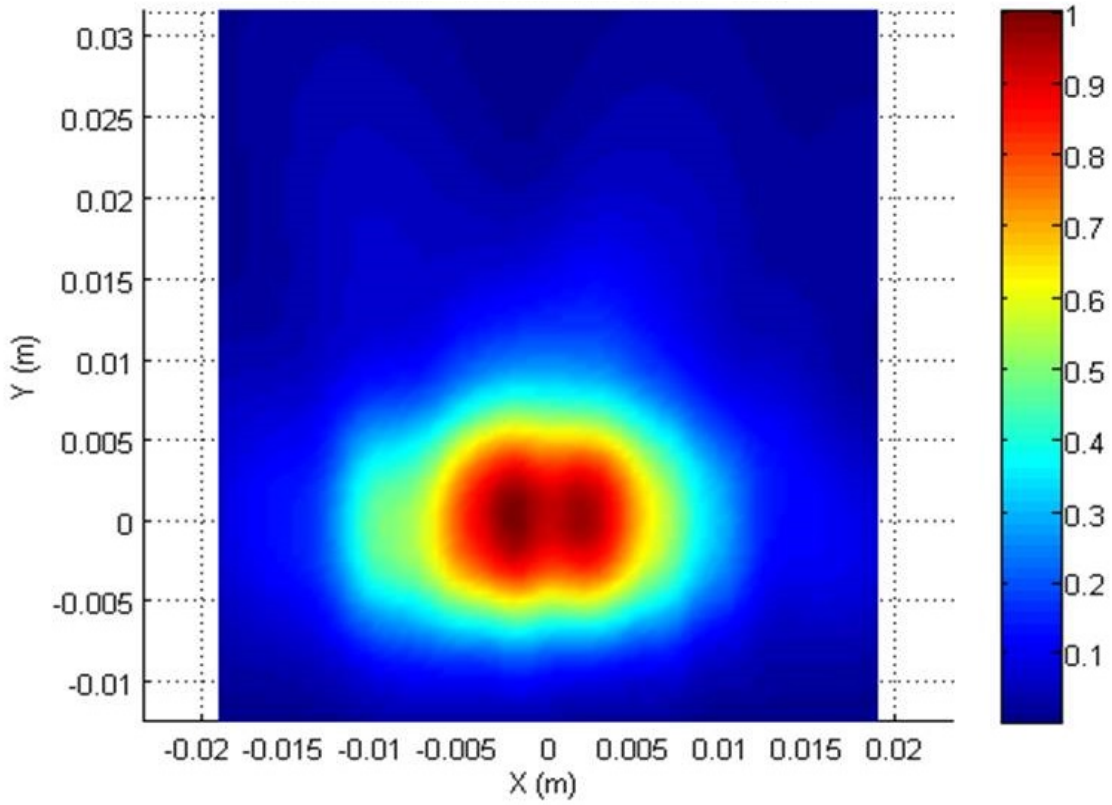

Figure 3-6: Normalized distribution of 1cm^2-averaged power density normally flowing to the exposure plane: (a) Antenna configuration #11; (b) Antenna configuration #13; (c) Antenna configuration #19

4 RF Exposure Measurement and Assessment Using Combination of PWS Method and Simulation-Based Scaling

The goal of the measurement is to capture the amplitude and phase of the E-fields along the planes parallel with the exposure plane for the identified three worst-case configurations, and then back-transfer the measured E-fields to the exposure plan using the Plane Wave Spectrum (PWS) method (described in Appendix D) to obtain the power density at the exposure plane to demonstrate the compliance.

Below flowchart explains the steps involved in the power density assessment for compliance demonstration of QCA9008-TBD1 802.11ad module.

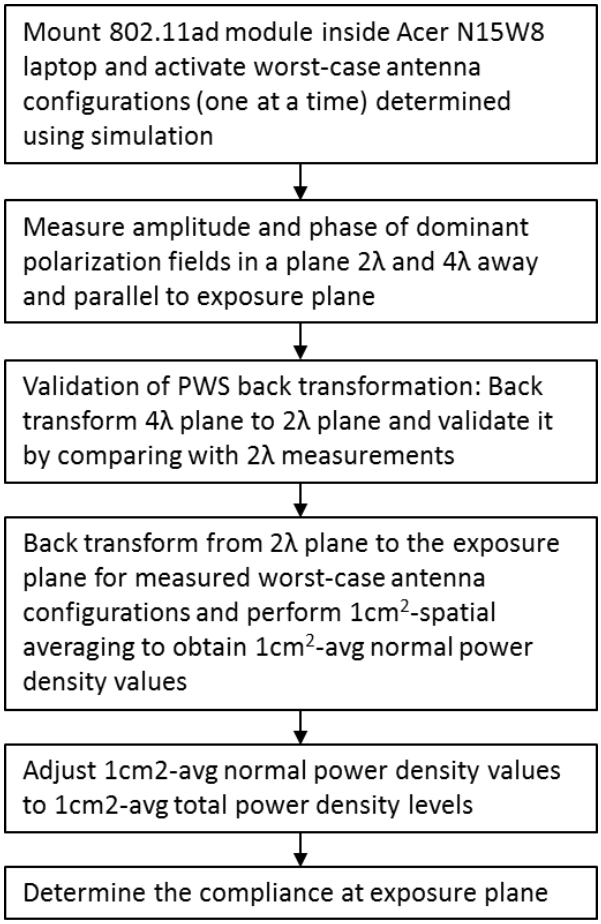

4.1 Test and measurement equipment

Table 4-1 lists all measurement equipment used in this test and their calibration information.

Table 4-1: Measurement equipment

MFR	Model	Description	Quantity	Calibration date
NSI	8x6 PNF	Planar Nearfield and Farfield scanner	1	7/4/2106
Keysight	N5247A	4-port Network Analyzer	1	6/23/2016
R&S	NRP2	Power Meter	1	1/21/2017
R&S	NRP-Z57	DC-67 GHz Power Meter Sensor	1	1/21/2017
Keysight	E8257D	250 KHz to 20 GHz PSG Analog Signal Generator	1	11/30/2016
Phillips	PM 2811	Power Supply	2	N/A
NSI	RF-WR15	Open-ended Waveguide Probe (50-75 GHz)	1	N/A

We calibrated the aperture waveguide (RF-WR15) in house. The Qualcomm® in-house calibration report is provided in Appendix E.

4.2 Measurement setup

4.2.1 General

The block diagram of the test setup is shown in Figure 4-1.

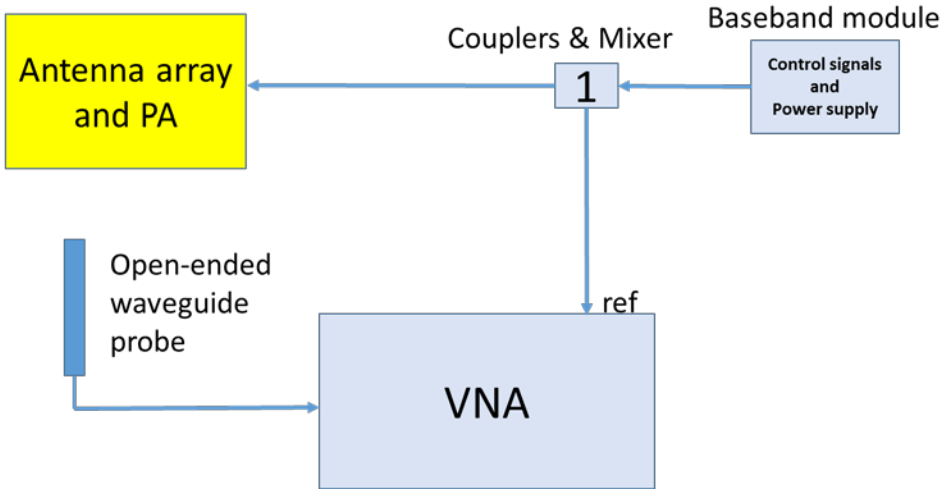

Figure 4-1: Measurement block diagram

The measurement setup uses an open-ended waveguide WR-15 probe fixed to a positioner as shown in Figure 4-2.

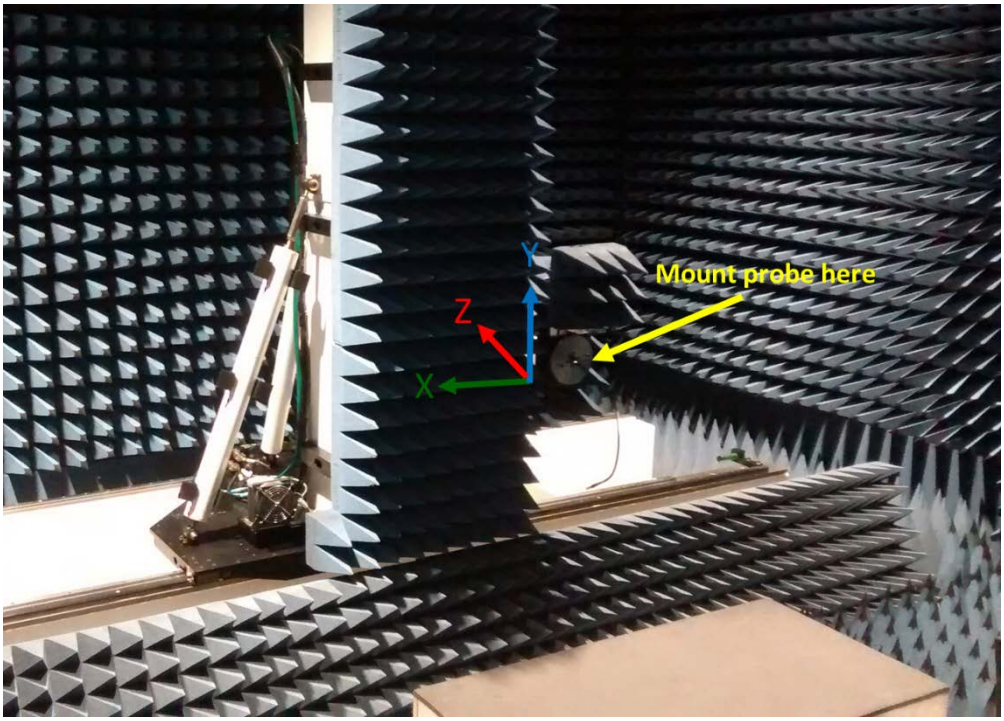

(a)

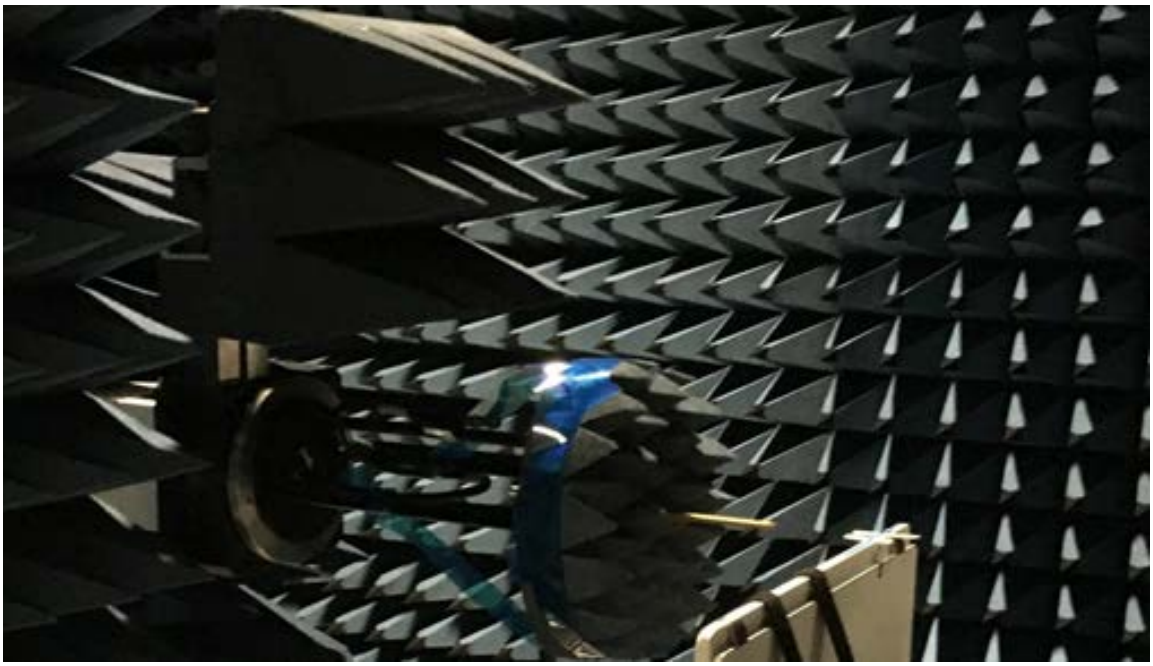

(b)

Figure 4-2: (a) Probe positioner system; (b) Waveguide probe in place surrounded by absorbers

The positioner can move along the rectilinear grid, which was used to perform 2D area scans in a vertical plane (XY-plane). The Acer N15W8 was positioned such that the exposure plane is aligned with the XY-plane as shown in Figure 4-3. The aperture of the open-ended waveguide is placed in parallel to the exposure plane (XY-plane) in order to capture the E-fields that are tangential to the scan planes corresponding to the power propagation direction normal to the scan plane.

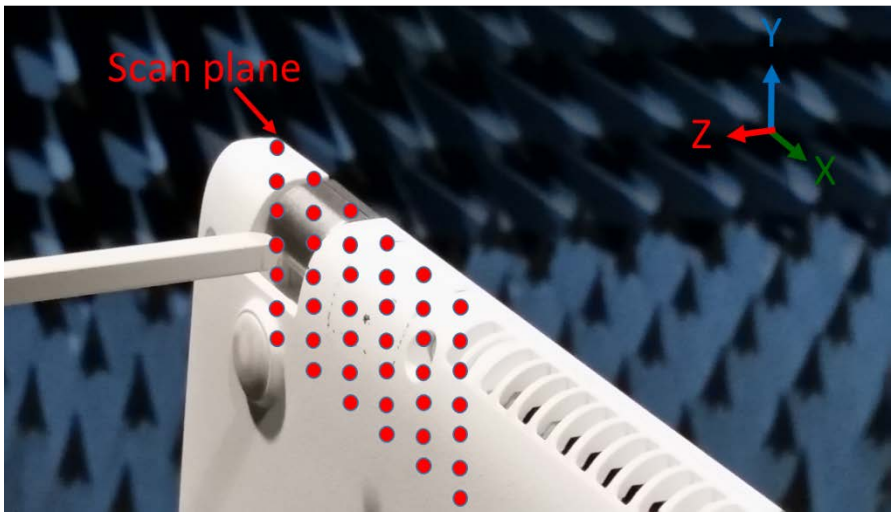

Figure 4-3: Acer N15W8 measurement setup

The waveguide probe was connected to a vector network analyzer (VNA) to measure the relative amplitude and phase of the incident electric field. The 2D area scan measured was 228 mm x 228 mm at a resolution of 2 mm recording about 114x114 points for each area scan. One polarization of E-fields was significantly dominant, the orthogonal polarization of E-fields was about 10 dB lower. Therefore, only dominant fields were recorded. Based on the measured dominant E-fields, the normal component of power density (PD_{normal}) was derived at the exposure plane using PWS back transformation, and then the total power density (PD_{total}) was calculated by adding the difference of simulated PD_{total} and simulated PD_{normal} using the simulation approach described in Section 3. FCC has accepted this approach for this device and filing only and considering the validations in Appendix F.

4.2.2 Other considerations

Note that when measuring only dominant fields, measurement time is cut in half since only one polarization is measured. However, only normal power density can be computed from single polarization data. In order to estimate total power density, in this case, simulation data need to be employed where simulation delta between normal and total power density can be used to adjust the measurement data. This requires additional validation as shown in Appendix F. Alternatively, if both polarizations are measured then total power density can directly be computed using PWS method (Appendix D.2). However, it will take twice the measurement time, but more important limitation is that the measurement system should have high sensitivity to accurately capture the amplitude and phase of non-dominant (weak) polarization of fields over the entire measurement scan area. Otherwise, the computed total power density using the PWS method could be erroneous.

4.2.3 Reference level setting using power meter

Since the VNA measures amplitude and phase relative to the reference signal, an absolute power measurement was also conducted at peak location of the area scan using an R&S NRP-Z57 power sensor to scale the measured relative 2D distribution of fields into absolute values.

4.3 Measurement results

Amplitude and phase of E-fields of dominant polarization were measured for the worst three antenna configurations #11, #13 and #19 at 10mm (~2λ) from the bottom surface (exposure plane) of the laptop. Using the Plane Wave Spectrum (PWS) method described in Appendix D, the measured dominant polarization fields were back transformed to the exposure plane in order to compute the normal power density component and then spatially averaged over 1 cm^2. Here, the back transformed data for normal component of power density was computed at 1.0 mm resolution in the exposure plane. 1 cm^2 spatial averaging was obtained by moving 1cm x 1cm square window, every 1.0 mm step size in the exposure plane. From spatially averaged normal power density, total power density was computed by adding the difference in simulated Total Power Density (PD_{total}) and simulated Normal Power Density (PD_{normal}) obtained in Section 3. For the circumstances with this device and filing, FCC is accepting the approach shown in Appendix F using the simulated difference between PD_{normal} and PD_{total} obtained in Section 3. The corresponding point power density and 1 cm^2-averaged power density distributions back transformed from 2λ distance to the exposure plane are shown in Figure 4-4, Figure 4-5, and Figure 4-6. The plots of the 1-D profile through the peak location are also provided.

a. **Antenna configuration #11: Peak Point Power Density (PD_{normal}) = 6.6 W/m^2**

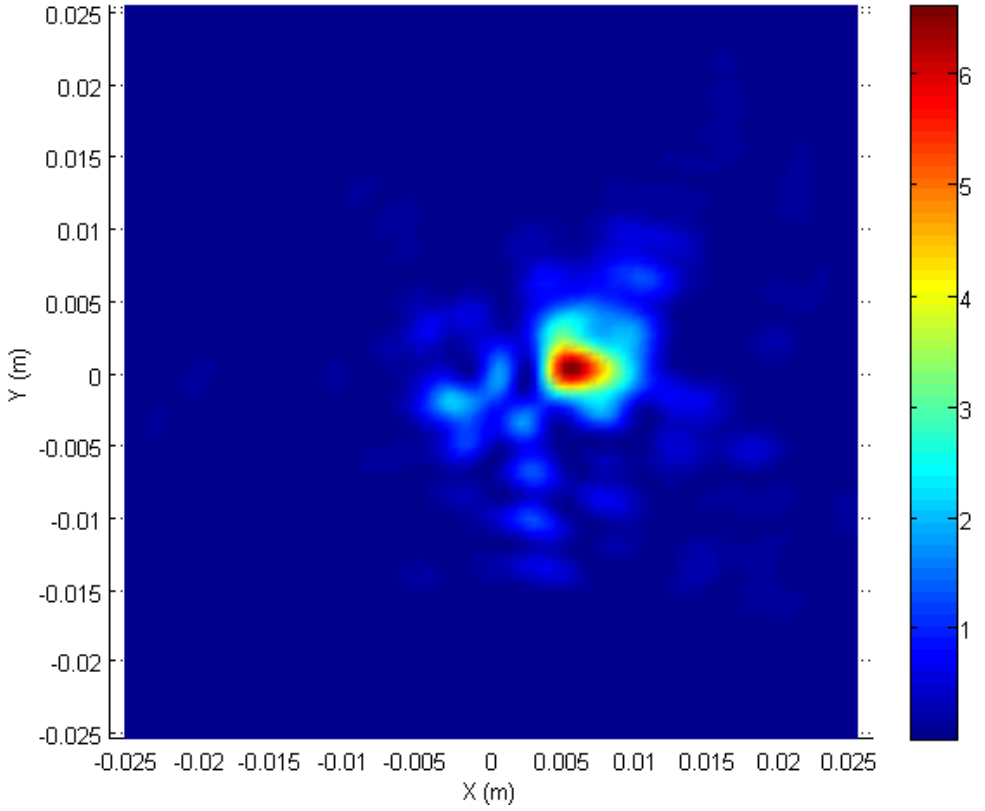

b. **Antenna configuration #11: point PD_{normal} along X-axis through peak location**

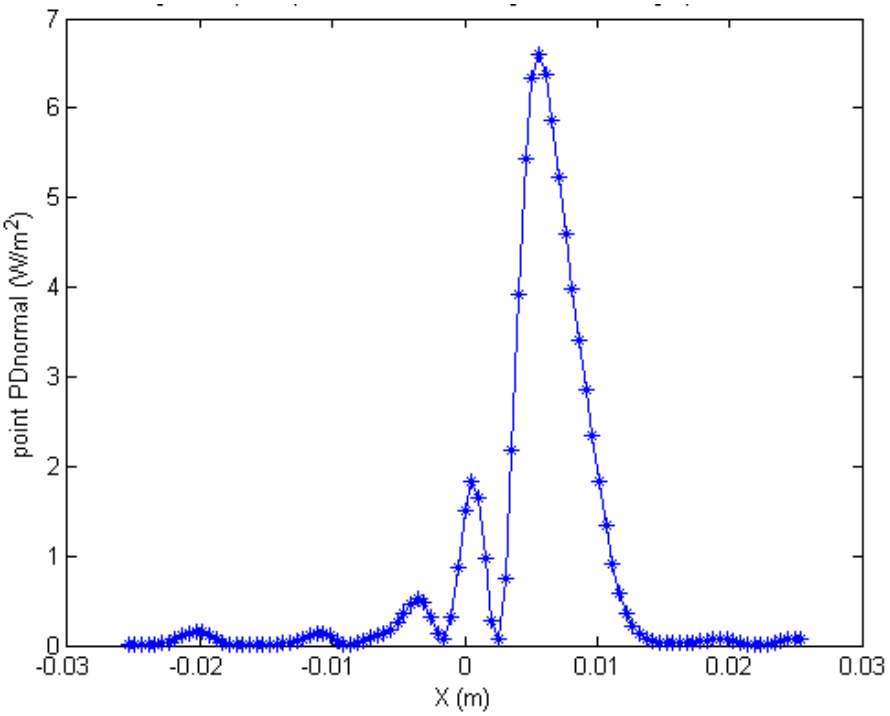

c. **Antenna configuration #11: Peak $1cm^2$-averaged PD_{normal} = 1.66 W/m^2**

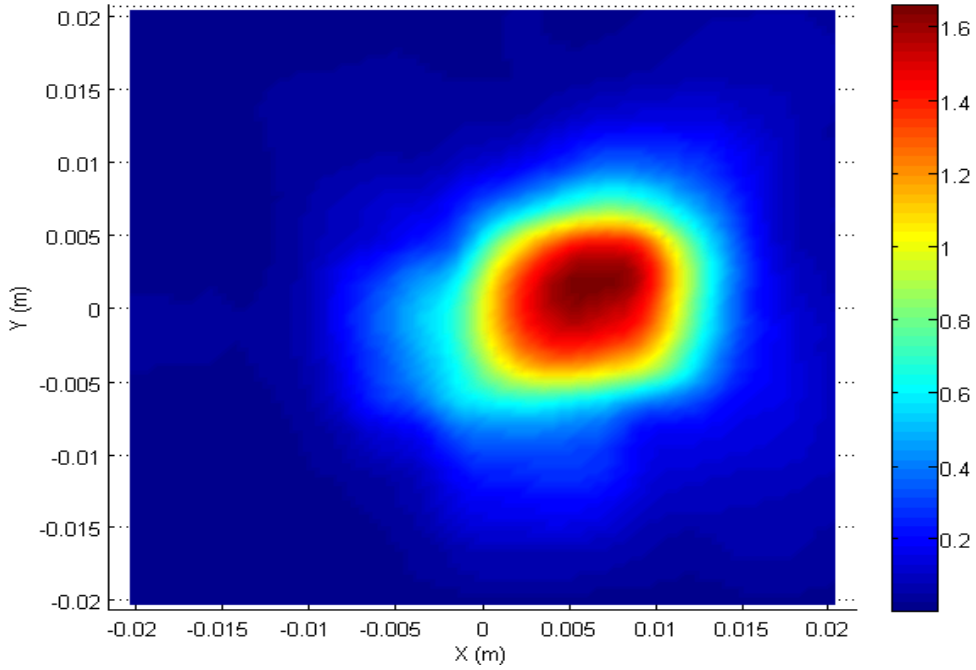

Figure 4-4: Power density distributions in the exposure plane for Antenna configuration #11: (a) Point PD_{normal} distribution; (b) 1-D profile plot through the peak location for point PD_{normal} distribution along X-axis; (c) $1cm^2$-averaged PD_{normal} distribution

a. **Antenna configuration #13: Peak Point Power Density (PD_{normal}) = 23 W/m²**

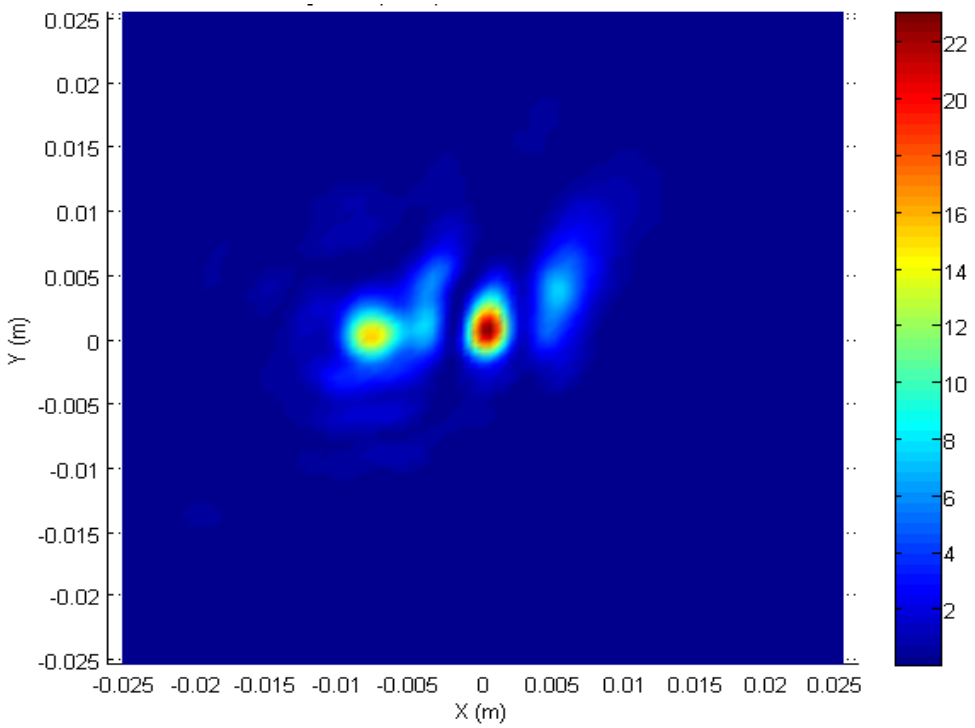

b. **Antenna configuration #13: point PD_{normal} along X-axis through peak location**

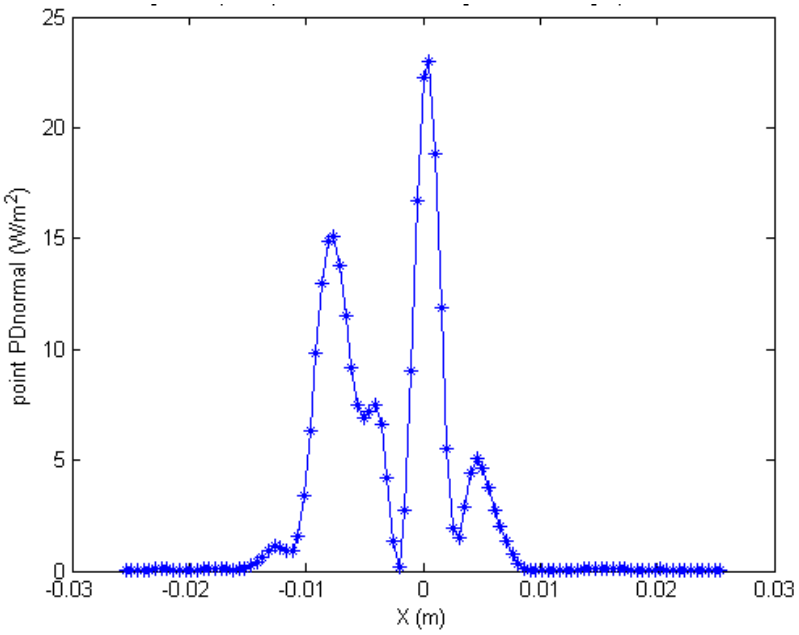

c. **Antenna configuration #13: Peak 1cm^2-averaged PD_{normal} = 4.66 W/m^2**

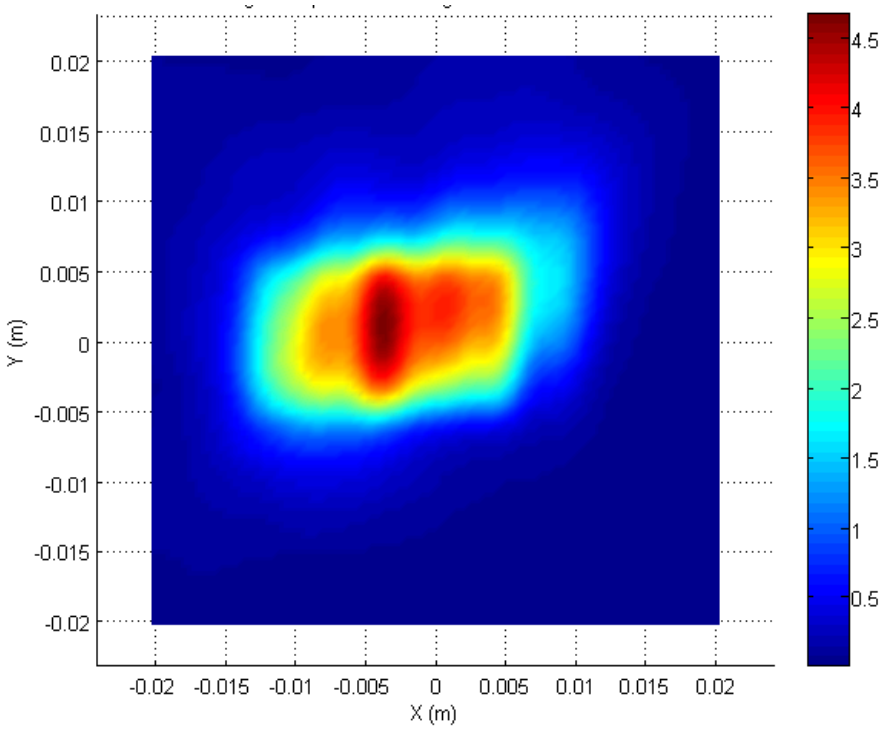

Figure 4-5: Power density distributions in the exposure plane for Antenna configuration #13: (a) Point PD_{normal} distribution; (b) 1-D profile plot through the peak location for point PD_{normal} distribution along X-axis; (c) 1cm^2-averaged PD_{normal} distribution

a. **Antenna configuration #19: Peak Point Power Density (PD_{normal}) = 8.49 W/m^2**

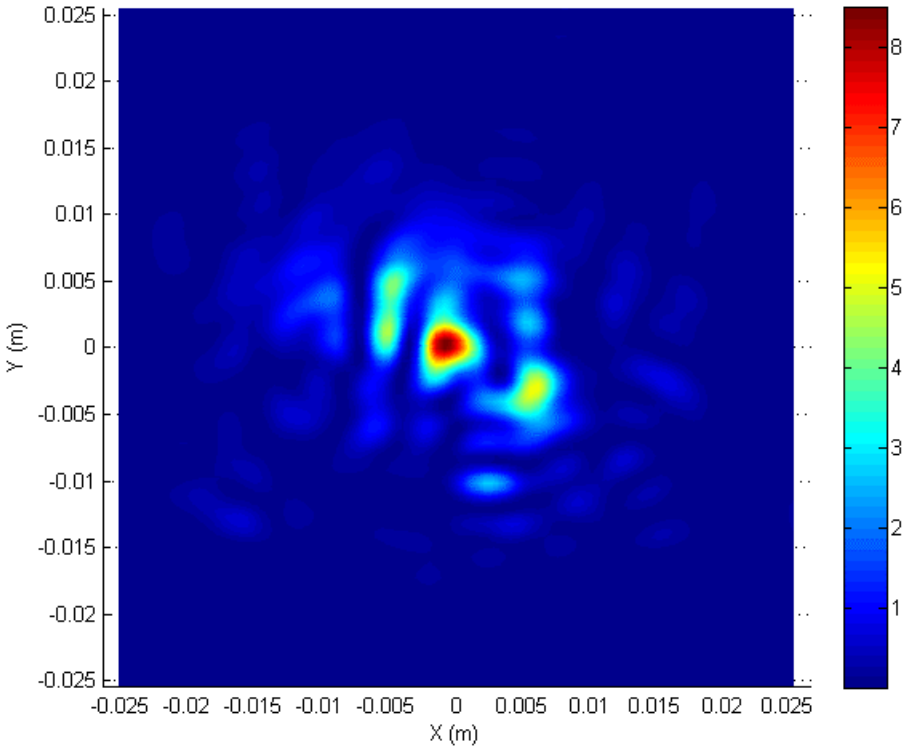

b. **Antenna configuration #19: point PD_{normal} along X-axis through peak location**

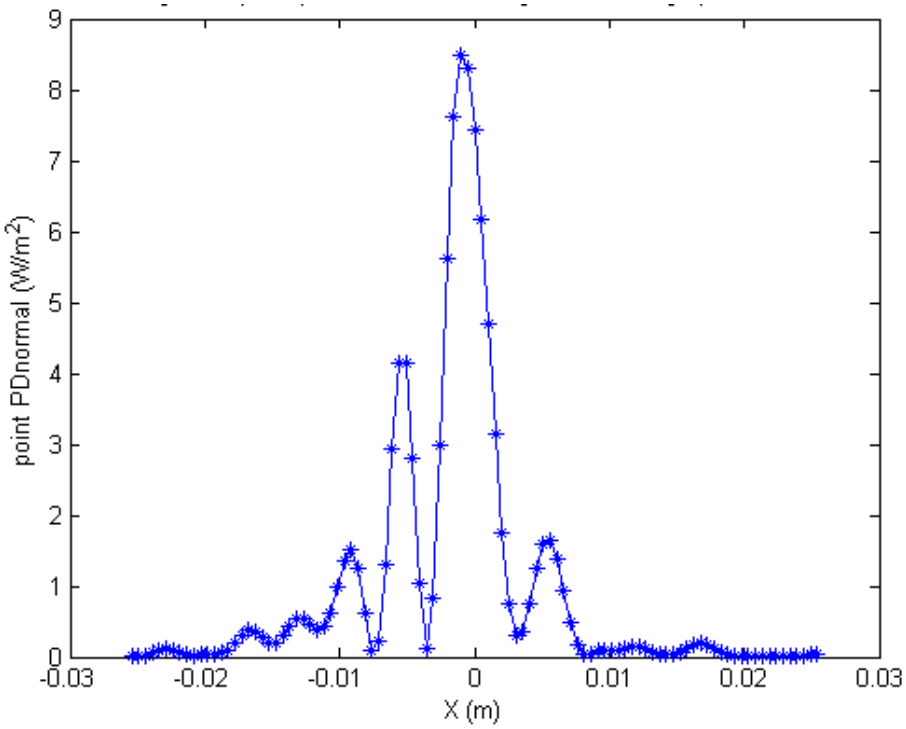

c. **Antenna configuration #19: Peak 1cm^2-averaged PD$_{normal}$ = 2.15 W/m^2**

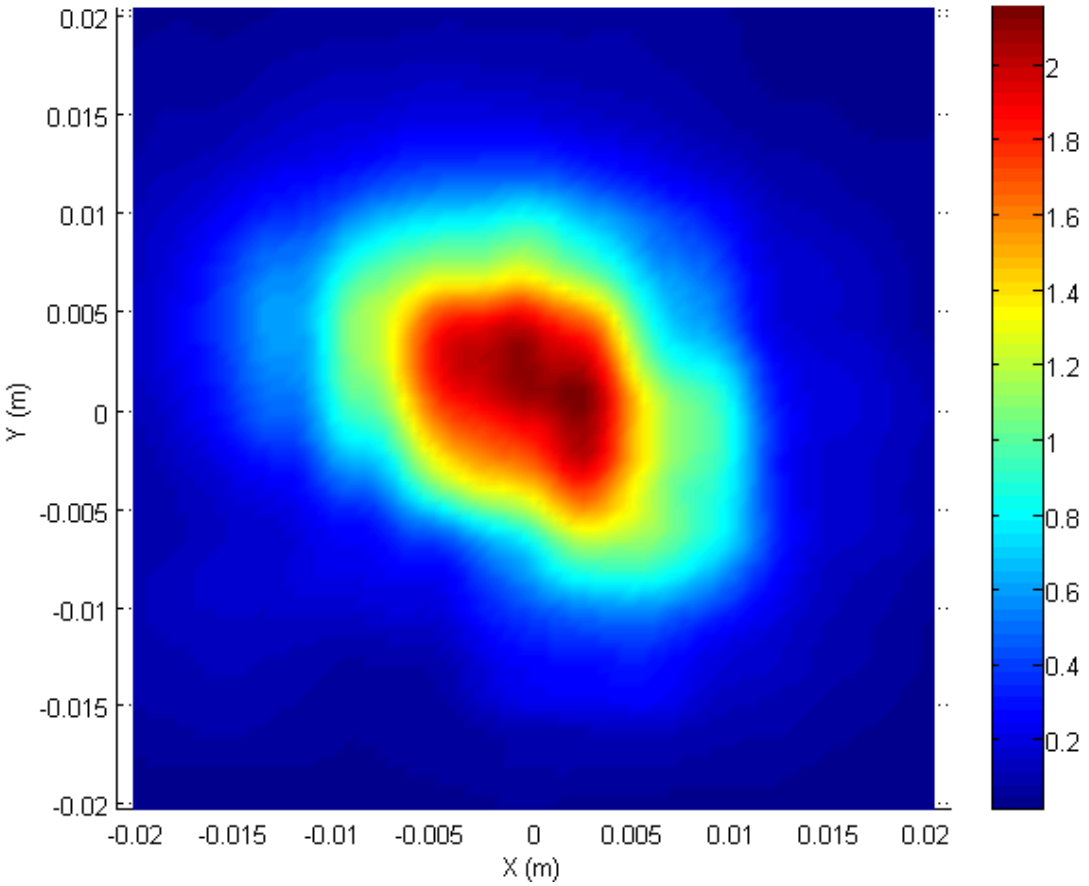

Figure 4-6: Power density distributions in the exposure plane for antenna configuration #19: (a) Point PD$_{normal}$ distribution; (b) 1-D profile plot through the peak location for point PD$_{normal}$ distribution along X-axis; (c) 1cm2-averaged PD$_{normal}$ distribution

Table 4-2 lists the peak point power density and peak 1 cm^2-averaged power density back transformed from 2λ separation distance, these are the normal components of power density at the exposure plane.

Table 4-2: Worst-case normal component Power Density (PD$_{normal}$) values

Config #	Peak point PD$_{normal}$ (W/m^2) Measured at 2λ and back transformed	Peak 1cm^2 averaged PD$_{normal}$ (W/m^2) Measured at 2λ and back transformed
11	6.60	1.66
13	23.0	4.66
19	8.49	2.15

In addition to the preceding PD$_{normal}$ results, to obtain total power density (PD$_{total}$) at exposure plane, we took the simulation approach described in Section 3 to find the relation between the normal power density (PD$_{normal}$) and total power density (PD$_{total}$) when simulated in free space

condition, then calculate the 1 cm^2-averaged PD_{total} for final product configuration (802.11ad module inside Acer N15W8) by adding the difference of simulated 1 cm^2-averaged PD_{total} and simulated 1cm^2-averaged PD_{normal} to the measured 1 cm^2-averaged PD_{normal} values listed in Table 4-2. The difference between PD_{normal} and PD_{total} in free space is listed in Table 4-3 for the identified three worst cases.

Table 4-3: Difference of simulated PD_{total} and simulated PD_{normal}

Antenna configuration #	Difference of PD_{total} and PD_{normal} (dB)
11	0.31
13	1.8
19	0.04

Thus, the peak 1 cm^2-averaged total power density levels for the three worst-case antenna configurations are as shown in Table 4-4. Note that the adjustment between PD_{total} and PD_{normal} for this Acer N15W8 application has been validated as shown in Appendix F, and it is accepted by FCC for this particular device and filing only.

Table 4-4: Worst-case peak 1cm^2-averaged total Power Density (PD_{total}) values

Antenna configuration #	PD_{total} (W/m^2)
11	1.78
13	7.05
19	2.17

All the power density values listed in Table 4-4 passed the 10 W/m^2 (or 1mW/cm^2) compliance limit with 7.05 W/m^2 as the highest level.

5 Validation Using Single-Element Simulation and Measurement

The simulation approach was taken for relative comparison evaluation in order to identify the three worst-case configurations having the highest power density value. The PWS-based measurement was used to demonstrate the compliance. Therefore, it is important to validate the assessment methodology in the following aspects:

1. Accuracy of the absolute amplitude measurement
2. Validity of the PWS implementation

Below flowchart explains the steps involved in this validation process:

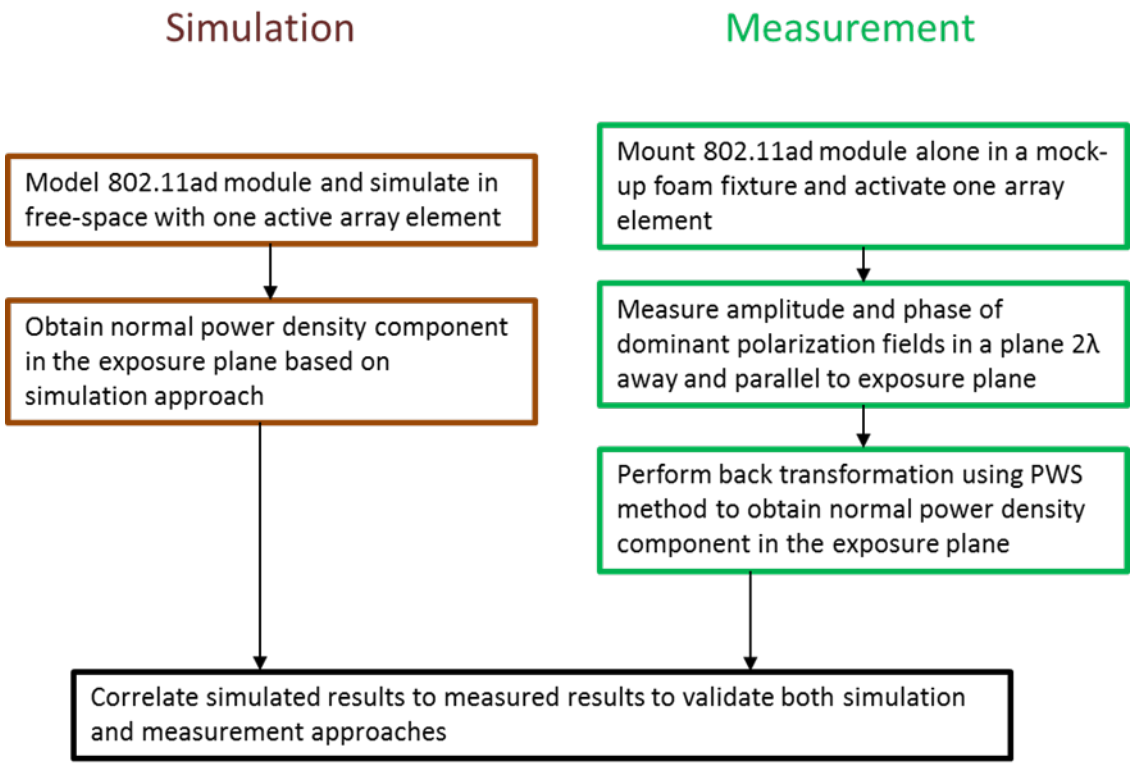

5.1 Absolute amplitude measurement validation using single-element modelling and measurement

The accuracy of the field distribution recovered from PWS back transformation relies on accurate relative amplitude and phase measurement at a scan plane, while the determination of the compliance depends on the accuracy of the absolute amplitude measurement. The validation for relative amplitude and phase is shown in Section 5.2 as part of PWS implementation, whereas validation for absolute amplitude measurement is shown in this section.

In order to validate that the test setup is accurate for absolute amplitude measurement, we compared the measurement results with simulated results. Since the measurement and simulation are two independent approaches, those two methods can validate each other, i.e. one method compliments the other.

5.1.1 Simulation for validation

As part of the validation, QCA9008-TBD1 802.11ad module was simulated in free-space with one active antenna element (patch antenna on the front side (see Figure 2-4) of the 802.11ad module's PCB as highlighted in Figure 5-1). This antenna element was fed with 4.74 dBm of power at the port.

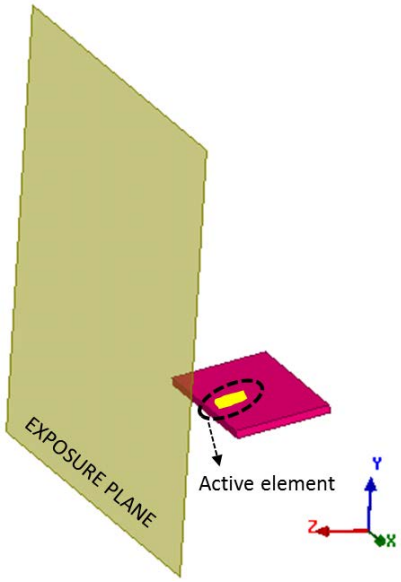

Figure 5-1: Simulation validation setup of QCA9008-TBD1 802.11ad module

Power density distribution and amplitude was assessed in the exposure plane. 1 cm^2 area spatial averaging was performed to extracted real part of normal component of Poynting vector in the exposure plane. Figure 5-2 shows the 1cm^2-averaged PD_{normal} distribution. (Note that we have done extensive validation as shown in Appendix G and F, therefore, for this device and filing, the FCC accepted our approach to compare only the normal power density).

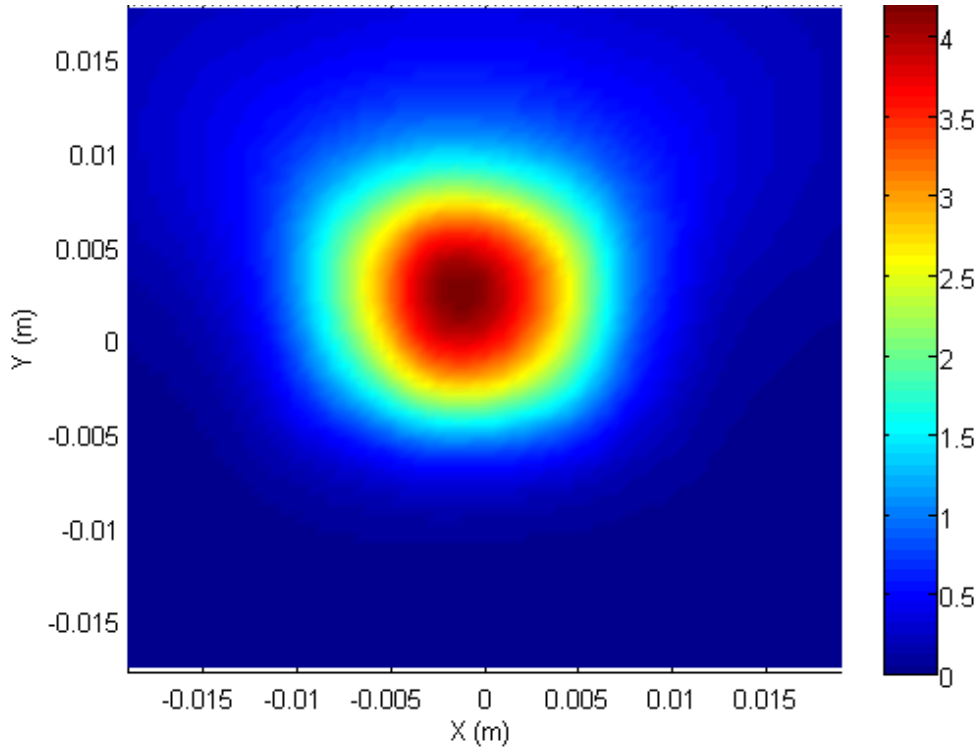

Figure 5-2: Simulated 1cm^2-averaged normal power density (PD_{normal}) in exposure plane with one active element in QCA9008-TBD1 802.11ad module

5.1.2 Measurement for validation

The QCA9008-TBD1 802.11ad module was also tested in free-space (non-perturbing support) with the same active antenna element as circled in Figure 5-1. For this purposes, the same test setup described in Sections 4.1 and 4.2 was used. In order to obtain the power density distribution in the exposure plane, amplitude and phase of electric field was measured for the dominant polarization in a plane 10mm (~2λ) away and parallel to the hypothetical bottom surface (i.e., exposure plane shown in Figure 3-1). Since the measurements were conducted in XY-plane (vertical plane) of the positioner, the 802.11ad module was oriented such that the exposure plane will be vertical (see Figure 5-3). The aperture of the open-ended waveguide is placed in parallel to the exposure plane (XY-plane) in order to capture the power density component normal to the exposure plane along Z-axis. Here, the dominant polarization was recorded to compute the normal power density at the exposure plane. Additionally, since the VNA measures amplitude and phase relative to the reference signal, an absolute power measurement was also conducted at peak location of the area scan using an R&S NRP-Z57 power sensor to scale the measured relative 2D distribution of fields into absolute values.

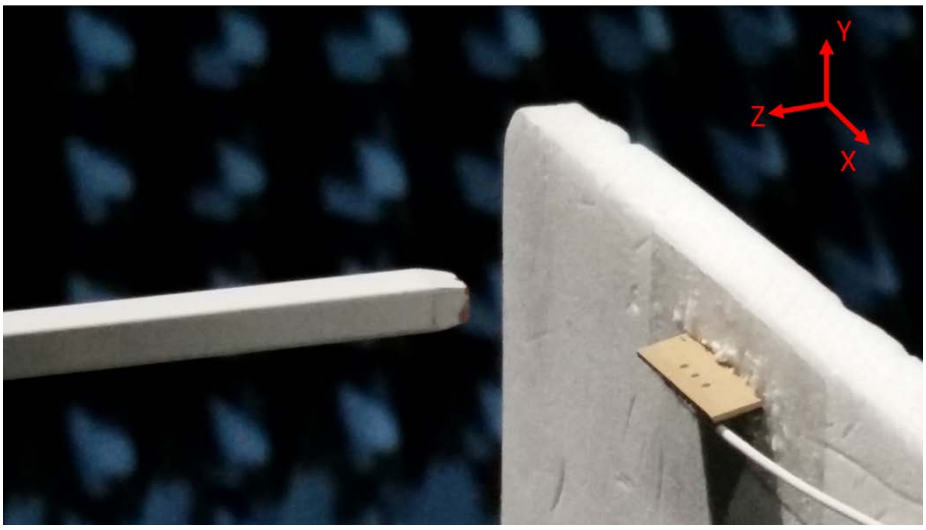

Figure 5-3: Measurement setup for validation

The measured fields at 10 mm separation distance from exposure plane were back transformed to the exposure plane using plane wave spectrum method described in Appendix D. The normal power density was spatially averaged over 1cm^2 area resulting in the distribution shown in Figure 5-4.

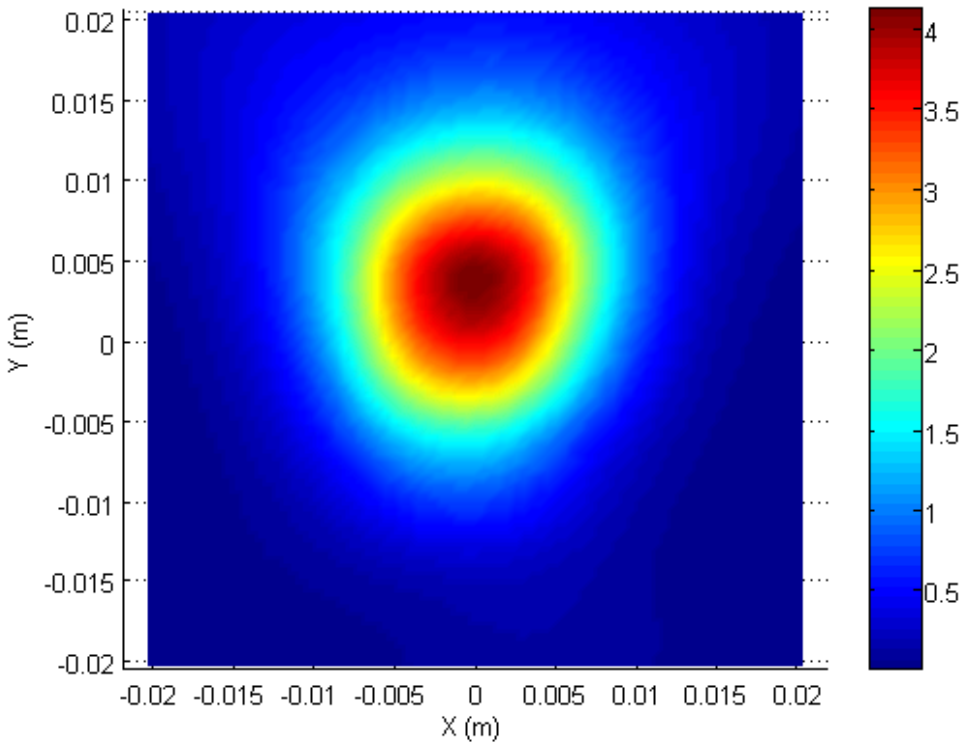

Figure 5-4: Measured normal power density was back transformed to the exposure plane averaged over 1cm^2 spatial area for one active element in QCA9008-TBD1 802.11ad module

5.1.3 Correlation between simulation and measurement results

It can be seen in Table 5-1 that the peak 1 cm^2-averaged normal power density and peak point normal power density are correlated to within 0.1 dB and 0.43 dB from the simulated values, respectively. Figure 5-5 shows the 1-D profile plot through the peak location for measured and simulated point normal power density along X-axis. Both comparisons are well within the combined uncertainty budget (see Appendix B). This confirms the accuracy of absolute amplitude measurement for our test setup, as well as validity of simulation and measurement approaches.

Table 5-1: Simulation and measurement correlation results

Assessment at exposure plane	Simulated normal power density (W/m2)	Measured normal power density (W/m2)	Delta (dB)
Peak 1cm^2-averaged	4.20	4.12	0.08
Peak point	7.64	6.92	0.43

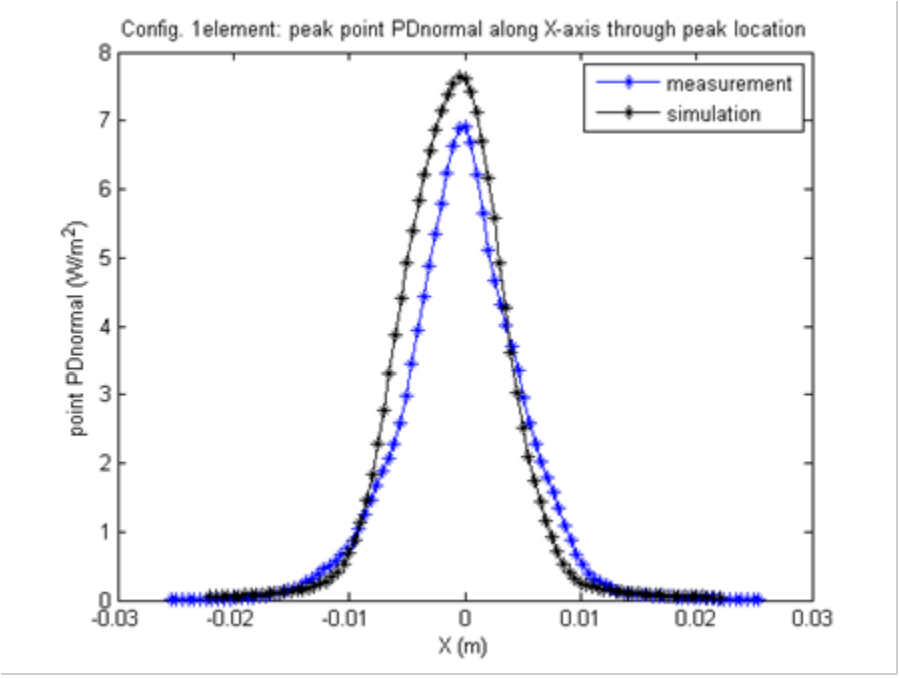

Figure 5-5: 1-D profile plot through the peak location for measured and simulated point normal power density along X-axis

5.2 Plane Wave Spectrum implementation validation

Appendix D describes the theory of the Plane Wave Spectrum (PWS), our PWS implementation, and shows the additional validation with a standard 2 x 4 antenna array.

In this section, to further validate our PWS implementation for Acer N15W8 application, we have done the followings:

a. Conducted near-field measurements at planes that are 2λ and 4λ away from the bottom of the Acer laptop and parallel to the exposure plane (see 2λ and 4λ planes shown in Figure 5-6), respectively, and recorded both amplitude and phase of E-fields for the

dominant polarization (E_y) as well as normal component of power density (PD_{normal}) at each plane,

b. Back-transformed the dominant polarization of fields (E_y) measured at 4λ to a closer plane that is 2λ away from the exposure plane to compute (PD_{normal}), and

c. Validated this back transformed PD_{normal} by comparing with the measured PD_{normal} in this 2λ plane.

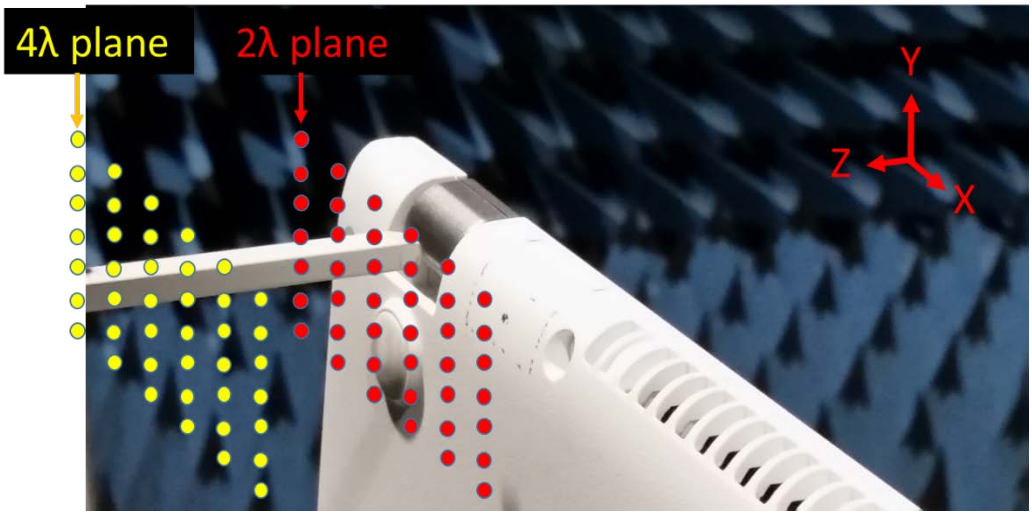

Figure 5-6: PWS implementation validation test setup

For the three worst case antenna configurations, the comparing data of back transforming 4λ plane to 2λ plane to measured data at 2λ plane is shown in Figure 5-7, where the good agreement in point power density distributions means good agreement in both amplitude and phase. The comparison of the corresponding peak power density values are shown in Table 5-2.

Table 5-2: Peak normal power density back transformed vs. the measured peak normal power density in 2λ plane

Config #	PD back transformed from 4λ to a plane 2λ away (W/m^2)	PD Measured in plane 2λ away from exp. Plane (W/m^2)	Delta (dB)
11	2.5 (Fig. 5-7a)	2.45 (Fig. 5-7b)	0.09
13	2.83 (Fig. 5-7c)	2.98 (Fig. 5-72)	-0.22
19	1.34 (Fig. 5-7e)	1.4 (Fig. 5-7f)	-0.19

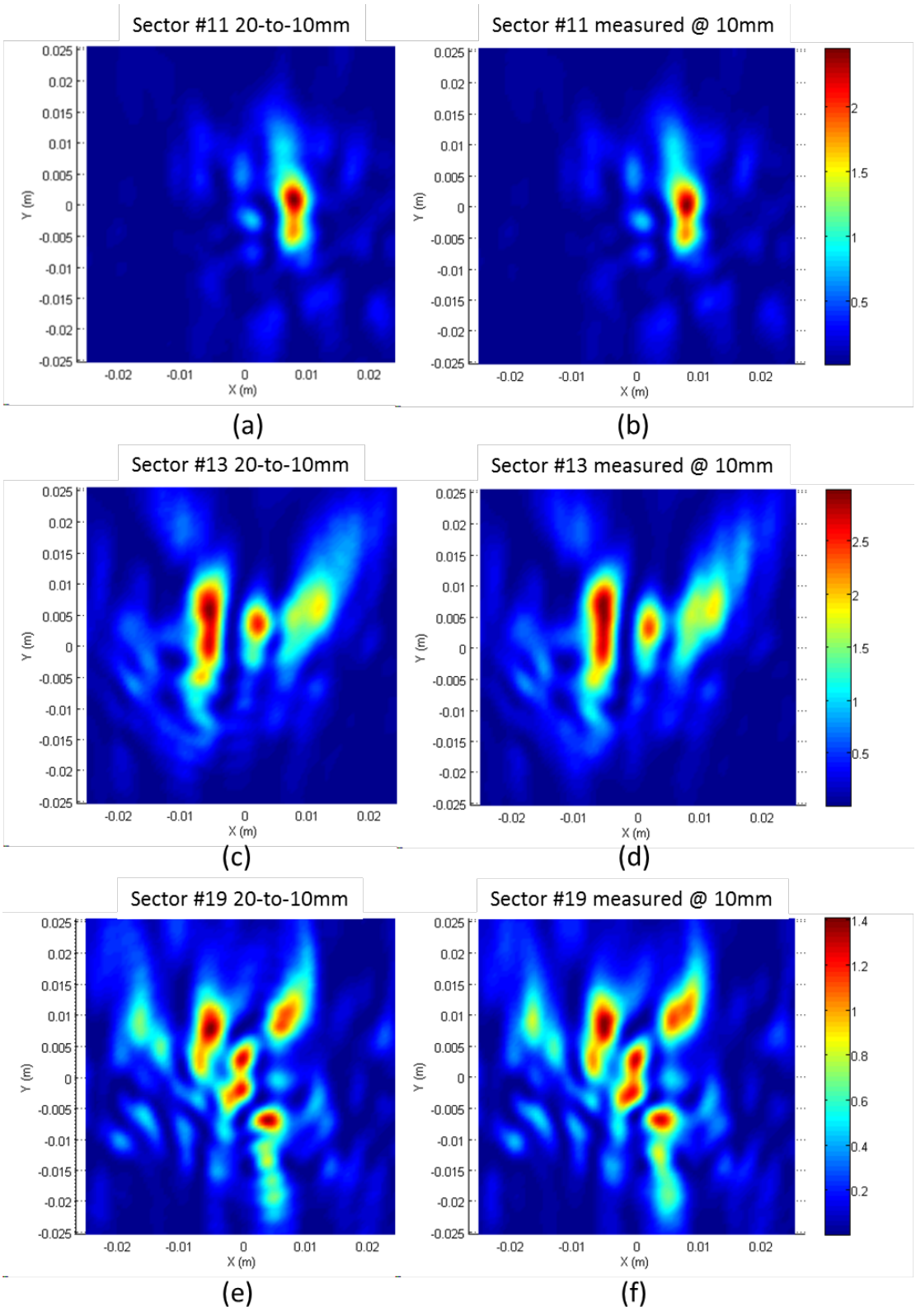

Figure 5-7: (a, c, e) show point PD_{normal} distributions of back transformed power density in 2λ plane from measured values in 4λ plane, (b,d,f) show point PD_{normal} distributions of measured power density in 2λ plane.

From the peak power density values and distributions shown above, the good agreement between back-transformed power density and measured power density in 2λ plane demonstrates the validity of our PWS implementation and associated measurement method. It should be noted this validation of the PWS method was performed on the compliance measurements of Acer product in final configuration, i.e., 802.11ad module placed inside the Acer laptop, for the three worst-case configurations identified. This data provides confidence for compliance demonstration since the same measurement data was used to back transform power density to the exposure plane.

5.3 Other Validation

On a general case basis, we further validated the accuracy of our absolute amplitude measurement with measuring and simulating the known sources. The adequate measurement distance from the source to minimize the probe perturbation was investigated as well. All the results are documented in Appendix G of this report.

6 Conclusions

General reporting requirements for RF exposure measurements and simulations described in KDB publication 865664 D02 were followed as shown in Appendix H.

In this report, we have performed RF exposure evaluation for QCA9008-TBD1 802.11ad radio in Acer N15W8 application by assessing the near-field power density using a combination of EM simulations and PWS-based near-field measurements.

QCA9008-TBD1 (FCC ID: PPD-QCA9008-TBD1) was installed inside N15W8 Acer laptop, and the 802.11ad module was mounted near the hinge. Since the user could place the laptop in the lap, i.e., closest possible distance to the QCA9008-TBD1 802.11ad module, power density was assessed at the bottom surface (exposure plane).

The PWS-based near-field measurement setup and EM simulations were validated by showing good correlation in power density in the exposure plane for a test scenario of 802.11ad module in free-space. EM simulations were used to reduce the number of measurements needed by determining the three worst-case antenna configurations for this particular application. Near-field measurements were performed for the identified three worst-case antenna configurations with 802.11ad module inside N15W8 Acer laptop at 10 mm and 20 mm separation distances from the exposure plane, and the measured fields were back transformed to determine the normal component of power density in the exposure plane.

The plane wave spectrum back transformation algorithm was also validated by showing good correlation between power density back transformed from 4λ scanning plane to 2λ plane and the power density measured in the 2λ plane.

1 cm^2 spatial averaging was performed on the back transformed normal power density in the exposure plane to determine the peak 1 cm^2-averaged power density values for the three worst antenna configurations. From spatially averaged normal power density, total power density was computed by adding the difference in simulated PD_{total} and simulated PD_{normal}. For this particular case, the FCC accepted our validation shown in Appendix F so that we can use this simulated difference. The adjustment of power density based on differences between the normal component of a Poynting vector and total field using the simulation results for the worst-case antenna configurations is only considered for the current circumstances and this permissive change filing.

The total power density values for the three worst-case antenna configurations were less than the compliance limit of 10 W/m^2, thus, complying with the RF exposure requirements.

In summary, the Acer N15W8 containing the QCA9008-TBD1 802.11ad radio is in compliance with FCC RF exposure requirement.

Table 6-1: Compliance summary

Worst case total power density (W/m^2) 1cm^2 averaged	Margin below limit (dB)	Conclusion
7.05	1.5	Complied

A Confidential Design Information of QCA9008-TBD1 802.11ad Module

This exhibit is confidential. It contains details on the QCA9008-TBD1 802.11ad module's design, details on all antenna configurations, antenna schematics, radiation pattern, and modeling details including the layout information. Refer to separate confidential exhibit "Appendix_A_Confidential Design Information of QCA9008-TBD1 802.11ad Module_RevC"

B Uncertainty Budget

B.1 Simulation uncertainty budget

Table B-1: Standard uncertainty budget for simulated values of power density

#	Description	Uncertainty (%)	Prob. Dist.	Div.	Std. Unc.	Std. Unc (dB)
1	FEM Mesh Density	0.1%	Norm	1.0	0.1%	0.00
2	Boundary Condition	0.8%	Norm	1.0	0.8%	0.04
3	Source amplitude	12%	Norm	1.0	12%	0.51
4	Convergence	0.5%	Norm	1.0	0.5%	0.02
				Combined Standard Uncertainty	**12%**	**0.51**
				Expanded Standard Uncertainty	**25%**	**0.97**

For table:

[1] Mesh density on the exposure plane was changed by limiting the "max length" of mesh size from auto setting (9.6mm) to 2mm

[2] Simulation domain (volume) was decreased by 30% to check the influence of reflections from boundary conditions on power density

[3] Simulated EIRP was compared with measured EIRP to determine the uncertainty in source amplitude. This test was conducted for one array element to estimate the source variation. We measured the EIRP with the QCA9008-TBD1 802.11ad module in free space with the single element enabled to a power level of 4.74 dBm, the EIRP is 11dBm. We also performed the simulation for the same configuration resulting in antenna gain of 5.7dBi. Knowing the input power for this antenna element is 4.74dBm, resulting in the simulated EIRP = 4.74+5.7=10.44dBm. Thus, we concluded the uncertainty in source amplitude as 0.5dB. In theory, this uncertainty includes both source variation as well as measurement uncertainty.

[4] 5% versus 3% convergence criteria were compared in Ansys Electromagnetics Suite 17.0.0.

B.2 Measurement uncertainty budget

Table B-2: Standard uncertainty budget for measured values of power density

#	Description	Uncertainty (%)	Prob. Dist.	Div.	Std. Unc.	Std. Unc (dB)
1	Power sensor meter	3.0%	Norm	1	3%	0.13
2	Cable and connector loss	12.0%	Norm	1	12%	0.49
3	Probe near-field perturbation	15.0%	Norm	1	15%	0.61
4	Positioning accuracy	12.6%	Norm	1	13%	0.51
5	Signal generation (IF accuracy)	2.3%	Norm	1	2%	0.10
6	Signal generation (LO accuracy)	2.3%	Norm	1	2%	0.10
7	Source power drift	1.2%	Norm	1	1%	0.05
				Combined Standard Uncertainty	**23%**	**0.91**
				Expanded Standard Uncertainty	**47%**	**1.67**

Notes for table:

[1] Power sensor uncertainty for R&S NRP-Z57

[2] Cable loss and connector loss uncertainty

[3] Difference in incident power density with and without open-ended waveguide probe (Appendix E)

[4] Influence of positioning accuracy to +/-1mm in separation distance between DUT and measurement plane. Here, only uncertainty along z-axis (separation distance) was accounted as the probe was manually positioned for separation distance from the bottom surface of the laptop. Automated probe positioning system has a much higher accuracy in positioning (can be set to within one-thousandth of an inch = 0.0254mm ~ λ/200), hence uncertainty of positioning in scan plane (XY plane) is negligible.

[5,6] Influence of external feed signals (IF and LO) to the source. IF and LO were changed by +/- 5dBm.

[7] Source signal stability over a time period of 10 minutes.

B.3 Combined uncertainty budget

Table B-3: Combined overall uncertainty budget for power density

#	Description	Std. Unc.	Std. Unc (dB)
1	Simulation Uncertainty	12.4%	0.51
2	Measurement Uncertainty	23.4%	0.91
Combined Overall Standard Uncertainty		**27%**	**1.02**
Expanded Overall Standard Uncertainty		**53%**	**1.85**

C Complete Simulation Results

The simulated power density in free-space was estimated by extracting the real component of Poynting vector radiating outwards normally to the bottom surface (exposure plane) of the laptop. The below figure shows the normalized peak PD_{normal} levels for the 36 antenna configurations that were evaluated to determine the worst case antenna configuration after applying $1cm^2$ area spatial averaging. Antenna configurations #11, #13, and #19 are identified as the worst configurations having the highest power density in the exposure plane.

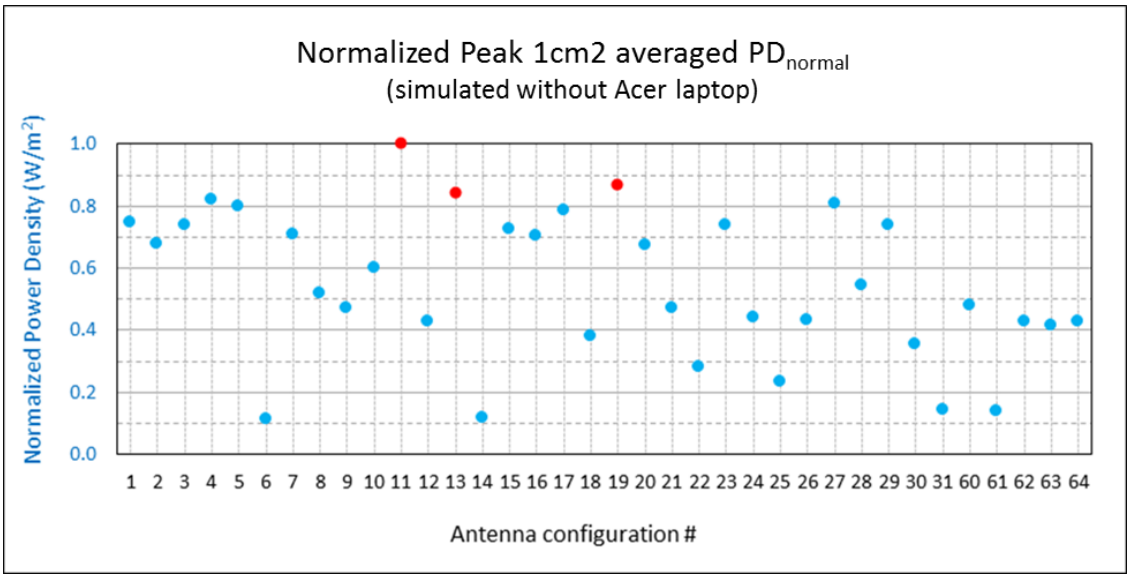

The distributions of PD_{normal} power density with $1cm^2$ spatial averaging are shown on the following pages for all antenna configurations.

Antenna configuration 1

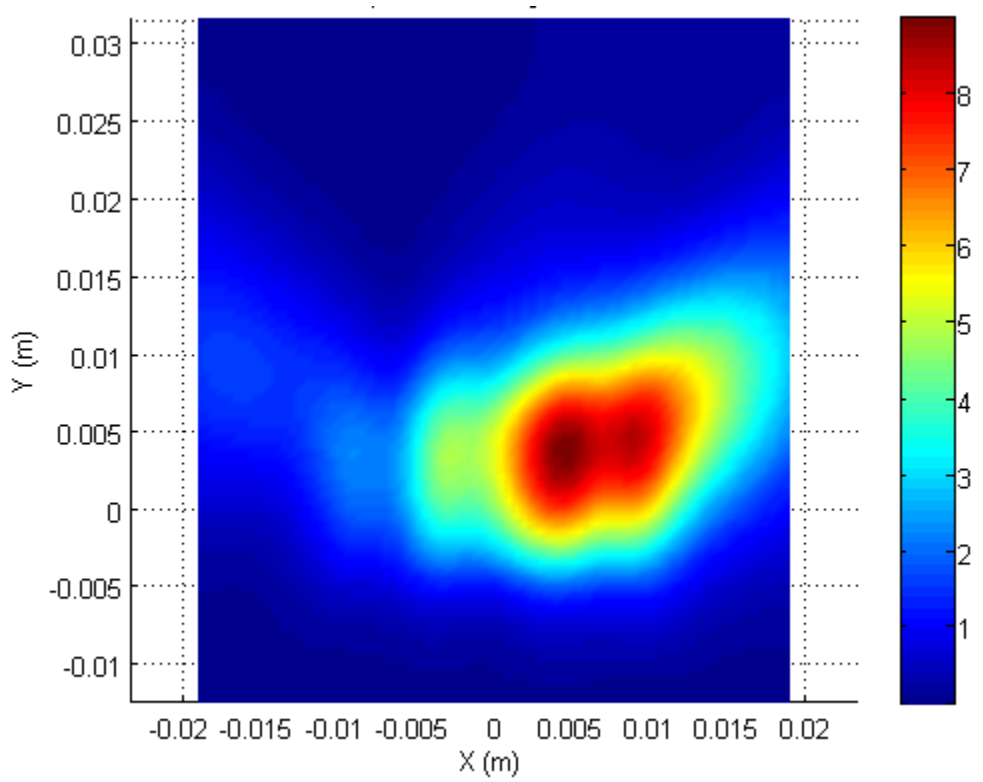

Antenna configuration 2

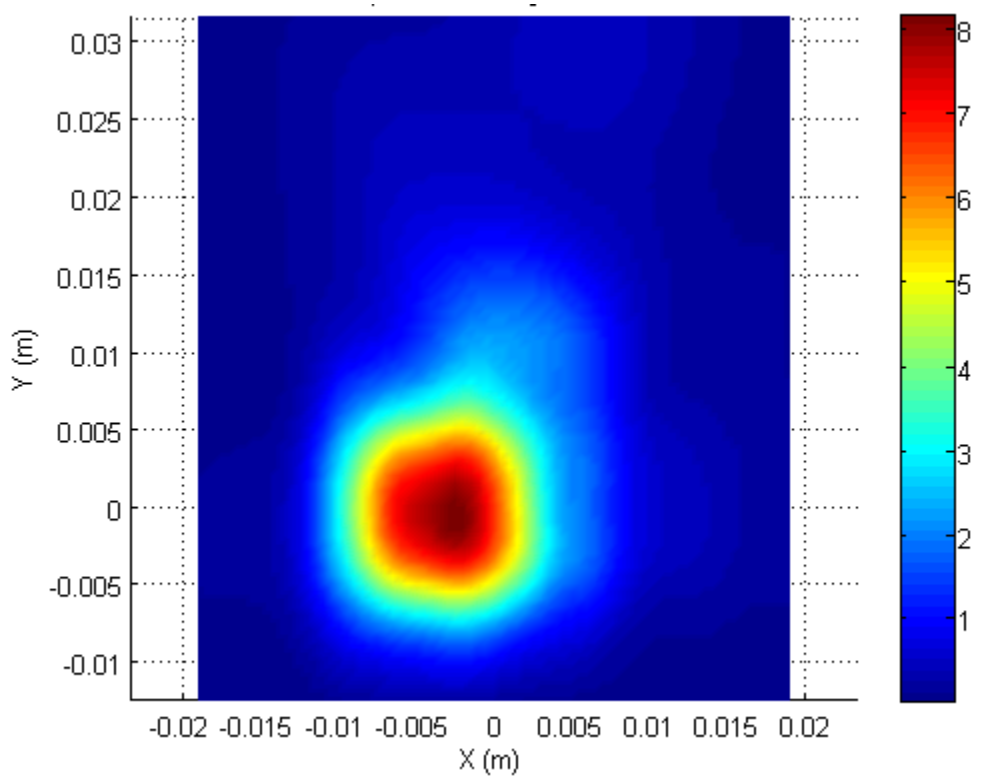

Antenna configuration 3

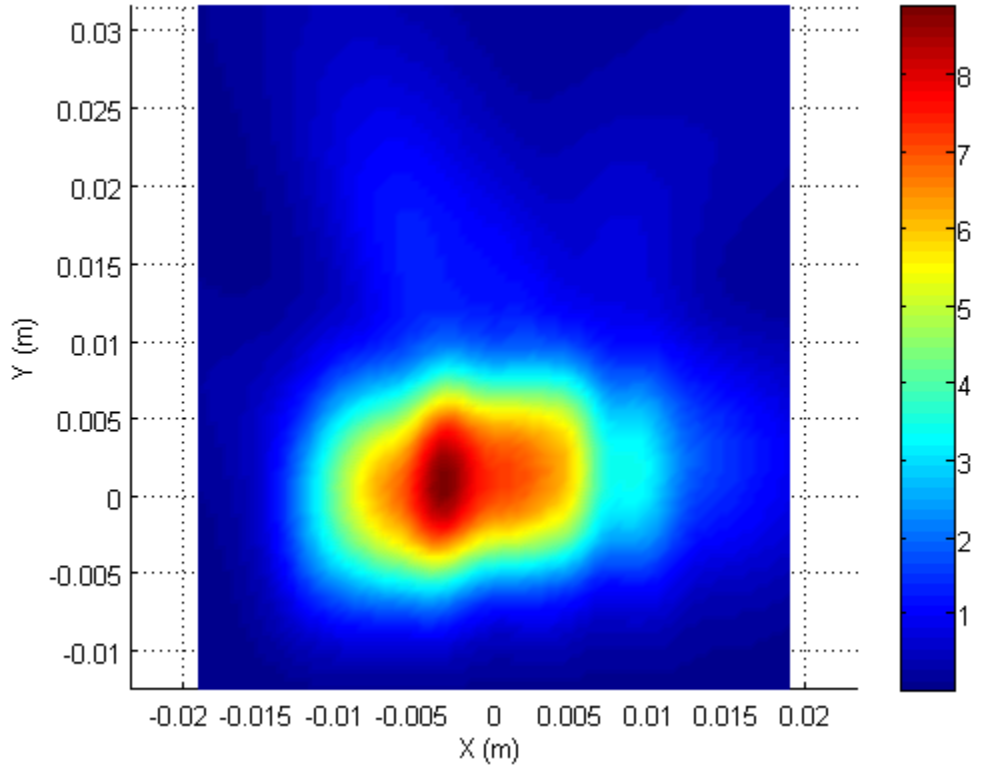

Antenna configuration 4

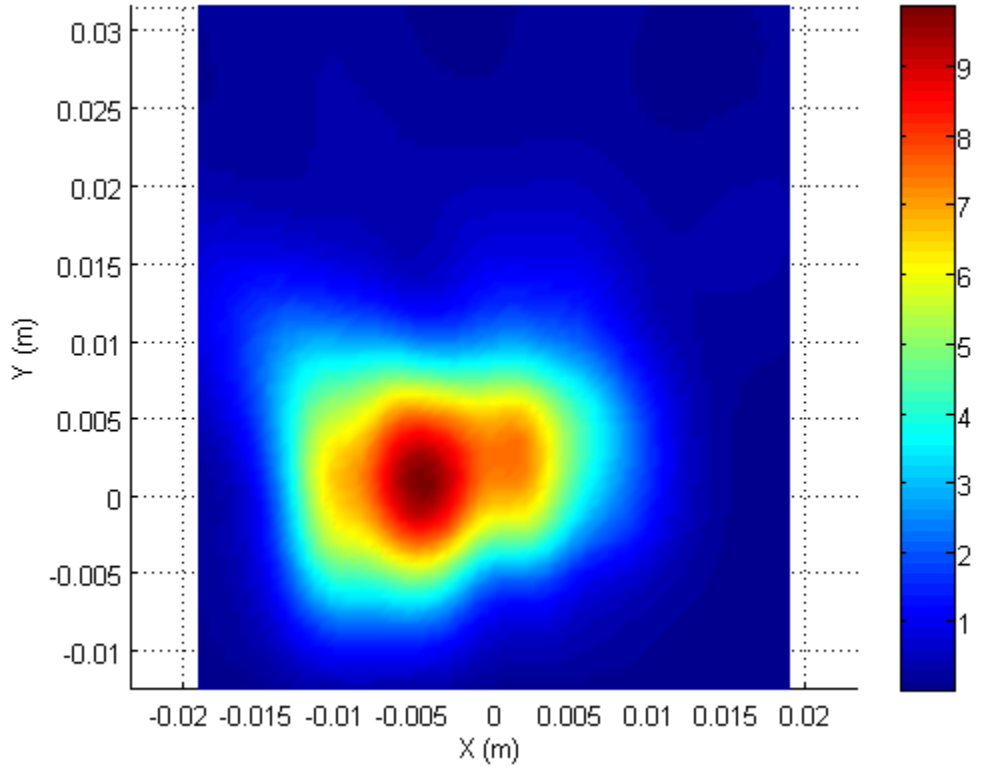

Antenna configuration 5

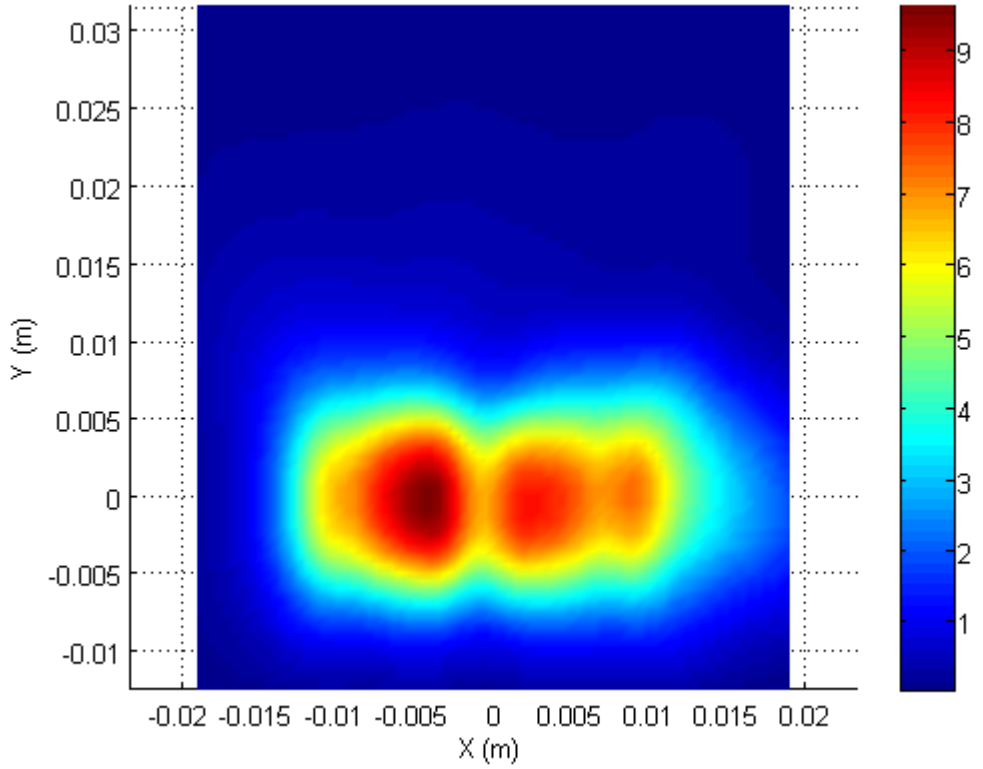

Antenna configuration 6

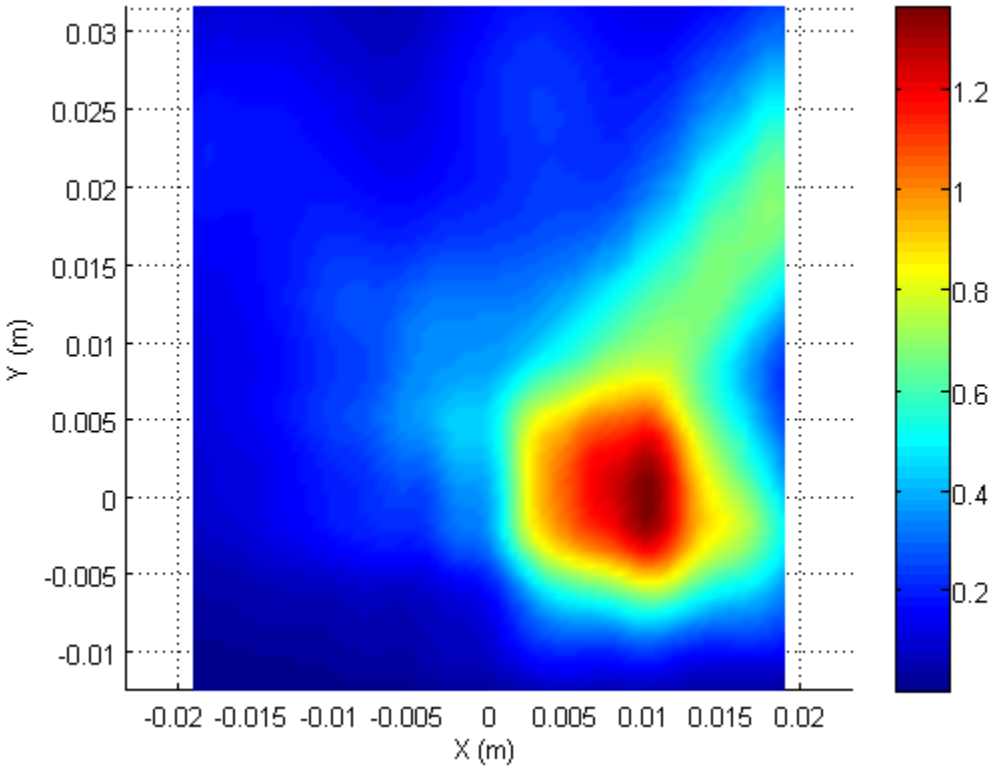

Antenna configuration 7

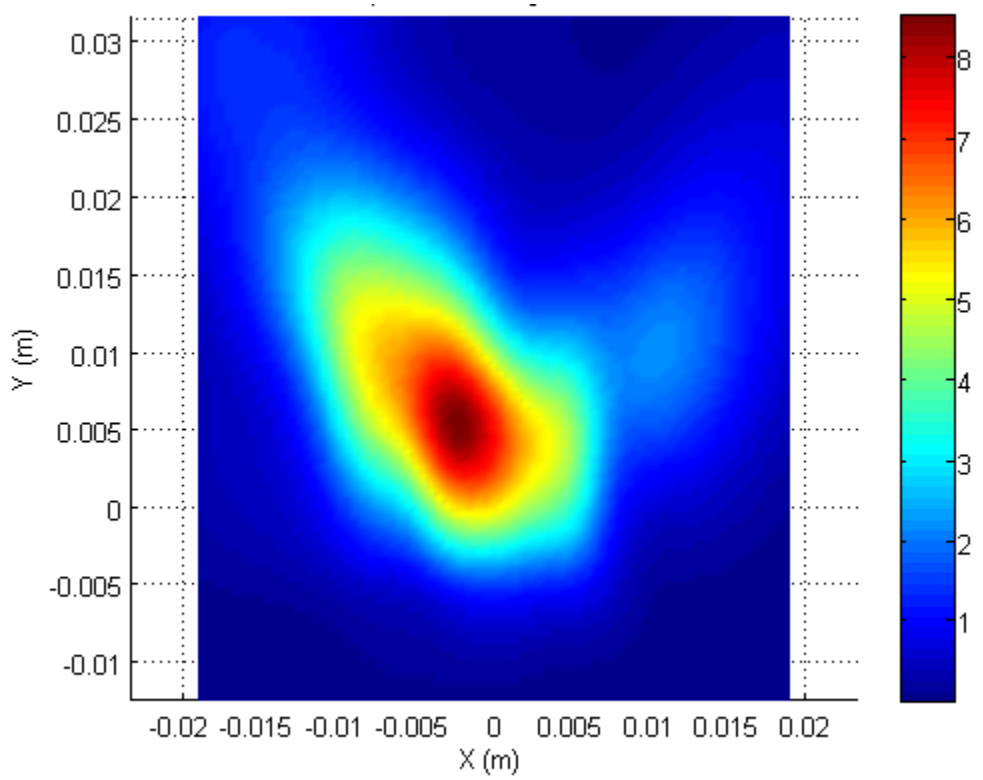

Antenna configuration 8

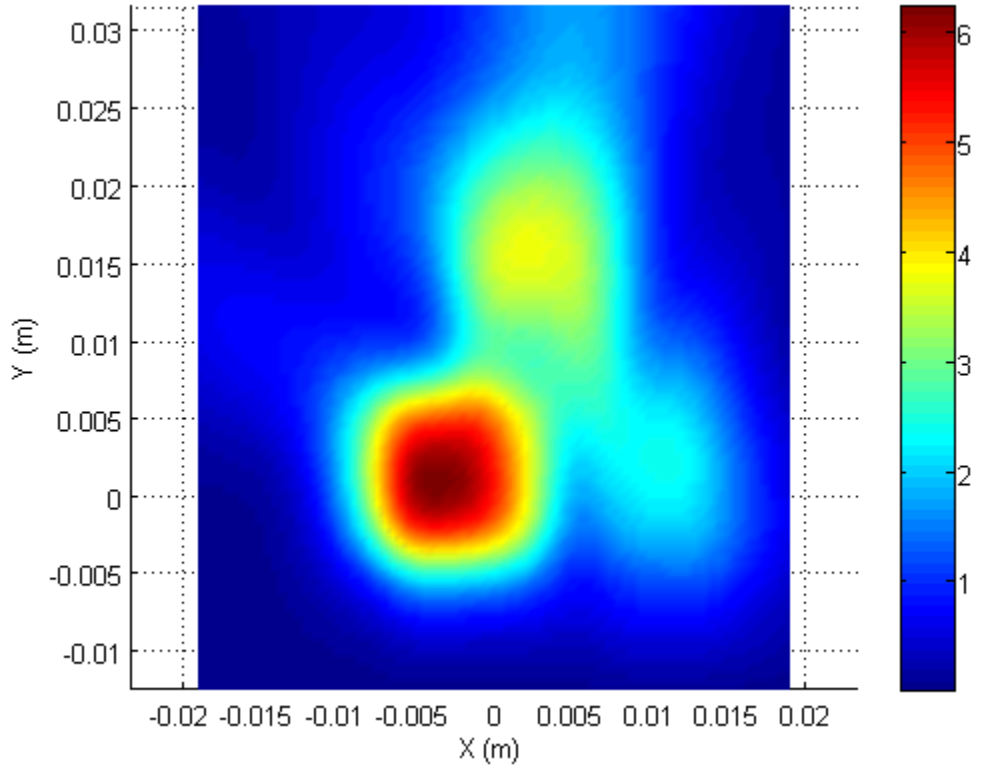

Antenna configuration 9

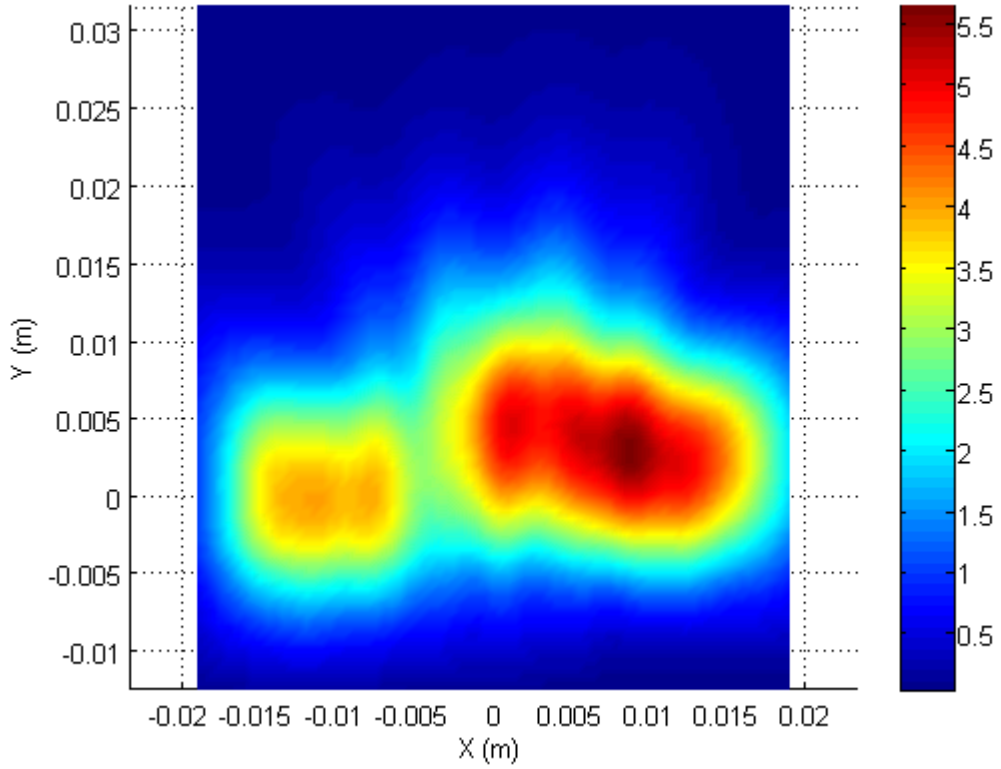

Antenna configuration 10

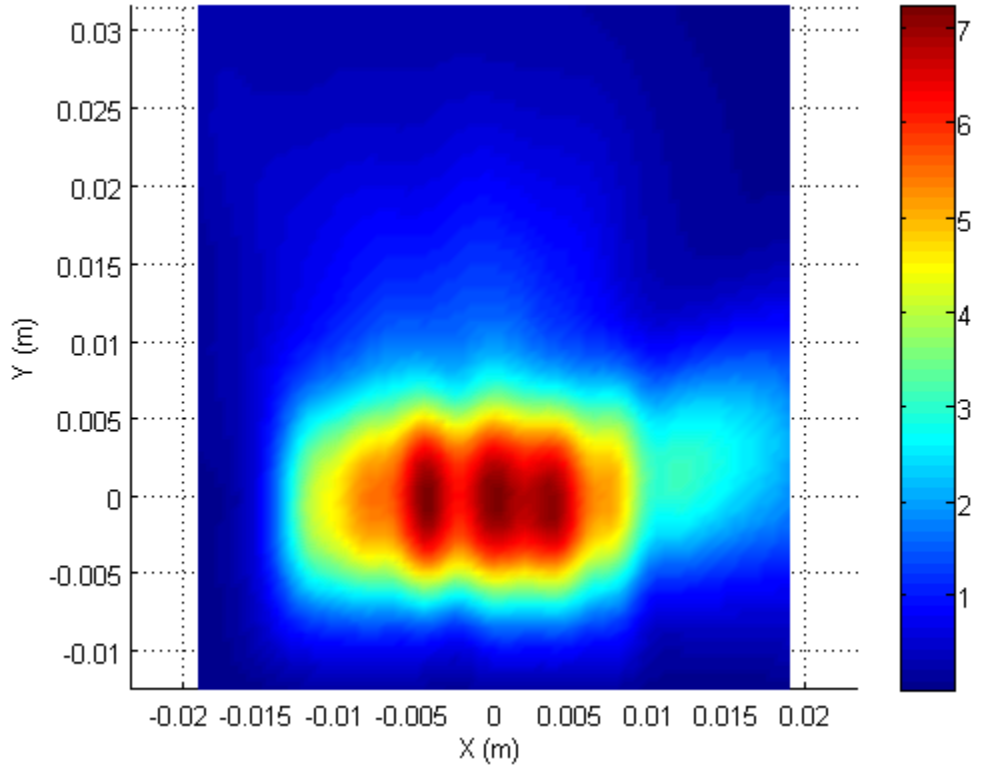

Antenna configuration 11

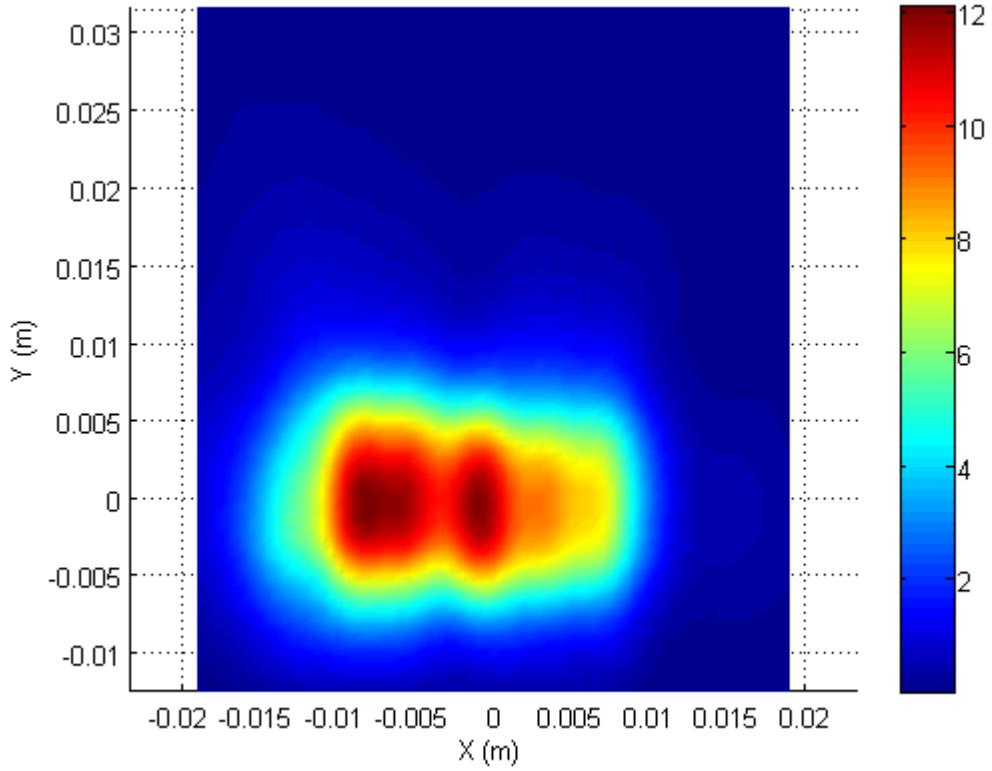

Antenna configuration 12

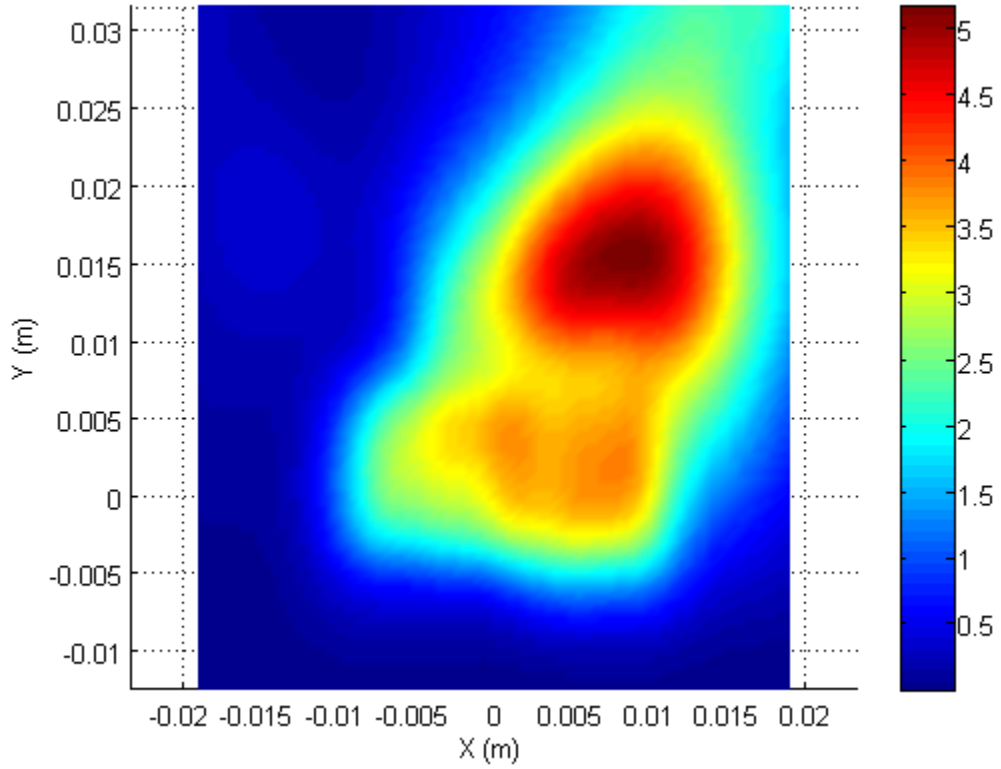

Antenna configuration 13

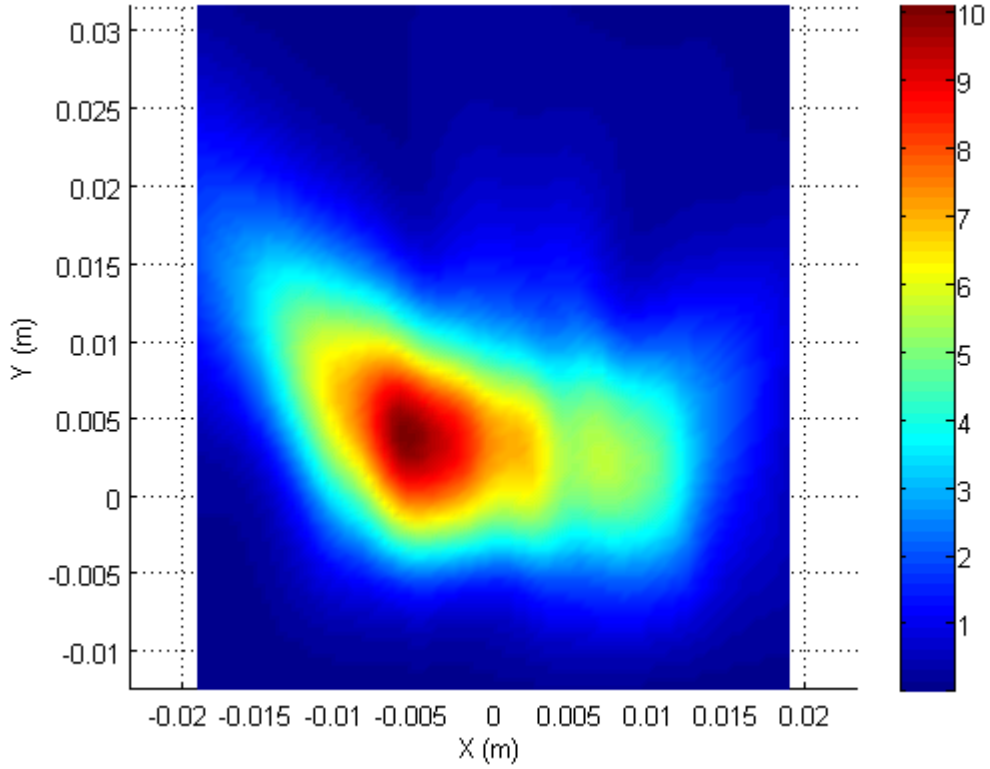

Antenna configuration 14

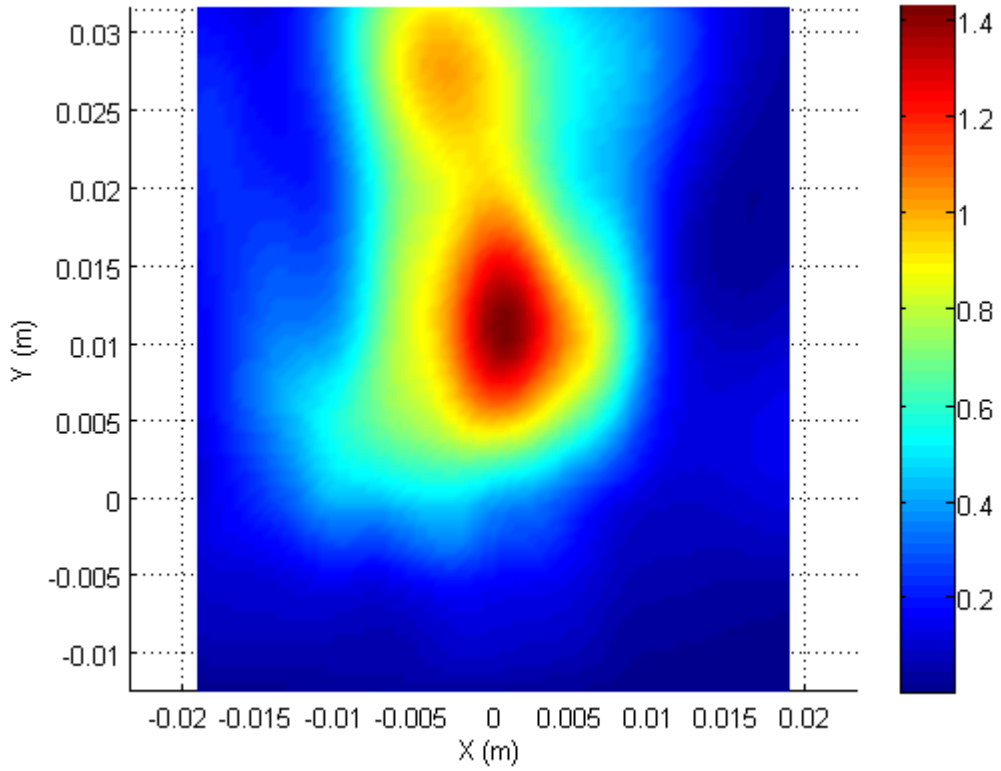

Antenna configuration 15

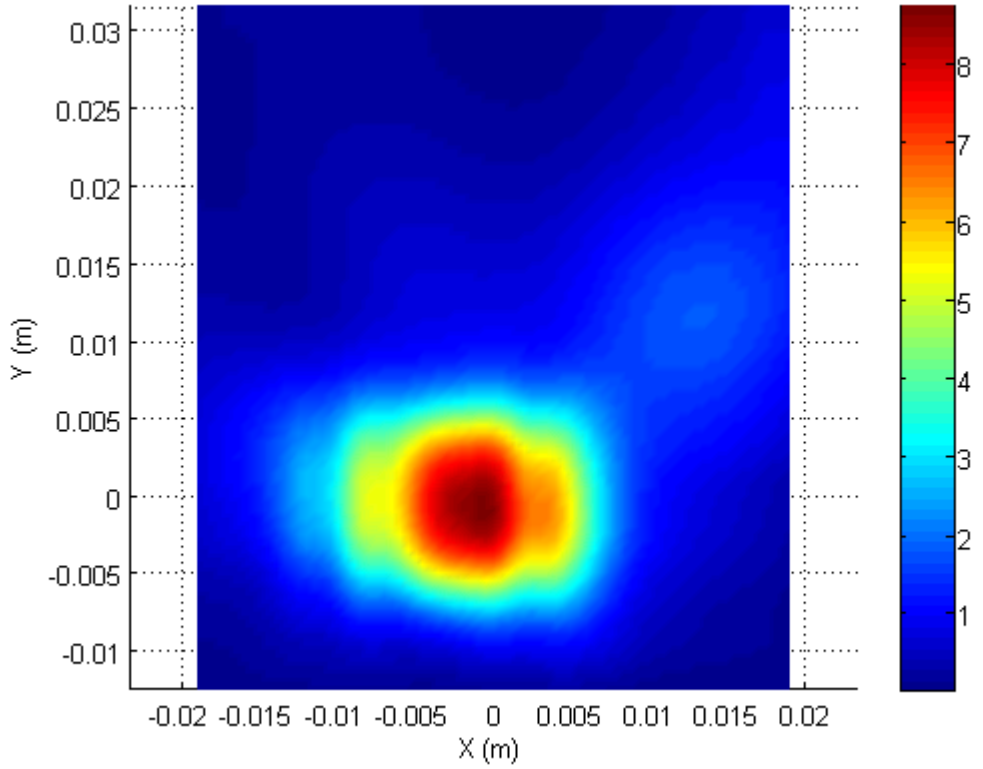

Antenna configuration 16

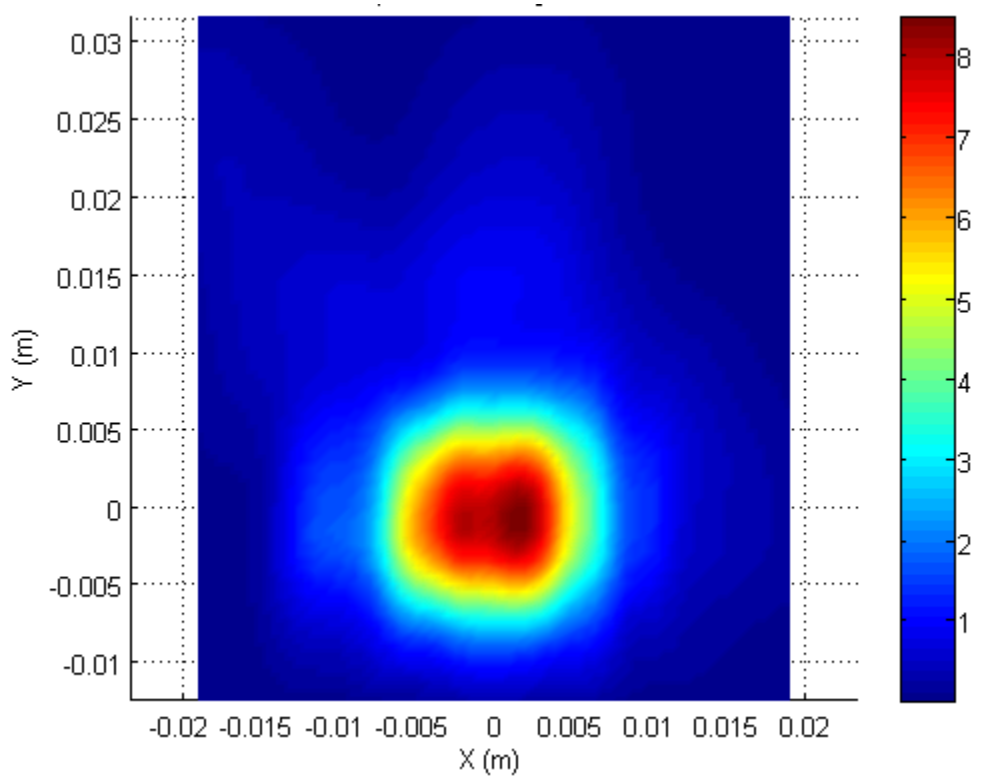

Antenna configuration 17

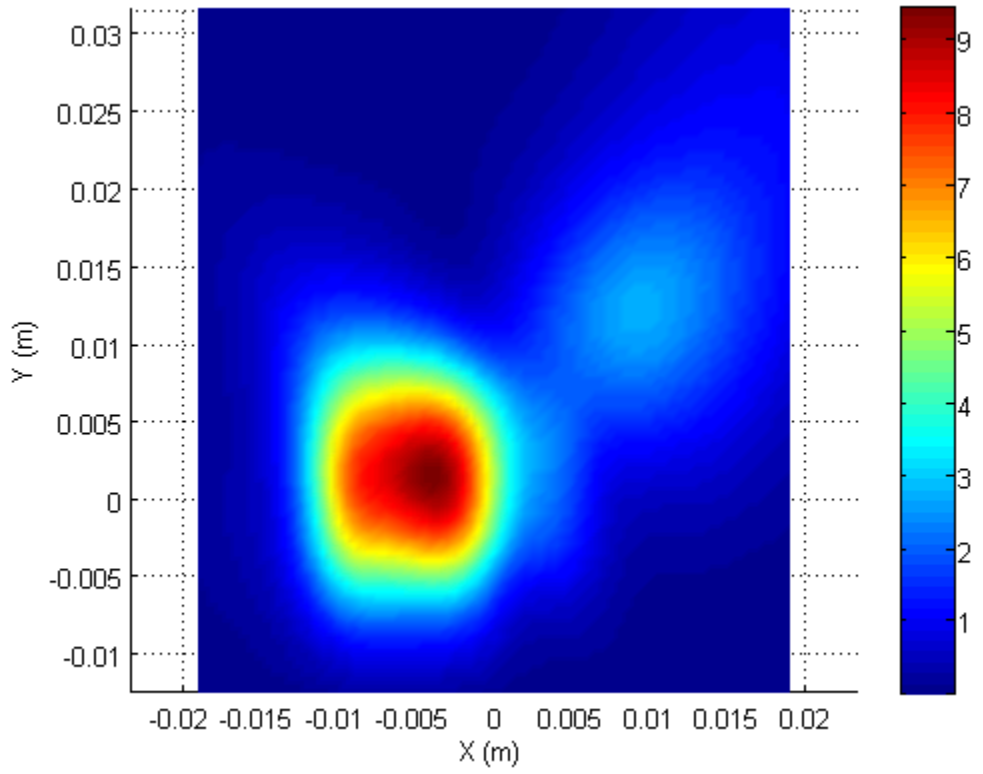

Antenna configuration 18

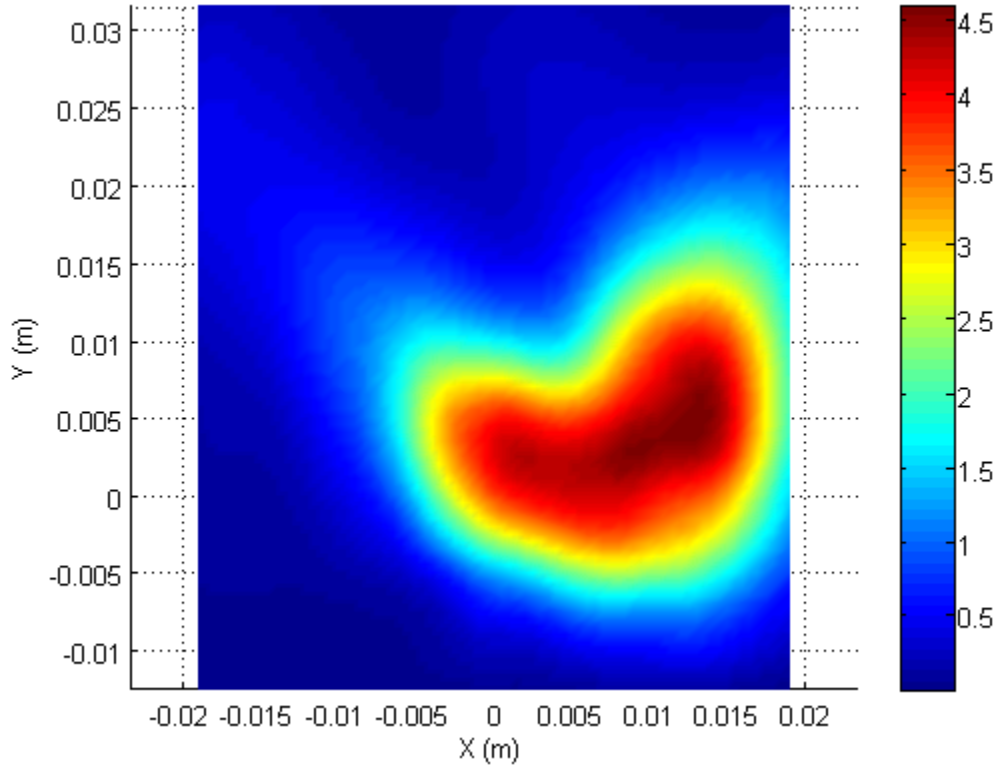

Antenna configuration 19

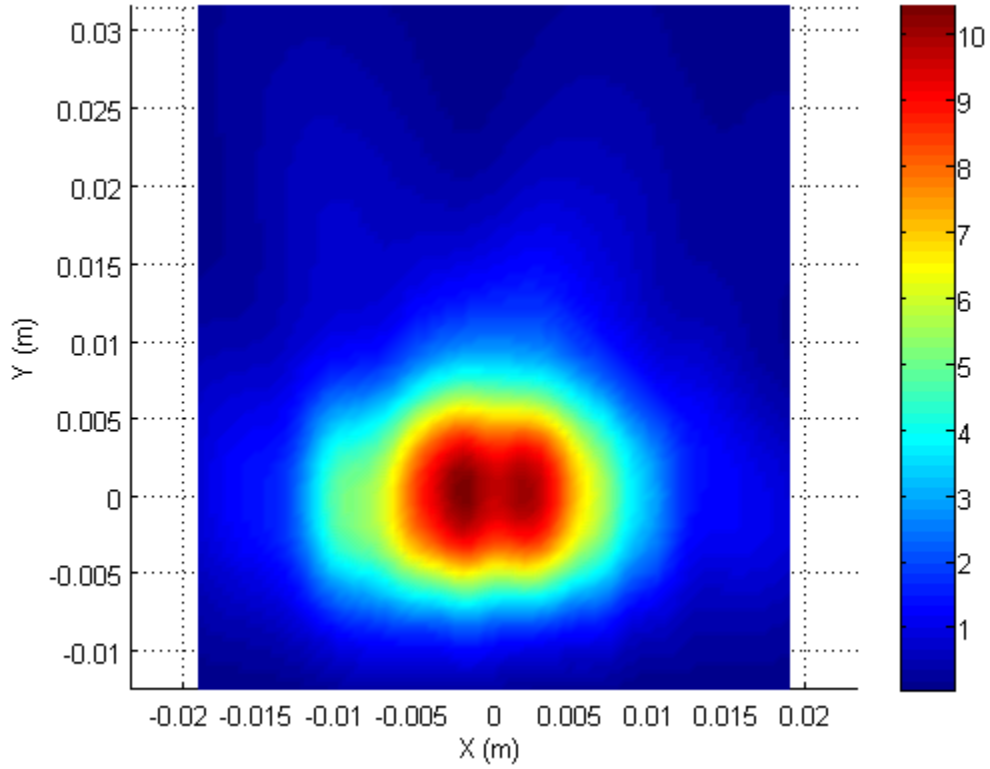

Antenna configuration 20

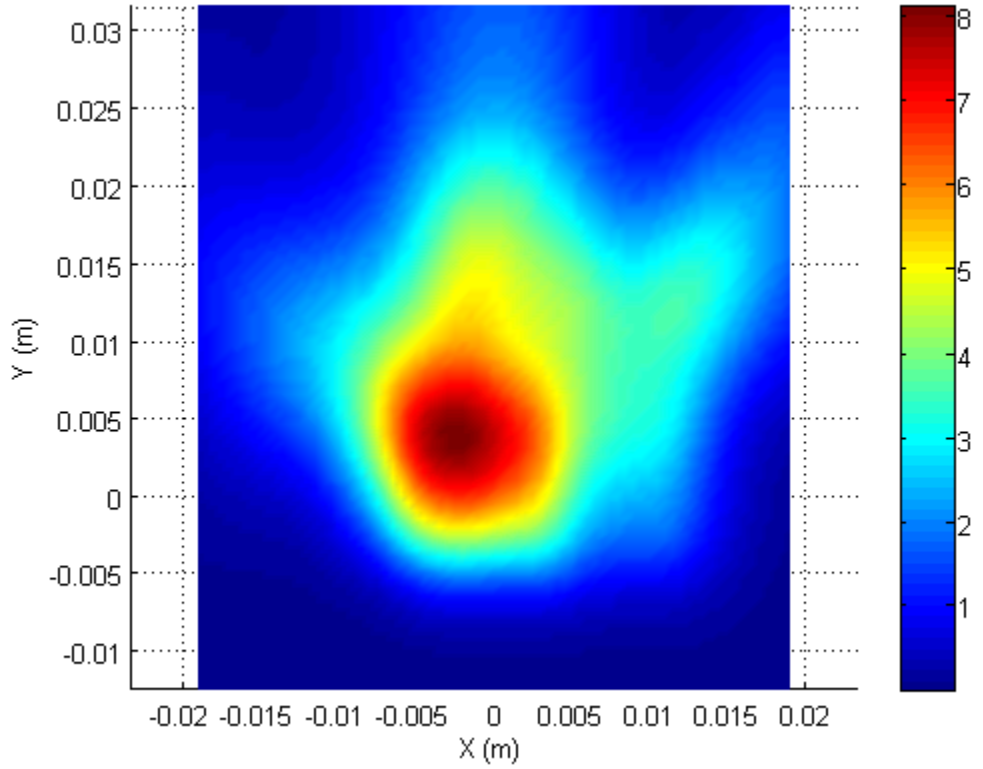

Antenna configuration 21

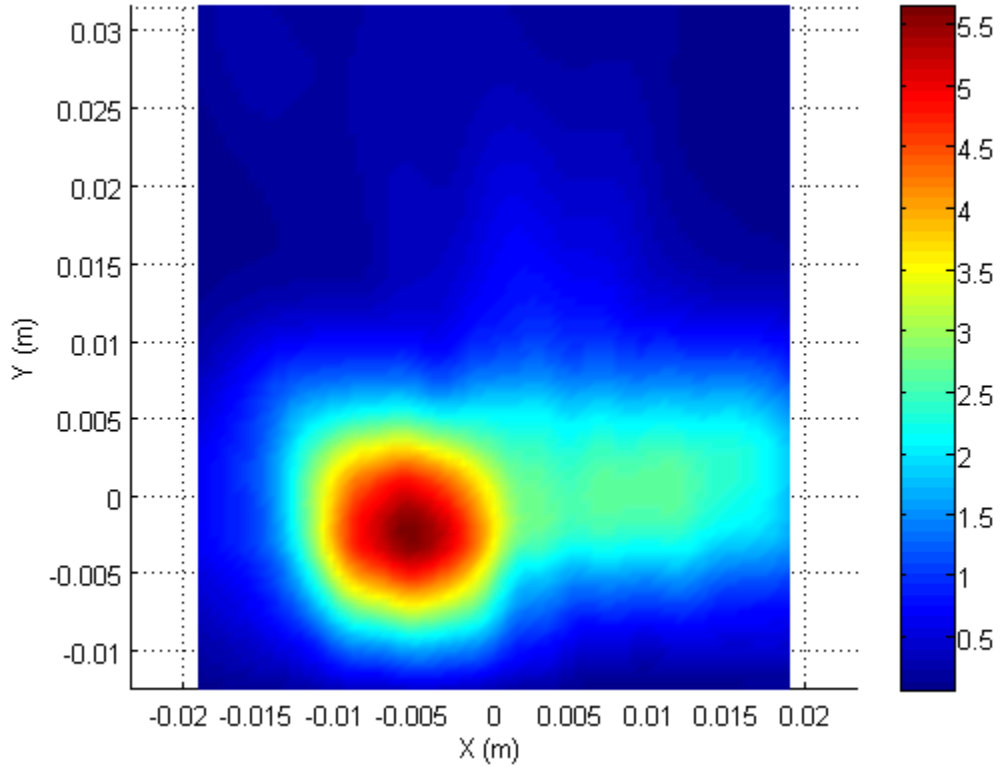

Antenna configuration 22

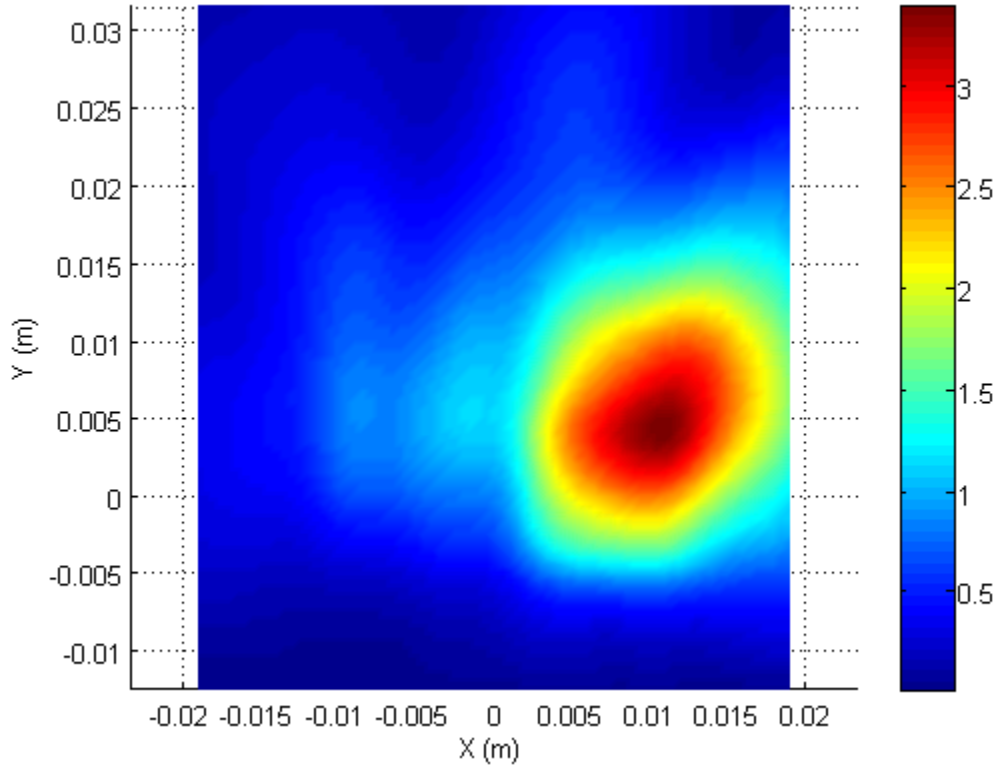

Antenna configuration 23

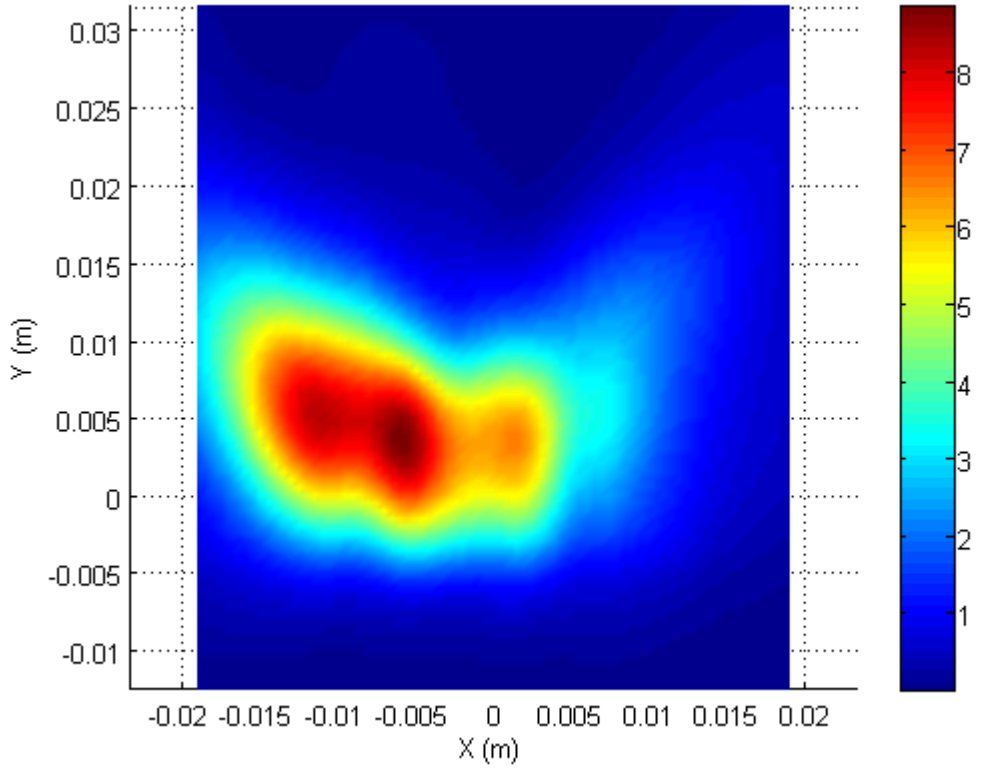

Antenna configuration 24

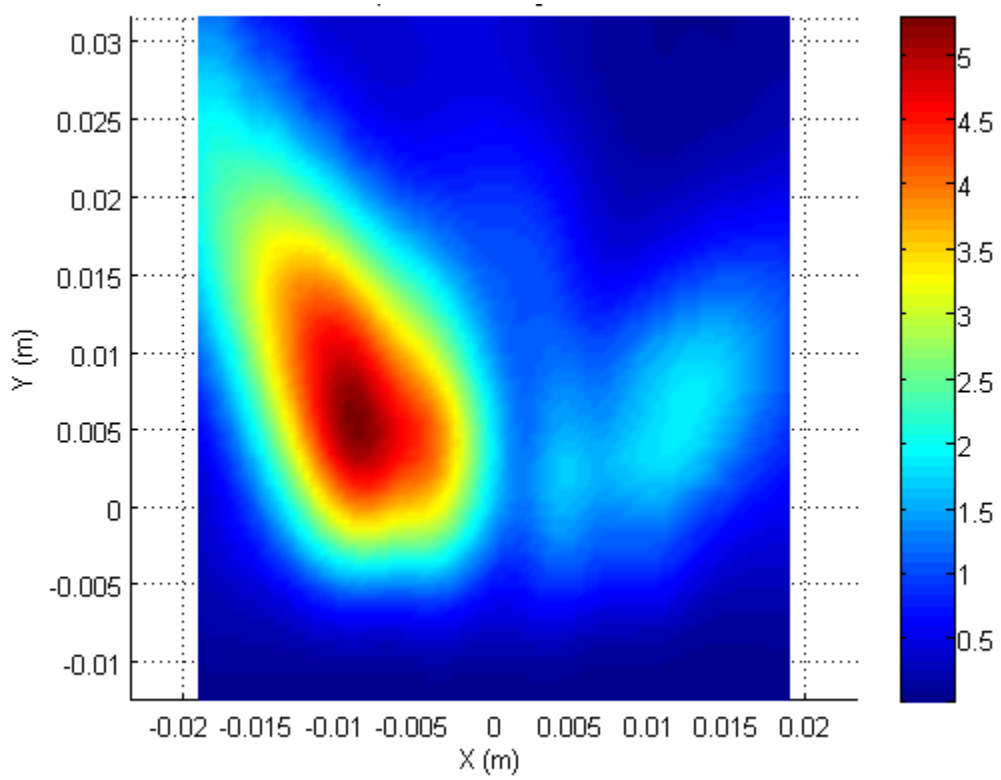

Antenna configuration 25

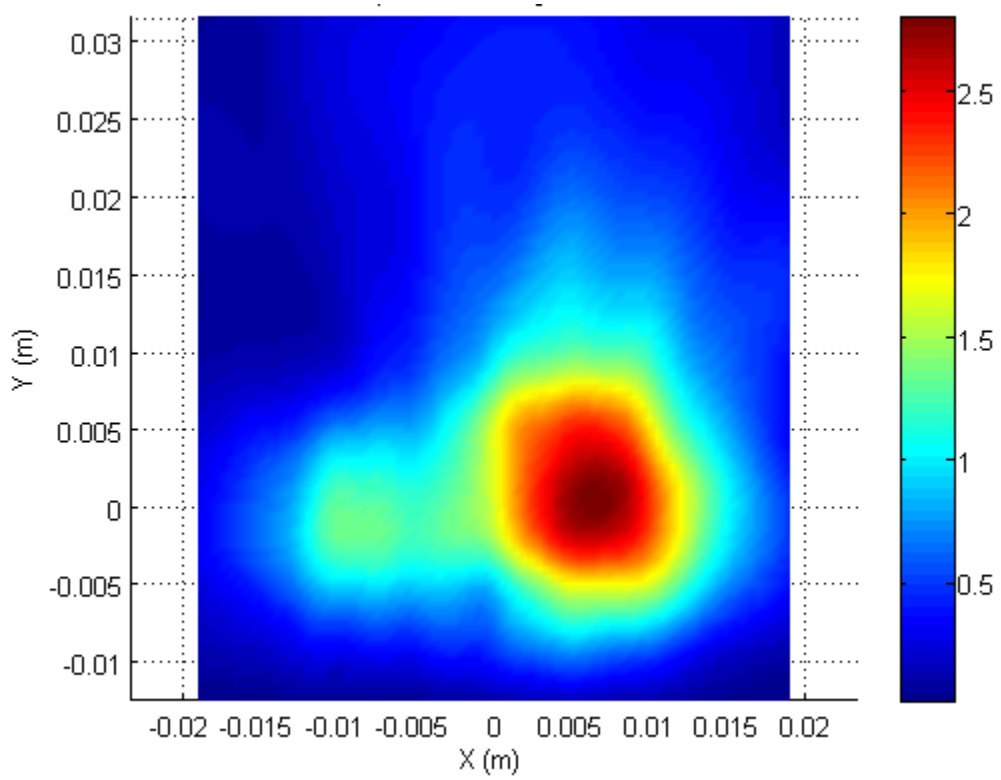

Antenna configuration 26

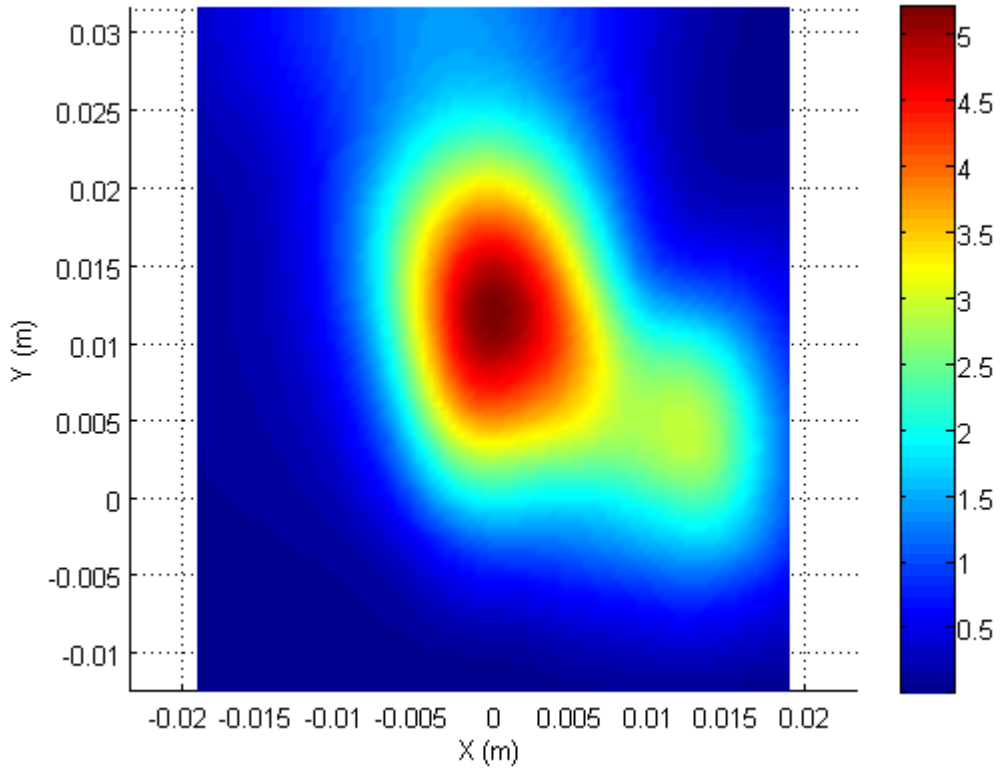

Antenna configuration 27

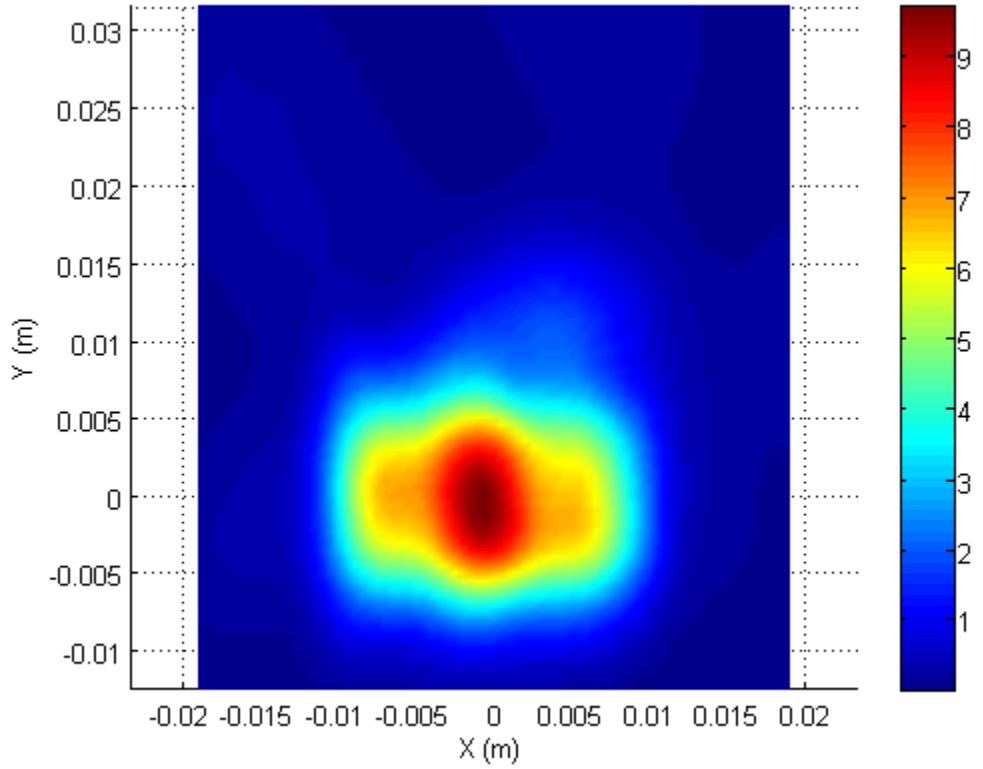

Antenna configuration 28

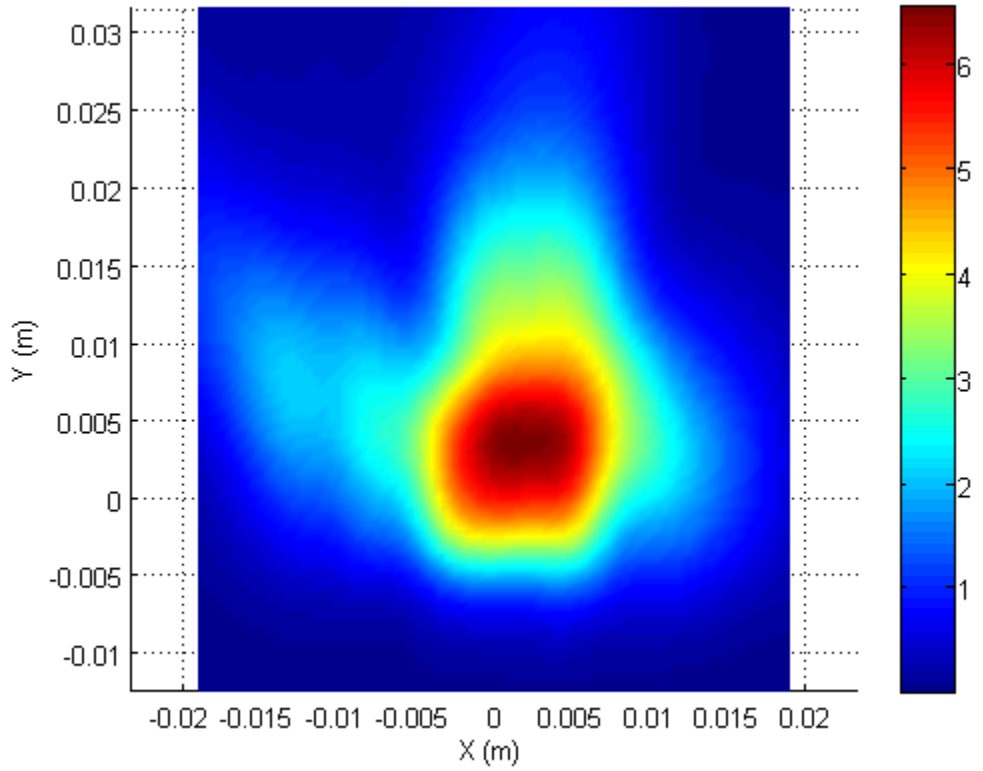

Antenna configuration 29

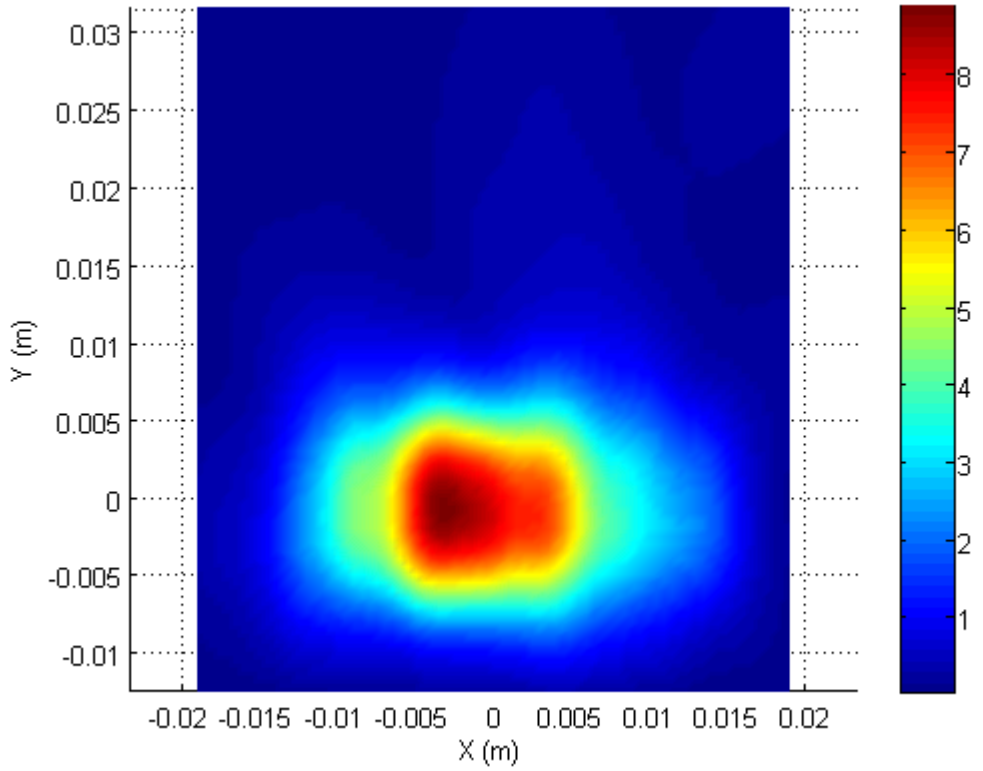

Antenna configuration 30

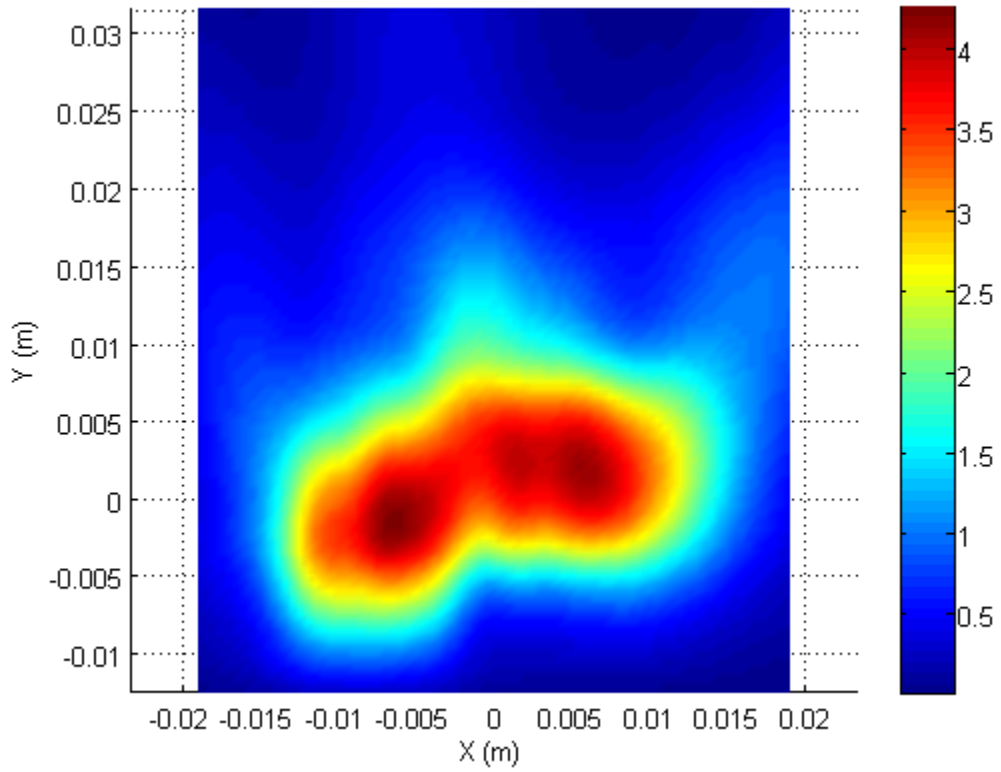

Antenna configuration 31

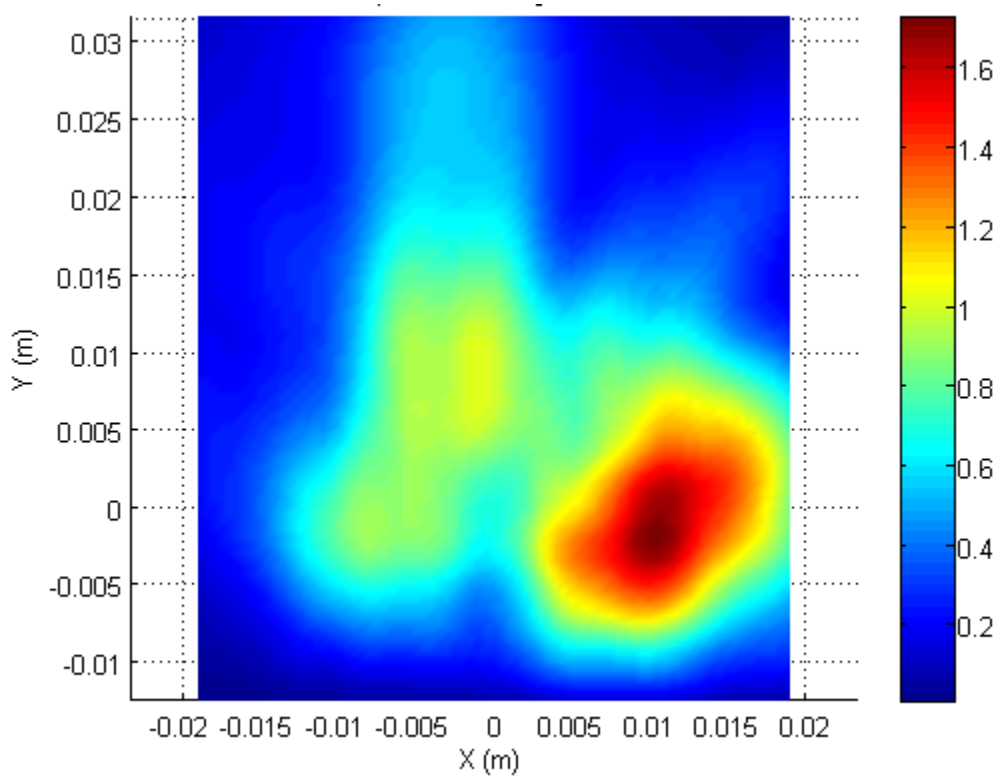

Antenna configuration 60

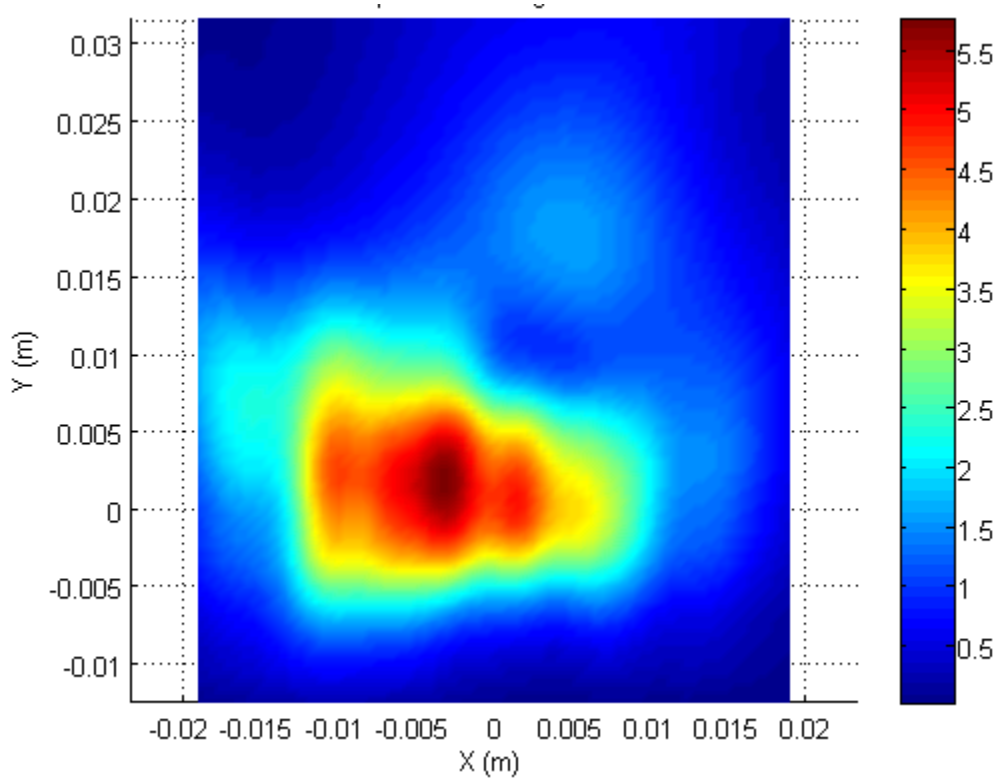

Antenna configuration 61

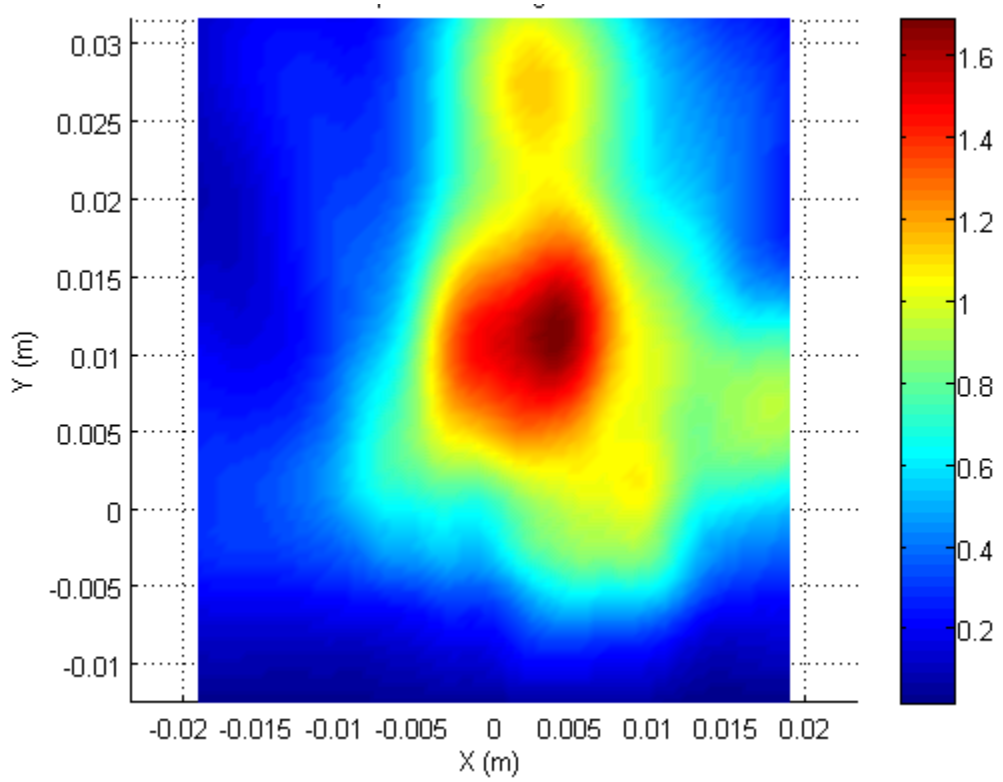

Antenna configuration 62

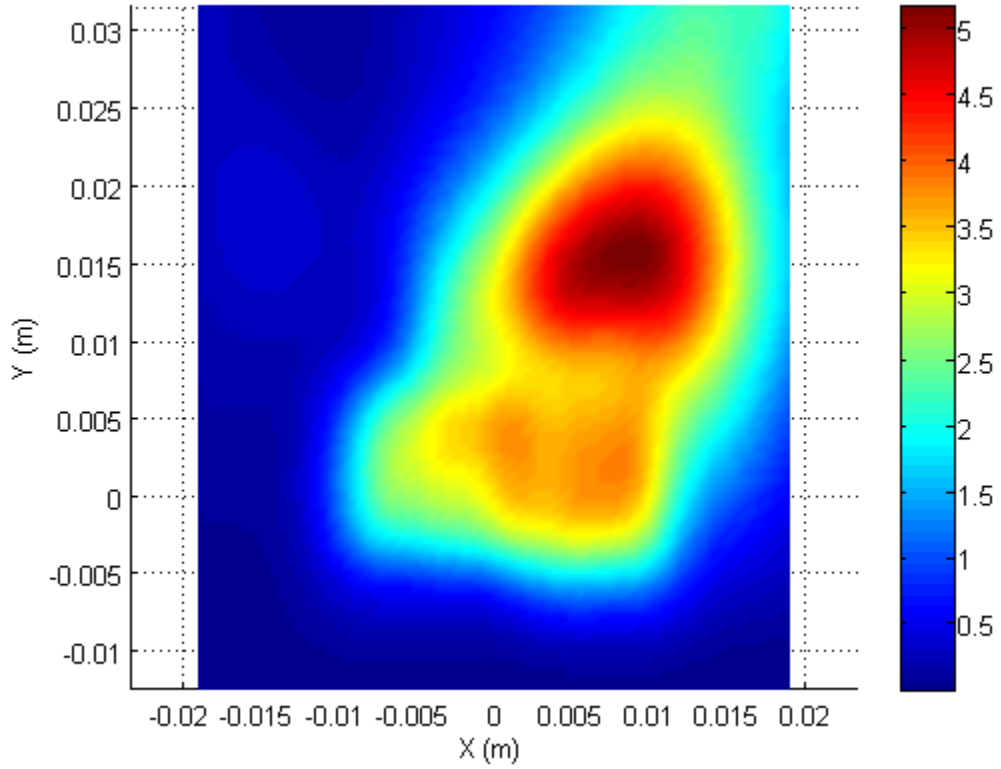

Antenna configuration 63

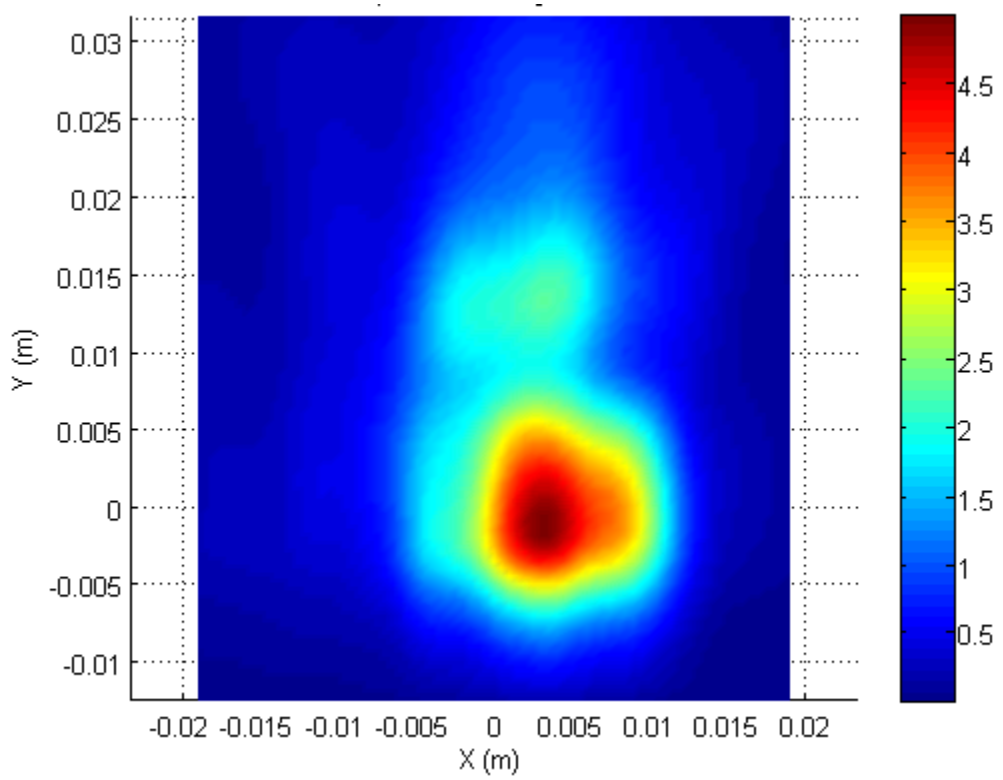

Antenna configuration 64

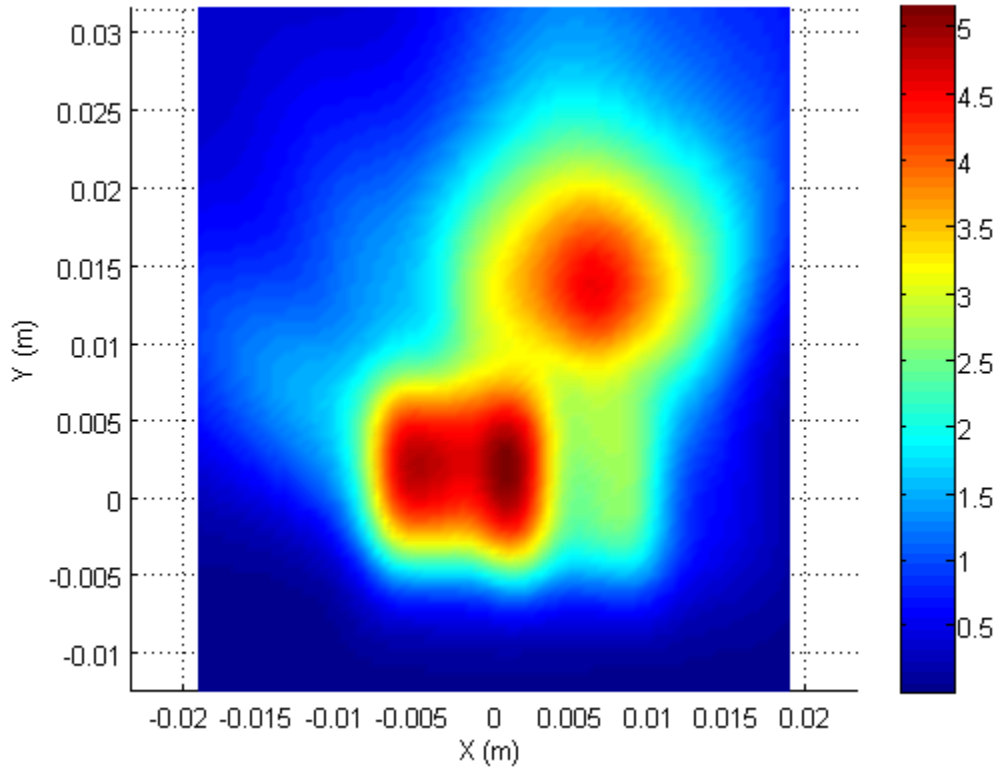

D Near-Field Back Transformation

D.1 Plane Wave Spectrum (PWS) method

Performing planar near-field measurements typically involves measuring at a distance of few wavelengths in order to prevent E/H-fields perturbation due to the presence of mmWave field probe. Compliance with mmWave exposure requires the estimation of power density at the closest plane to the wireless device. Therefore, this involves near-field measurement at few wavelengths away and back transforming the measured fields to a closer plane in order to demonstrate compliance. The plane-wave spectrum (PWS) method widely used for this purpose is explained below.

Assuming the source (transmitting antenna) is in XY plane at z=0, then the solution to the Maxwell equations for z >=0 and satisfying the boundary conditions for the source plane are given by[1,2]:

$$\boldsymbol{E}(x,y,z) = \frac{1}{2\pi}\int_{-\infty}^{\infty}\int_{-\infty}^{\infty} \boldsymbol{A}(k_x,k_y)e^{-j\boldsymbol{k}\cdot\boldsymbol{r}}\,dk_x\,dk_y \qquad (1)$$

$$\boldsymbol{H}(x,y,z) = \frac{1}{2\pi\omega\mu}\int_{-\infty}^{\infty}\int_{-\infty}^{\infty} \boldsymbol{k}\times\boldsymbol{A}(k_x,k_y)e^{-j\boldsymbol{k}\cdot\boldsymbol{r}}\,dk_x\,dk_y \qquad (2)$$

$$\boldsymbol{k}\cdot\boldsymbol{A}(k_x,k_y) = k_xA_x(k_x,k_y) + k_yA_y(k_x,k_y) + k_zA_z(k_x,k_y) = 0 \qquad (3)$$

where,

$$\boldsymbol{k} = k_x\hat{x} + k_y\hat{y} + k_z\hat{z} \qquad (4)$$

$$k^{\boldsymbol{2}} = \boldsymbol{k}\cdot\boldsymbol{k} = \frac{\omega^2}{\mu\varepsilon} \qquad (5)$$

$$\boldsymbol{r} = x\hat{x} + y\hat{y} + z\hat{z} \qquad (6)$$

$$\boldsymbol{A}(k_x,k_y) = A_x(k_x,k_y)\hat{x} + A_y(k_x,k_y)\hat{y} + A_z(k_x,k_y) \qquad (7)$$

Here, k is the wavenumber and $\boldsymbol{A}$ is referred to as the PWS because the expression $\boldsymbol{A}(k_x,k_y)e^{-j\boldsymbol{k}\cdot\boldsymbol{r}}$ represents a uniform plane wave propagating in the direction $\boldsymbol{k}$. k_x and k_y are real variables, from which, k_z can be calculated as below:

$$k_z = \begin{cases} \left(k^2 - k_x^2 - k_y^2\right)^{1/2}, & \text{if } k_x^2 + k_y^2 \le k^2 \\ -j\left(k_x^2 + k_y^2 - k^2\right)^{1/2}, & \text{if } k_x^2 + k_y^2 \ge k^2 \text{ and } z \ge 0 \\ j\left(k_x^2 + k_y^2 - k^2\right)^{1/2}, & \text{if } k_x^2 + k_y^2 \ge k^2 \text{ and } z < 0 \end{cases} \qquad (8)$$

[1] Zhao, J., Lu, H., Deng, J., "Application of the planar-scanning technique to the near-field dosimetry of millimeter-wave radiators", *Bioelectromagnetics*, 36: 108-117, 2015.
[2] Wang, J.J.H, "An examination of the theory and practices of planar near-field measurement", *IEEE Transactions on Antennas and Propagation*, 36(6): 746-753, June 1998.

An imaginary k_z corresponds to evanescent PWS, which rapidly attenuate away from z=0 plane. In our back-transformation, evanescent waves are ignored. So, imaginary k_z is replaced with 0.

At measured distance, z=d, the electric-field **E** can be expressed as (9) below

$$\boldsymbol{E}(x,y,d) = \frac{1}{2\pi}\int_{-\infty}^{\infty}\int_{-\infty}^{\infty}\boldsymbol{A}(k_x,k_y)e^{-jk_z d}e^{-j(k_x x+k_y y)}\,dk_x\,dk_y = \frac{1}{2\pi}\int_{-\infty}^{\infty}\int_{-\infty}^{\infty}\boldsymbol{A}(k_x,k_y,d)e^{-j(k_x x+k_y y)}\,dk_x\,dk_y \quad (9)$$

From the measured E-fields, PWS can be computed using Fourier transform:

$$\boldsymbol{A}(k_x,k_y,d) = \frac{1}{2\pi}\int_{-\infty}^{\infty}\int_{-\infty}^{\infty}\boldsymbol{E}(x,y,d)e^{j(k_x x+k_y y)}\,dx\,dy \quad (10)$$

Here,

$$\boldsymbol{A}(k_x,k_y) = \boldsymbol{A}(k_x,k_y,d)e^{jk_z d} \quad (11)$$

A_x and A_y components can be computed from measured E_x and E_y components (see section D.2 for further clarification). A_z component can be computed from A_x and A_y using equation (3). Fields at closer distances (say, at source, z=0), can be derived as:

$$\boldsymbol{E}(x,y,0) = \frac{1}{2\pi}\int_{-\infty}^{\infty}\int_{-\infty}^{\infty}\boldsymbol{A}(k_x,k_y)e^{-j(k_x x+k_y y)}\,dk_x\,dk_y \quad (12)$$

In actual measurements, the scan area is finite and limited to $x \in [-x_m, x_m]$ and $y \in [-y_m, y_m]$ in the XY plane with finite resolutions Δx and Δy. Uniform intervals of Δx and Δy will result in PWS equally spaced in k-domain with $k_x \in [-k_{xm}, k_{xm}]$ and $k_y \in [-k_{ym}, k_{ym}]$.The sample spacings and spectral extents are related as follows:

$$\Delta x = \frac{\pi}{k_{xm}}, \Delta y = \frac{\pi}{k_{ym}} \quad (13)$$

Similarly, for inverse DFT, selection of spectral spacings Δk_x and Δk_y in k-domain with $k_x \in [-k_{xm}, k_{xm}]$ and $k_y \in [-k_{ym}, k_{ym}]$ will lead to equally spaced in (x,y) domain. The spectral spacings and spatial extents are related as follows:

$$\Delta k_x = \frac{\pi}{x_m}, \Delta k_y = \frac{\pi}{y_m} \quad (14)$$

The selection of measurement scan area in the near-fields should include all the important fields in the aperture, such that Δk_x and Δk_y are sufficiently small to describe the PWS A_x and A_y, respectively. Similarly, the measurement resolution Δx, Δy should be small enough to capture sufficient spectral extents, i.e., k_x, k_y at least equal to k as higher values lead to evanescent PWS with $k_x^2 + k_y^2 \geq k^2$. This requires Δx, Δy ≤ λ/2 (Nyquist rate).

D.2 Implementation of PWS method

Measured amplitude of power density (PD) in both polarizations can be converted into corresponding E-field amplitude using below equation[1]. Here, (θ, φ) represent the direction angles of the source antenna relative to the probe, G is the probe gain pattern, and η is the free-space impedance.

$$|E_x|(x,y,d) = \sqrt{2\eta\frac{G(0,0)}{G(\theta,\varphi)}PD_x(x,y,d)}\sqrt{\frac{y^2+d^2}{x^2+y^2+d^2}} \quad (15)$$

$$|E_y|(x,y,d) = \sqrt{2\eta\frac{G(0,0)}{G(\theta,\varphi)}PD_y(x,y,d)}\sqrt{\frac{x^2+d^2}{x^2+y^2+d^2}} \quad (16)$$

If the probe correction factor for open-ended waveguide probe is already accounted for in the measurement setup, then the amplitude of E-field is determined using:

$$\left|E_{x,y}\right|(x,y,d) = \sqrt{2\eta PD_{x,y}(x,y,d)} \qquad (17)$$

The determined E_x and E_y fields over $[-x_m, x_m]$ and $[-y_m, y_m]$ spatial area in plane z=d, with Δx, Δy spatial resolutions are used to compute E-fields at closer plane $z=z_s$, by using Discrete Fourier Transform as shown below. The spectral extents and resolutions are calculated using (13) and (14).

$$\boldsymbol{A}(k_x,k_y,d) = \frac{1}{2\pi}\sum_{-x_m}^{x_m}\sum_{-y_m}^{y_m}\boldsymbol{E}(x,y,d)e^{j(k_x x+k_y y)}\,\Delta x\Delta y \qquad (18)$$

$$\boldsymbol{A}\left(k_x,k_y\right) = \boldsymbol{A}\left(k_x,k_y,d\right)e^{jk_z d} \qquad (19)$$

$$\boldsymbol{E}(x,y,z_s) = \frac{1}{2\pi}\sum_{-k_{xm}}^{k_{xm}}\sum_{-k_{ym}}^{k_{ym}}\boldsymbol{A}\left(k_x,k_y\right)e^{-jk_z z_s}e^{-j(k_x x+k_y y)}\,\Delta k_x\Delta k_y \qquad (20)$$

PWS components A_x and A_y were computed in the back transformed plane using measured E_x, E_y, and equations (18) – (19). Using equation (3), A_z component is calculated based on A_x and A_y. Using equation (20), E_x, E_y and E_z are computed in the back transformed plane. Similarly, using equation (2), H_x, H_y and H_z can be computed as shown below:

$$\boldsymbol{H}(x,y,z_s) = \frac{1}{2\pi\omega\mu}\sum_{-k_{xm}}^{k_{xm}}\sum_{-k_{ym}}^{k_{ym}}\boldsymbol{k}\times\boldsymbol{A}\left(k_x,k_y\right)e^{-jk_z z_s}e^{-j(k_x x+k_y y)}\,\Delta k_x\Delta k_y \qquad (21)$$

From all components of E-field and H-field, i.e., equations (20) – (21), power density can be computed as shown below:

$$\overrightarrow{\boldsymbol{PD}} = \vec{\boldsymbol{E}}\times\vec{\boldsymbol{H}} = \left(E_y H_z - E_z H_y\right)\hat{x} + \left(E_z H_x - E_x H_z\right)\hat{y} + \left(E_x H_y - E_y H_x\right)\hat{z} \qquad (22)$$

$$total\ power\ density\ \left|\overrightarrow{\boldsymbol{PD}}\right| = \sqrt{\left[|real(PD_x)|^2 + \left|real(PD_y)\right|^2 + |real(PD_z)|^2\right]} \qquad (23)$$

Normal vs. Total Power Density:

If only one dominant polarization is measured, i.e., either Ex or Ey, over $[-x_m, x_m]$ and $[-y_m, y_m]$ spatial area in plane z=d, with Δx, Δy spatial resolutions, then using equations (18) – (20), only one dominant polarization of E-field can be recovered at closer plane $z=z_s$. Therefore, only normal component of power density can be recovered in the closer plane (exposure plane) using equation (17).

If both polarizations are measured, i.e., both Ex or Ey, over $[-x_m, x_m]$ and $[-y_m, y_m]$ spatial area in plane z=d, with Δx, Δy spatial resolutions, then using equations (18)-(19), followed by equation (3), followed by equations (20)-(21), all components of E-field and H-field can be computed at closer plane $z=z_s$. Therefore, using equations (22)-(23), total power density can be computed. Note that the measurement system should have high sensitivity to accurately capture the amplitude and phase of both polarization of fields, particularly, the non-dominant polarization over the measured scan area. Otherwise, the computed total power density using PWS method could be erroneous.

D.3 Validation of PWS implementation for basic array antenna

D.3.1 Back transformation: parallel to aperture plane

Figure D-1 shows the 2x4 patch array used for validating the implementation of PWS method for back transforming fields.

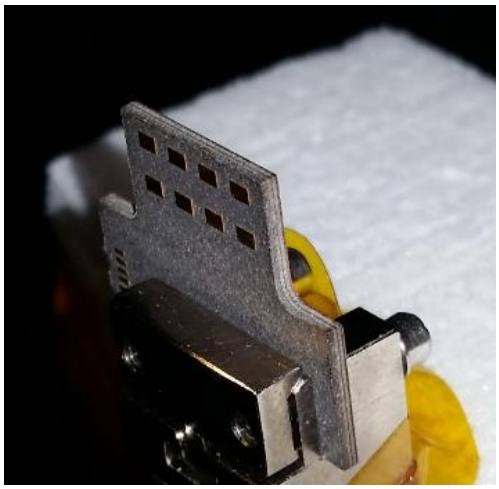

Figure D-1: 60GHz 2x4 patch array antenna

Figure D-2 shows the test setup used to measure both polarizations of the waveguide probe for capturing the normal component of power density propagating into the waveguide probe, with scan planes parallel with the antenna aperture at 2λ and 4λ separation distance.

(a) (b)

Figure D-2: Measure E-fields along the scan planes parallel with the antenna aperture: (a) vertical polarization; (b) horizontal polarization

The measured fields at 4λ distance were back transformed to 2λ distance, and were compared with measured fields at 2λ distance in Figure D-3. Good agreement in the power density distributions shows that the implementation of PWS method is accurate.

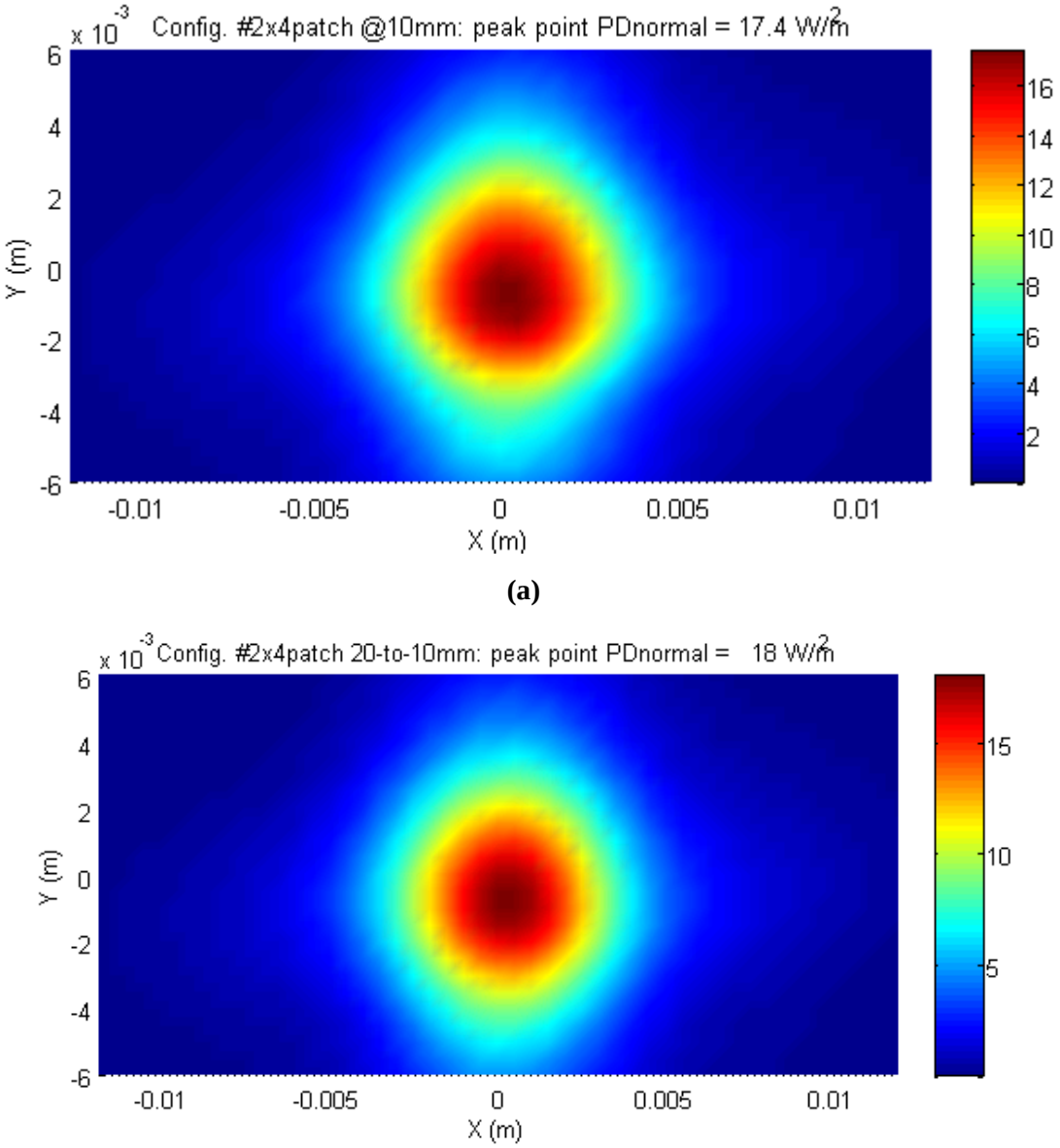

Figure D-3: Peak power density for 2x4 patch:(a) measured at 2λ, and (b) back transformed from 4λ

D.3.2 Back transformation: inclined to aperture plane

Using the 2x4 patch array as a source, two measurement scan planes were setup at two orientations, one measurement plane parallel to the aperture plane of the array and another measurement plane at an inclination (65 degrees) to the aperture plane. Measured fields were back transformed to closer planes and the total power density was compared at the intersection

line between the two back transformed planes, to validate PWS-based measurement approach for measurement conducted in planes that are at an inclination to the aperture plane.

Figure D-4 shows measured power density along the tilted planes at 4λ separation distance from the closest edge of the 2x4 patch array. The scan plane is 65 degree tilted relative to the main beam (aperture plane) of the 2x4 patch array. Similar to previous scans, waveguide probe was rotated 90 degrees to capture both polarizations.

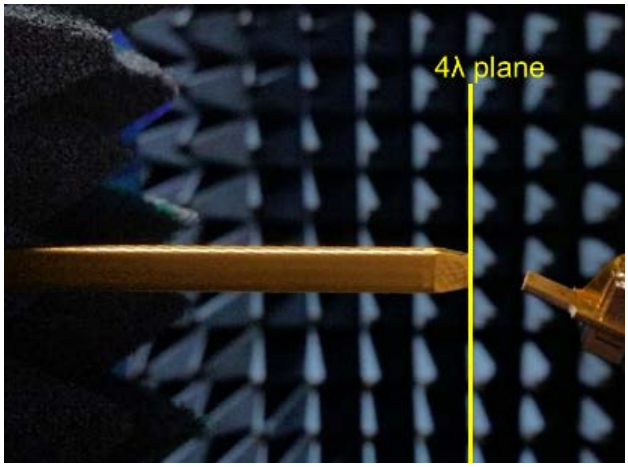

Figure D-4: Measured both polarizations of waveguide probe in the 65 degree tilted scan plane

Test Results and Correlation

Figure D-5 shows the geometry schematic of the two scan planes' orientations relative to the 2x4 patch array as well as the intersection of scan planes and intersection of their corresponding back-transformed planes.

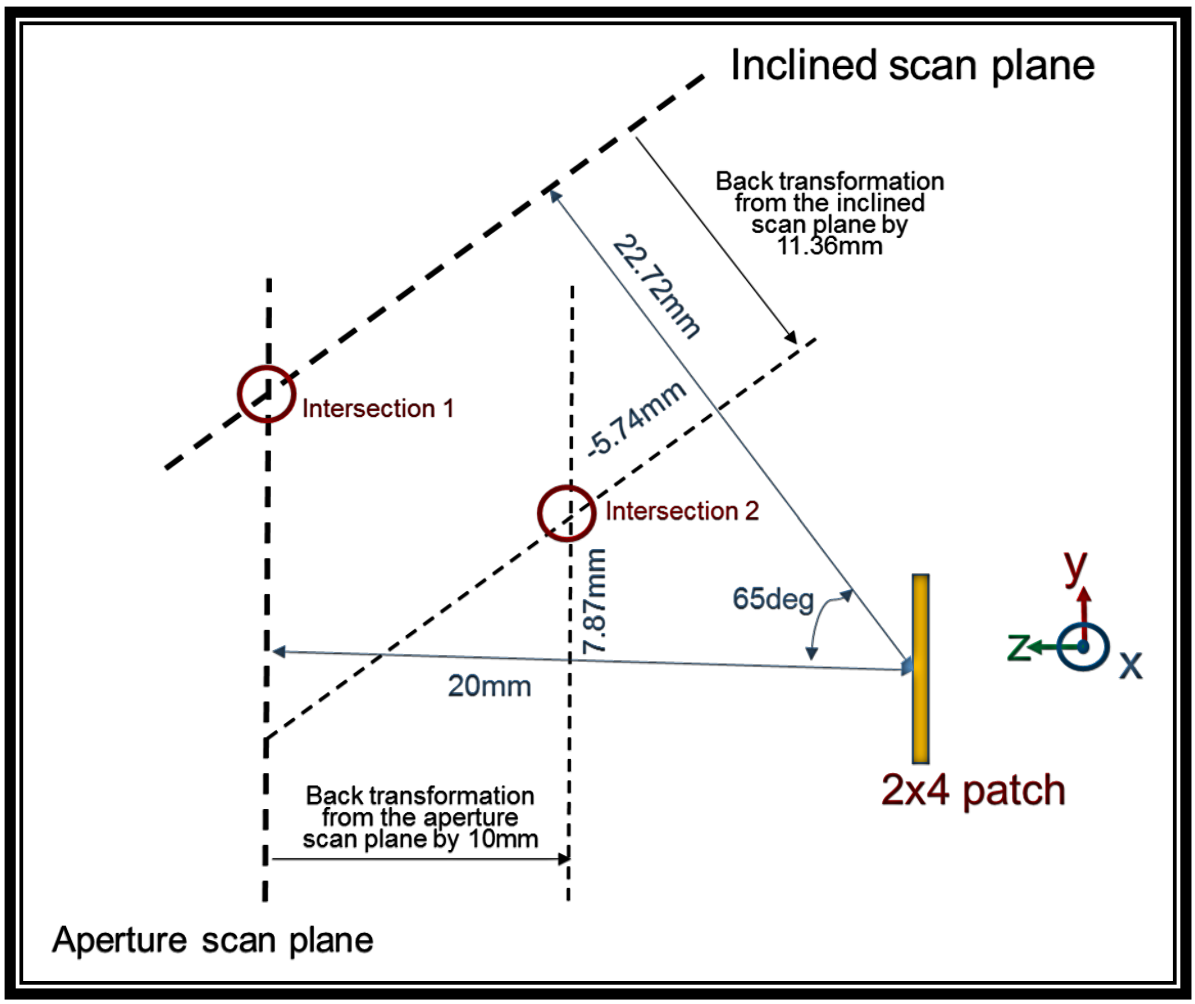

Figure D-5: Geometry relationship of the two orientated scan planes relative to the 2x4 array. Measurements are done at the planes represented by the thicker dashed lines. Aperture scan plane is "parallel" to the array plane.

We measured the two polarizations of the E-fields tangential to the scanning planes corresponding to the power density component normal to the scan plane. Figure D-6 shows the normal power density component along the intersection line (labeled "intersection 1" in Figure D-5) of these two measured scan planes. Note that at each location along this intersection line, amplitude of power density (PD) normal to each scan plane will depend on the angle between PD vector and unit vector normal to each measurement scan plane. Figure D-6 provides confidence in the positioning and validity of our measurement setup for performing scans at different angles relative to the aperture plane.

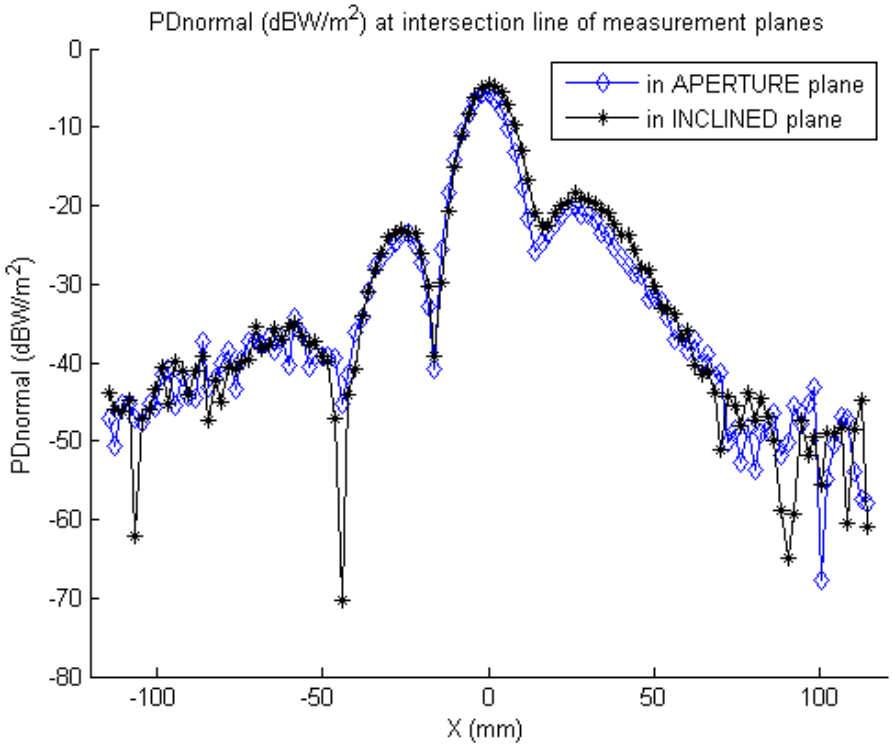

Figure D-6: In 2x4 patch array case, measured power density component normal to the scan planes along the intersection line ("intersection 1" in Figure D-5)

Based on the measured polarizations capturing two E-field components tangential to the scan plane, we derived the normal E-field component as well as all H-field components using the Plane Wave Spectrum equations (see equations (18)-(23)) to obtain the total power density in the back transformed planes that are parallel and inclined to the 2x4 patch antenna aperture plane. We verified the correlation along the intersection line of the back transformed planes (labeled "intersection 2" in Figure D-5). Figure D-7 shows the total power density along intersection 2 line obtained from back transformed planes parallel and inclined to the aperture plane, the simulated total power density at the corresponding location is also plotted in Figure D-7. The peak values are within 1 dB.

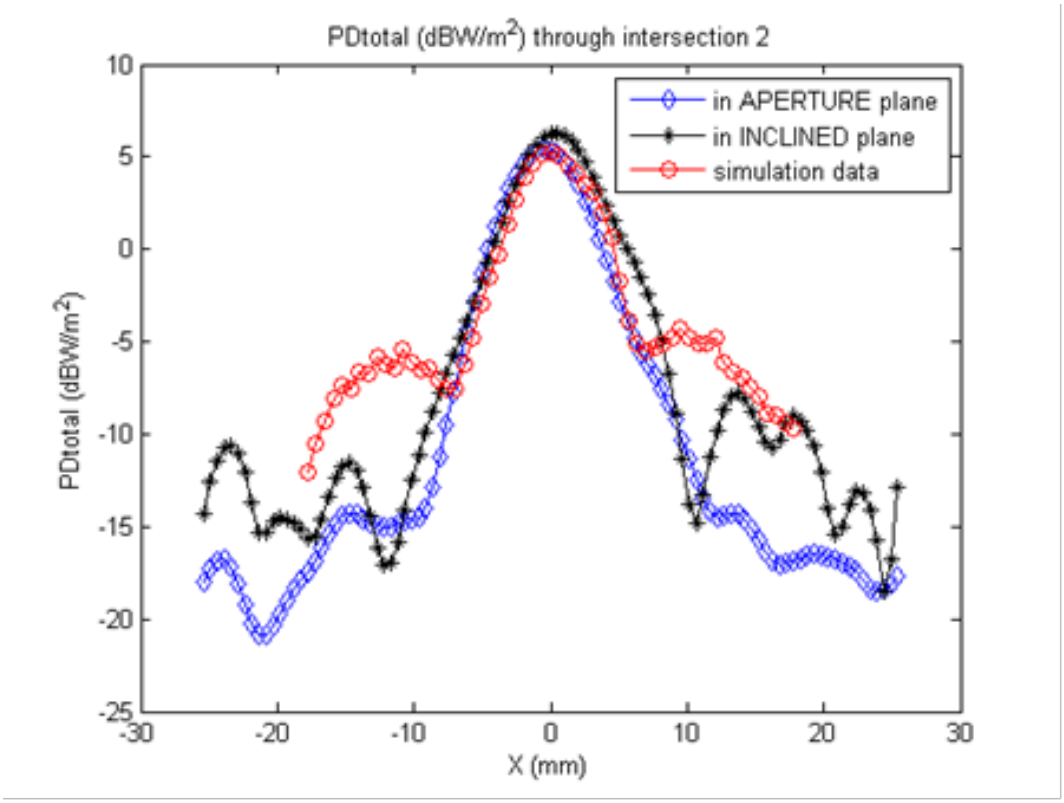

Figure D-7: In 2x4 patch array case, back transformed total power density along the intersection line ("intersection 2" in Figure D-5)

E Characterization of Aperture Waveguide (RF-WR15)

The RF-WR15 open-ended waveguide probe was calibrated in-house for its far field characteristic. The Qualcomm in-house calibration report is attached at the end of this Appendix. Additionally, the S11 of the probe was measured; the S11 is less than 10 dB across the 60 GHz band as shown in Figure E-1.

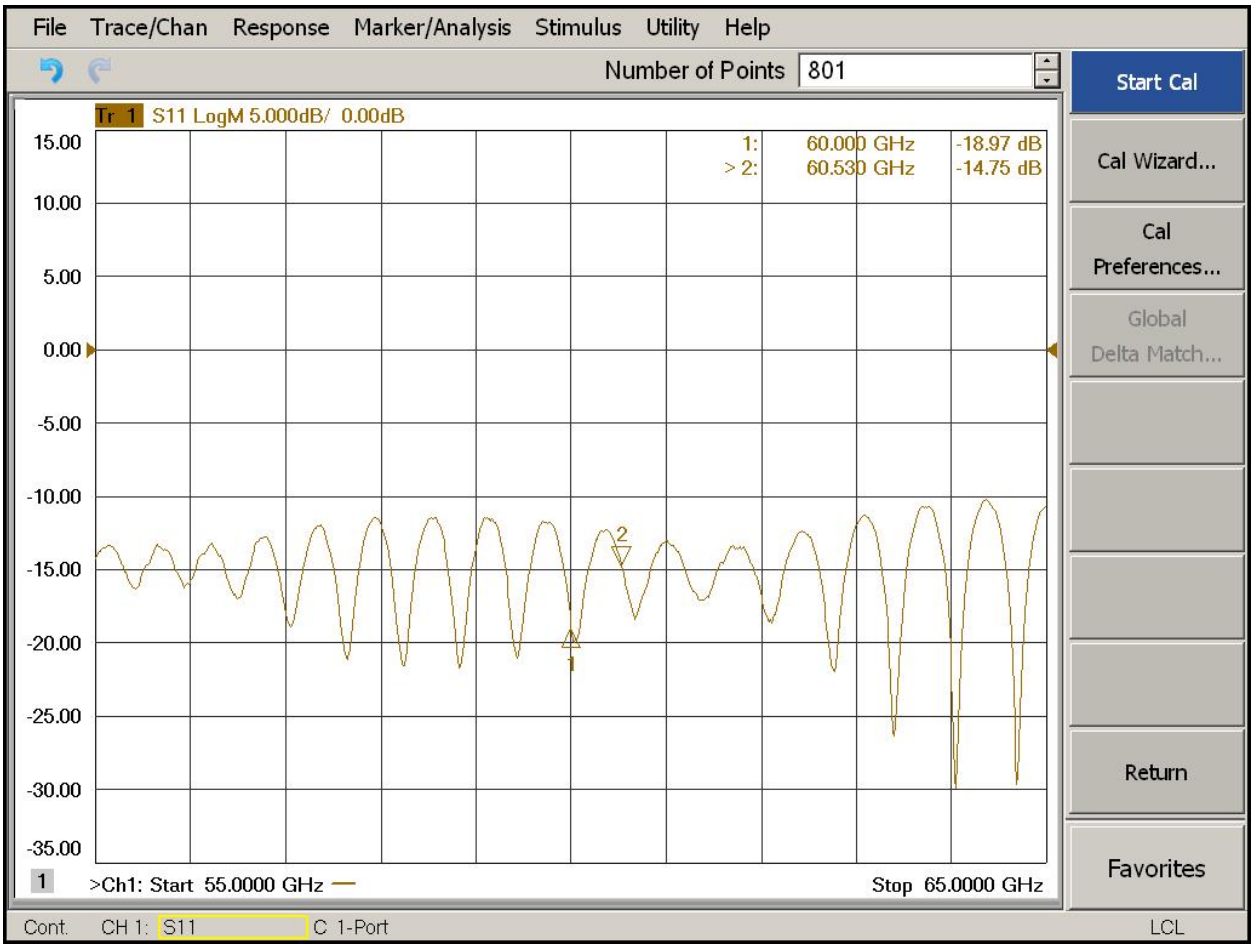

Figure E-1: RF-WR15 open-ended waveguide probe, measuring S11 of the probe

The variation of S11 between 58.32 (low channel) and 62.64 (high channel) is from -12 dB to -20 dB, which is about 1% ~ 6% of variation in power. Therefore, it does not have significant impact if all three channels require evaluation using this waveguide probe.

Furthermore, it needs to be noted that the waveguide probe, when used in the near field measurement, is effectively a transmission line. As described in Appendix G, we also validated the accuracy of near-field measurements using this RF-WR15 probe by measuring and simulating a standard horn antenna, and the 0.6dB of the probe perturbation (including transmission loss) reported in the Appendix G was accounted in the measurement uncertainty budget (see Appendix B). Therefore there is no conversion factor that needs to be applied to the final value of the total power density.

E.1 Purpose and scope

Gain measurements are made by comparing the resulting far-field level of the Antenna Under Test (AUT) to that of a known Standard Gain Horn (SGH) substituted under the same conditions (Reference, *IEEE 'Standard Test Procedures for Antennas' section 12.3 "Gain-Transfer Method*", IEEE Std 149-1979). The same cables are used for both tests (SGH and AUT). In this way, the losses for the cables do not matter to the measurement. The difference in measured signal level is the difference in gain between the AUT and the SGH.This gain standard can be any type of antenna whose gain has been previously measured or calculated. Often the gain standard is a pyramidal horn. If the antenna is constructed from the NRL (Naval Research Laboratory) standards, then published NRL gain curves can be used to describe the gain of the horn.

The purpose of this test was to measure the gain of NSI-MI Open Ended Wavegude Probe (OEWG), model NSI-RF-WR15. For measurements peformed at Qualcomm's NSI-MI Antenna Range, see Figure E-2.

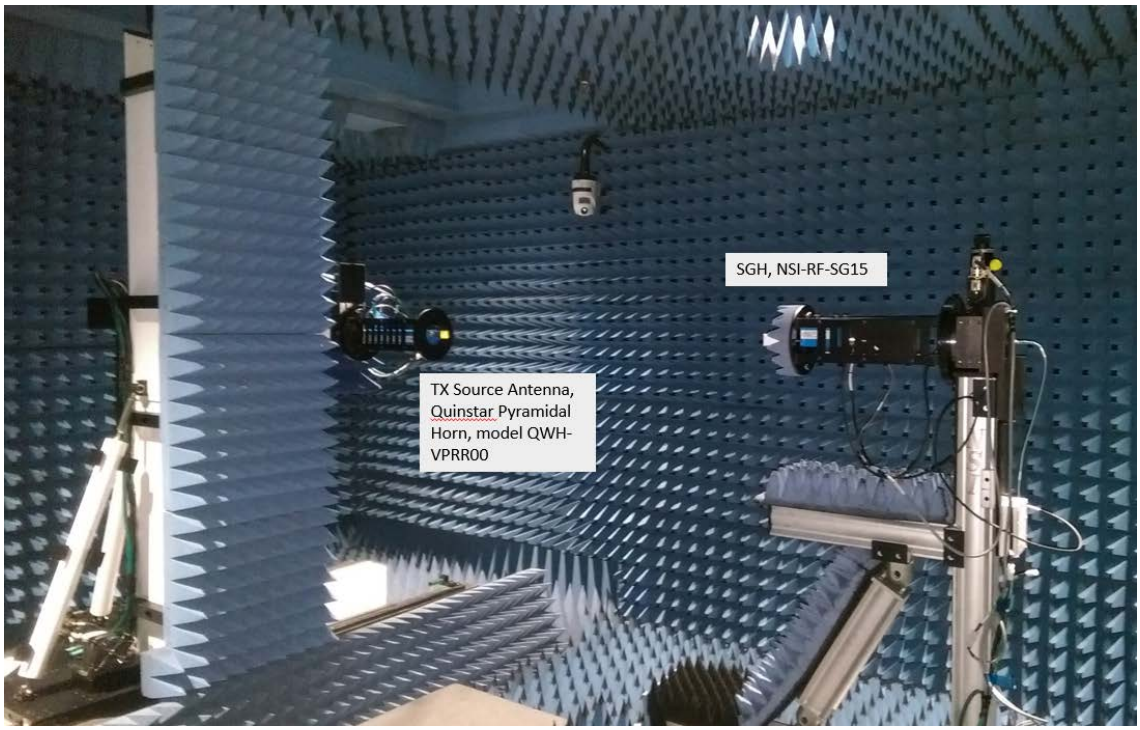

Figure E-2: Qualcomm NSI-MI far-field gain Measurement using standard gain horn

E.2 Gain measurement procedure

Measurement is performed using NSI 2000 antenna measurement software.

1. Measure the largest aperture dimensions of antennas (Source, SGH, and AUT)
2. Compute Far-field distance:

$$Far\ Field\ Distance \geq \frac{2D^2}{\lambda}$$

   D for NSI horn (largest aperture dimension) = 1.26”
   At 62.6 GHz, Far-field > 17”
   Far-field distance of 40” was used for tests

3. Mount and align the transmit source antenna and SGH, verify Far-field distance is adjusted to correct length. This is measured from the center-of-rotation of the azimuth stage to the front of the source antenna. Use a plumb bob to verify that the aperture of SGH is over azimuth rotater center-of-rotation. Place absorber material around AUT and support structures. Adjust transmit SGH for vertical polarization.
4. Perform laser alignment with precision mirror, see Figure E-3. Note: Typical alignment results can get system alignments to within about ± 0.1” and ±0.1°

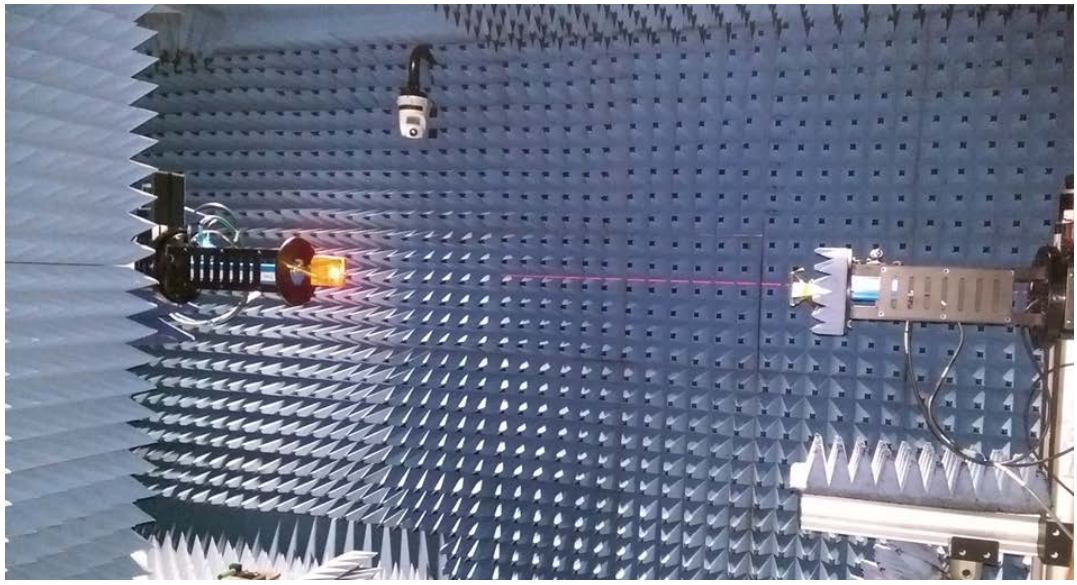

Figure E-3: Laser alignment using precision mirror

5. Adjust the SGH for vertical polarization.

6. For Far-field measurements the model tower is equiped with phi (“roll”) over azimuth rotation, the AUT is mounted to the model tower, while the TX source antenna is mounted to the X-Y scanner. Figure E-4 shows spherical coordinate system.

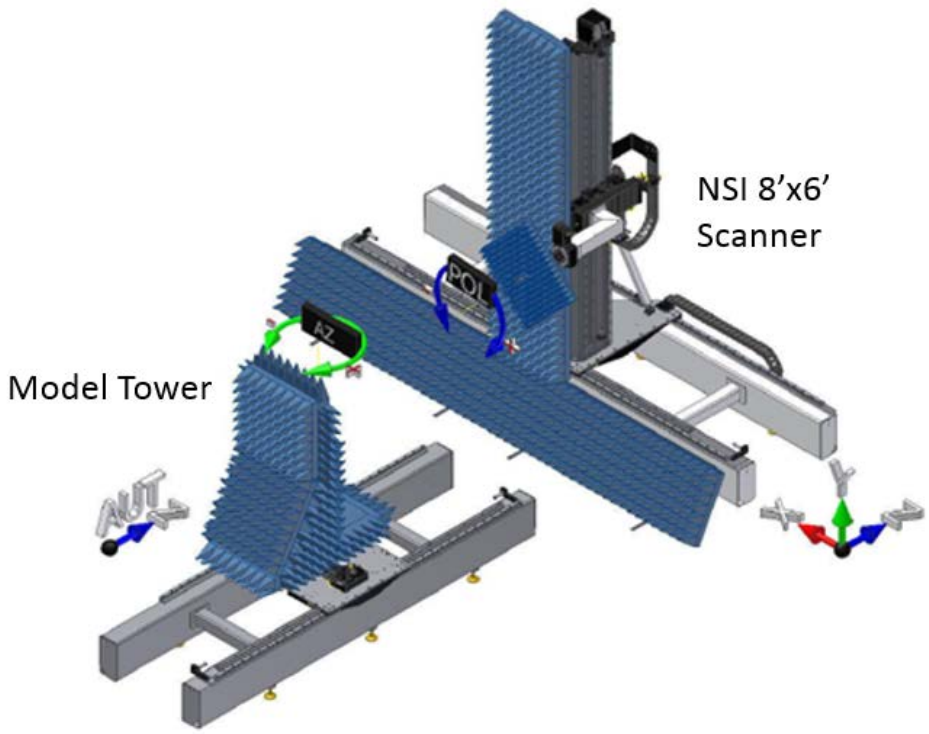

Figure E-4: Range coordinate system

7. Run the frequency bands script and select ‘50-75 GHz, AUT=RX mode’.
8. Make a calibration measurement (AUT = SGH). Peak up the SGH amplitude reading by adjusting the azimuth and elevation position in the move axes menu.
9. Set up the OEWG measurement. Remove SGH at model tower and replace with OEWG. Connect the AUT to the antenna cable. Place RF absorber material around AUT and support structures.
10. Align aperture of OEWG over model tower azimuth center-of-rotation. Follow the procedure to align the Source Antenna and AUT phi stage. Using plumb bob, adjust Z-Axis as necessary, and then check level of OEWG with precision level.
11. Adjust the OEWG for vertical polarization
12. Perform single-axis measurement.
13. Process the gain data using calibration file from SGH. This will compute the gain constant and the AUT calculated gain. The AUT calculated gain is computed by adding the gain constant, network offset, and AUT max far-field.

E.3 Results

Measured Gain of NSI-RF-WR-15 OEWG Probe:

- Tests performed at Qualcomm NSI-MI Far-field range on 4/15/16
- NSI-RF-SG15 Horn used as calibration reference

Measured gain is compared to theoretical far-field gain of common open-ended waveguide aperture with a two-to-one aspect ratio, i.e. a/b=2, provided by IEEE Std C95.3-2002(R2008) clause 5.5.1.1.3 equation (4)

$$G = 21.6\, f\, a$$

f is frequency in GHz

a is the width (larger dimension) of the waveguide aperture in (m)

Table E-1: Measured gain compared to theoretical far-field gain

Frequency (GHz)	a (m)	Theoretical Gain (dBi)	Measured Peak Gain (dBi)	Delta (dB)
58.30	0.00376	6.75	6.79	0.04
60.00	0.00376	6.88	7.47	s9
60.50	0.00376	6.91	7.31	0.40
62.60	0.00376	7.06	7.11	0.05

NOTE: All NSI-MI SGHs are designed and built to meet the requirements of NRL Report 4433 and include theoretical gain versus frequency curves. Frequency coverage is based on standard "WR" waveguide bands. The published curves are said to be accurate to +/ 0.3 dB.

F Normal vs. Total Power Density

In order to validate the applicability of simulated difference in normal power density (PD_{normal}) versus total power density (PD_{total}), this difference was verified through measurements for the Acer N15W8 laptop containing QCA9008-TBD1 802.11ad module operating in worst configuration (#13).

F.1 Test setup for Acer laptop

The far-field antenna pattern of Acer N15W8 laptop containing QCA9008-TBD1 802.11ad module operating in worst-case Antenna configurations #13 is shown in Figure F-1, where it can be seen that the main beam is about 65 degrees relative to the normal of defined exposure plane (bottom surface of laptop).

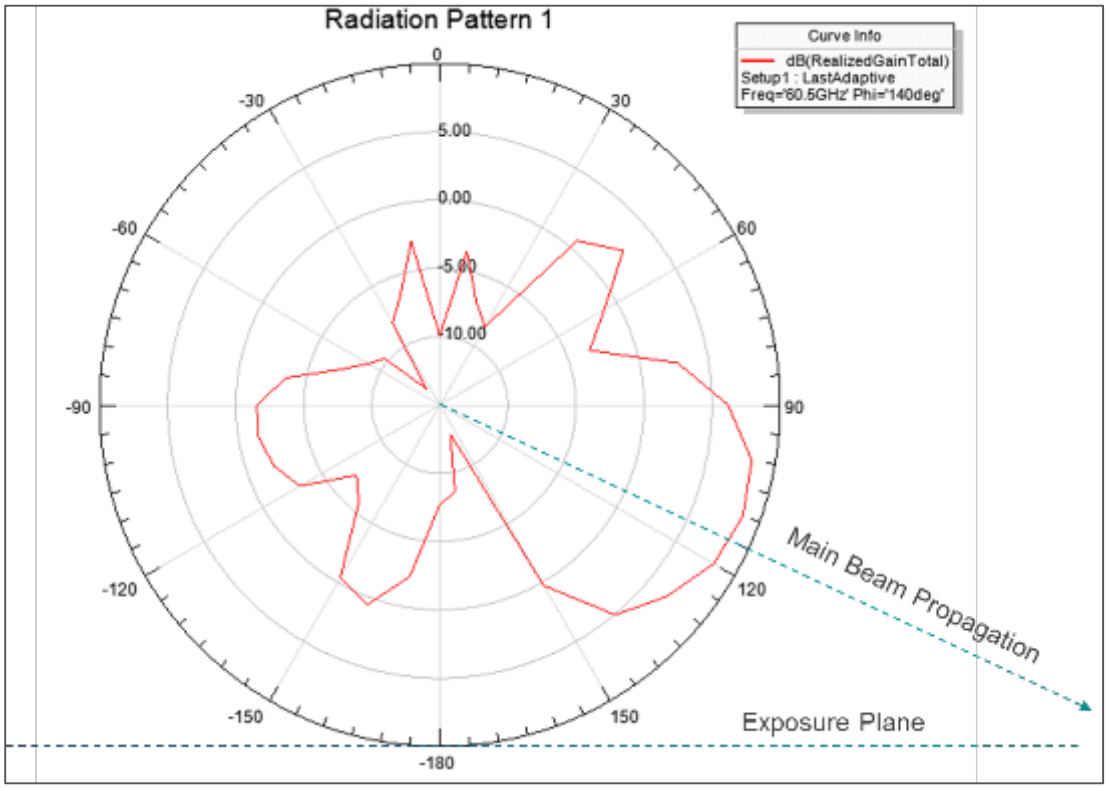

Figure F-1: Antenna pattern of configuration #13 and its orientation relative to the exposure plane

Based on the relative orientation of the main lobe direction and the exposure plane, the test setup shown in Figure F-2 was established for this validation. Note the two white foam sticks placed on the Acer N15W8 laptop edge along each side of the QCA9008-TBD1 802.11ad module were used for aligning the waveguide probe towards the center of the 802.11ad module, particularly when the Acer laptop was in a tilted position. The objective of the validation is to:

1. Scan the E-fields in both polarizations along the plane that is normal to main beam propagation (in other words, parallel with the antenna aperture)
2. Back-transform the fields to the hot spot location in the exposure plane identified in the main RF exposure assessment report
3. Compare the maximum power density level with what we reported (Figure 4-5), as well as provide the correlation along the intersection line (along X-axis) going through the hot spot in exposure plane.

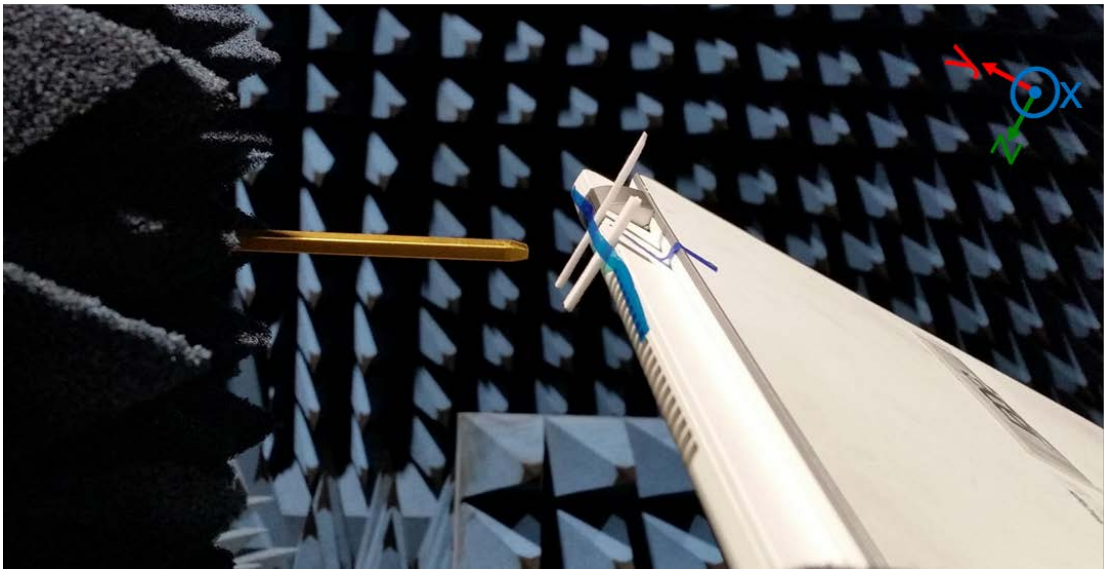

Figure F-2: Acer laptop positioned at 65 degree from the Y-axis

F.2 Acer Antenna configurations #13 test results and correlation

Figure F-3 shows the geometry schematic of the two scan planes' orientations relative to the Acer's QCA9008-TBD1 802.11ad module as well as the intersection of scan planes and the

intersection of their corresponding back-transformed planes going through the hot spot in the exposure plane.

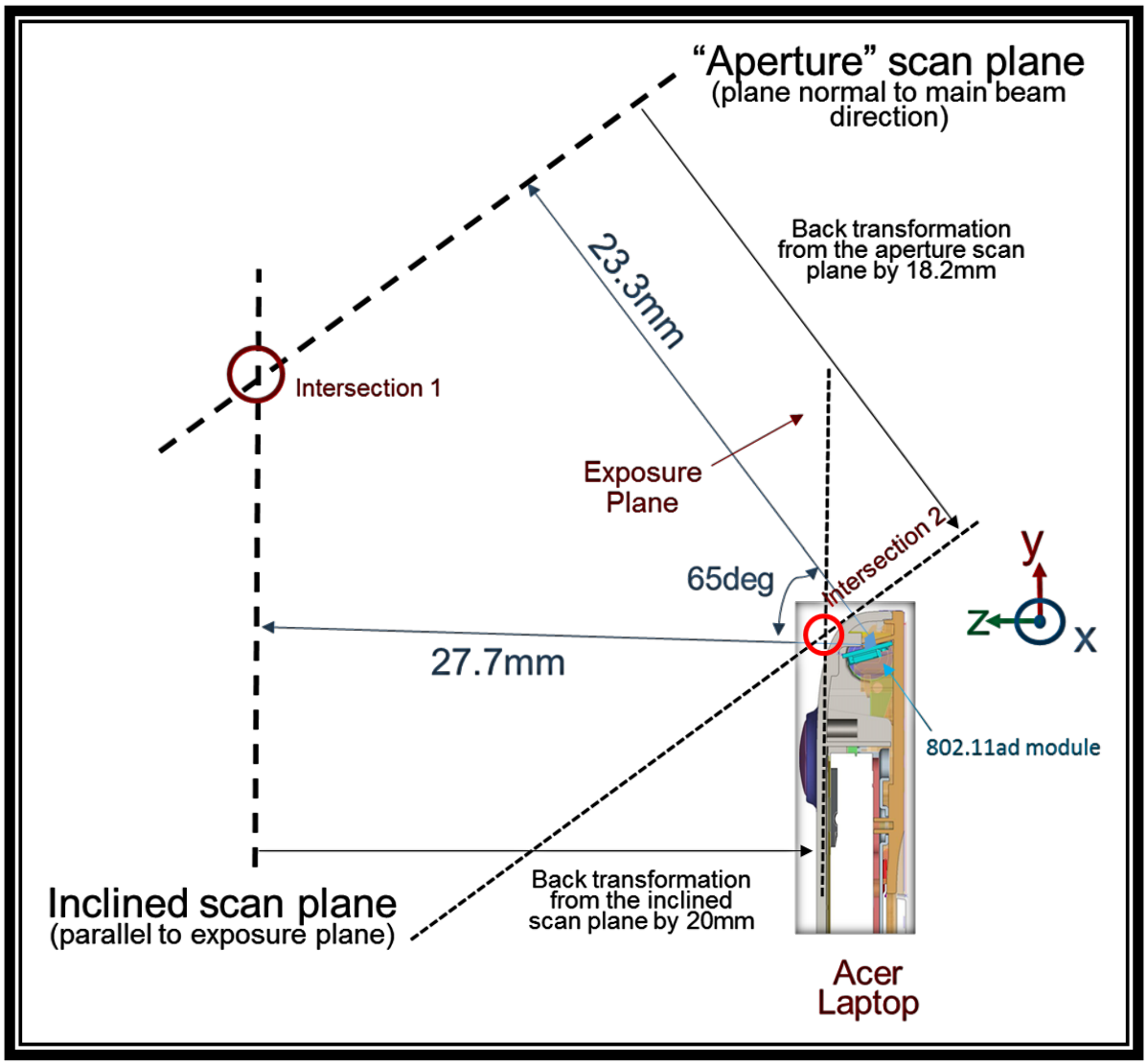

Figure F-3: Geometry relationship of the two orientated scan planes relative to QCA9008-TBD1 802.11ad module installed in Acer

We measured both the polarizations of the E-field components tangential to the measured scan planes (indicated in Figure F-3). It should be noted that "inclined scan plane" in Figure F-3 corresponds to the results shown in Figure 4-5. Figure F-4 shows the normal power density component along the intersection line (labeled "intersection 1" in Figure F-3) of these two measured scan planes.

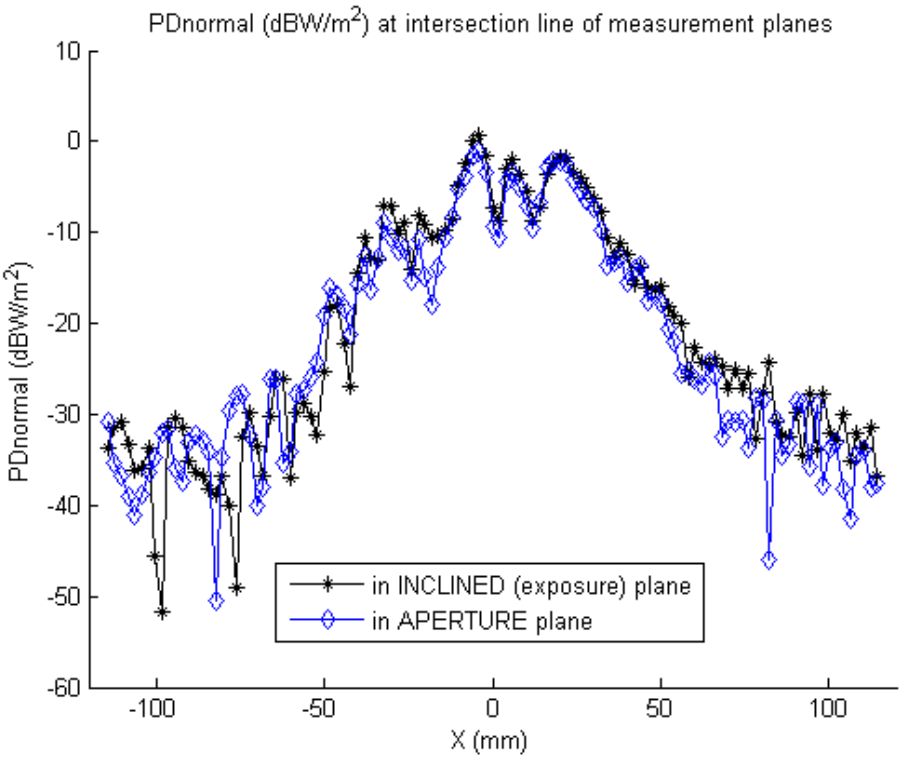

Figure F-4: In Acer laptop case, measured power density component normal to the scan planes along the intersection line ("intersection 1" in Figure F-3)

Based on measured data, we derived the corresponding normal component of E-field as well as all H-field components using the Plane Wave Spectrum equations to obtain total power density in the back-transformed planes. Here, fields were back-transformed to planes going through the exposure plane hot spot location (labeled "intersection 2" in Figure F-3) identified in the main report.

Figure F-5 shows the total power density along the intersection line of these two back-transformed planes going through the exposure plane hot spot (labeled "intersection 2" in Figure F-3).

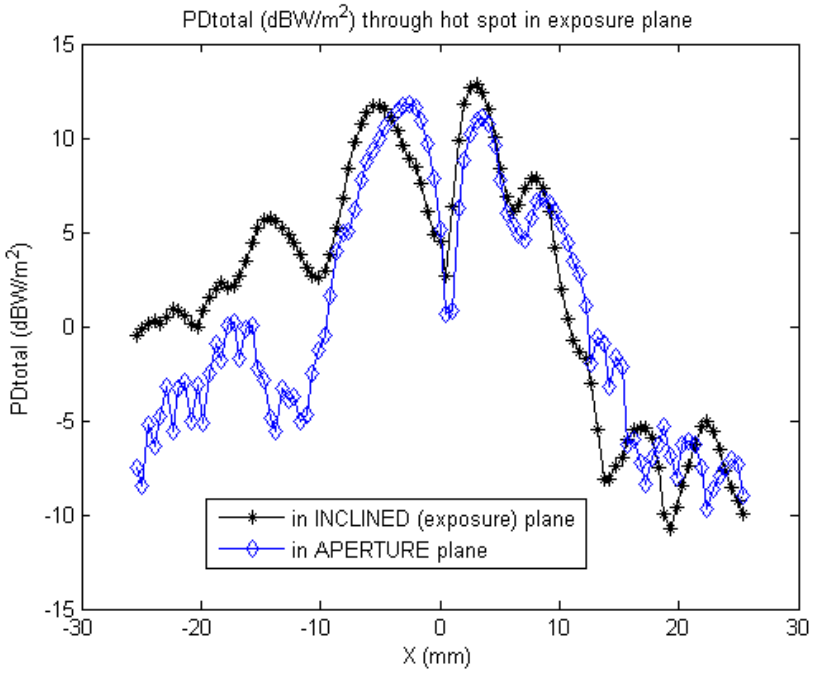

Figure F-5: Back transformed total power density along the intersection line ("intersection 2" in Figure F-3) in the exposure plane (bottom surface of Acer N15W8 laptop).

Figure F-1 lists the maximum 1 cm^2-averaged total power density levels obtained from:

a. Back-transforming the field measured in a plane parallel to exposure plane

b. Back-transforming the field measured in a plane parallel to "aperture" plane (main beam direction)

c. Back-transforming the PD_{normal} measured in a plane parallel to exposure plane (value obtained from Table 4-2), and adding the free space simulated delta (1.8dB) of (PD_{total}-PD_{normal})

Table F-1: Maximum 1 cm^2-averaged total power density levels

	(a) Based on measured data in parallel to **exposure plane** and back transformed PD_{total} to exposure plane	(b) Based on measured data in parallel to **aperture plane** and back transformed PD_{total} to exposure plane	(c) Based on measured dominant polarization data in parallel to exposure plane and back transformed PD_{normal} to exposure plane and applied free space simulated delta (1.8dB) of (PD_{total}-PD_{normal})
1cm^2-averaged PD_{total} (W/m^2) at the hot spot in exposure plane	6.6	5.56	7.05 (=4.66 *$10^{(1.8/10)}$)

Therefore, the adjustment of normal component of power density and total power density using simulated difference is conservative.

G Near-Field Measurement Validation

This section addresses two key aspects in near-field measurement:

- Determine the separation distance to minimize probe perturbation
- Evaluate test setup for accuracy of absolute amplitude measurement

G.1 Near-field perturbation of probe

To assess the influence of WR-15 open-ended waveguide probe on the power density in the near-field of the source, FEM simulations were performed at 60 GHz using Ansys Electromagnetics Suite 17.0.0 for a 2x4 patch antenna array and power density was assessed at various separation distances with and without the waveguide probe (see Figure G-1).

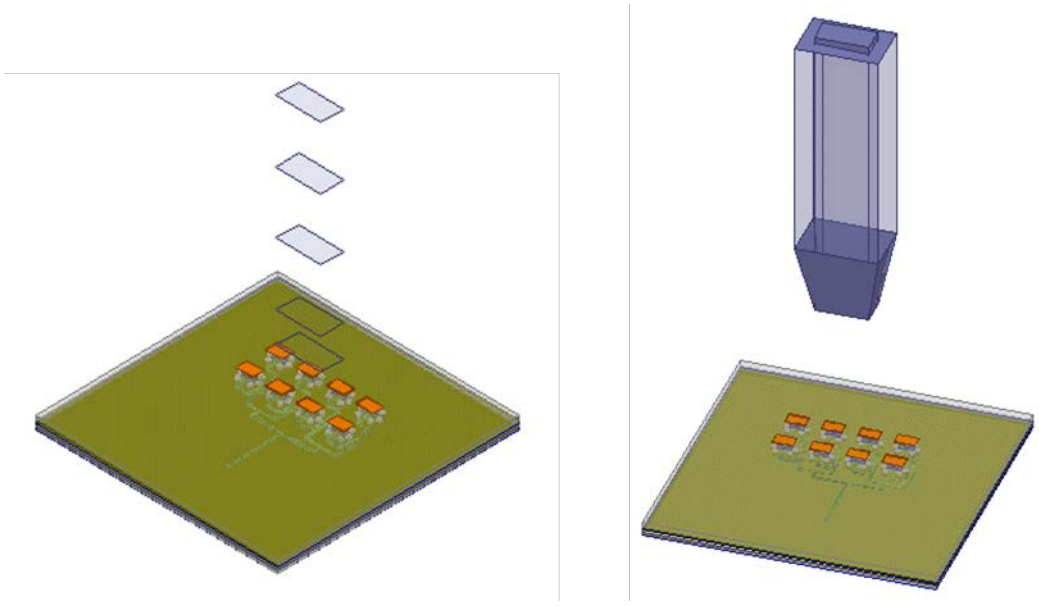

(a) (b)

Figure G-1: (a) 2x4 patch array simulated in free-space to determine total power propagating normal to the probe aperture at various separation distances. (b) 2x4 patch array was simulated with WR-15 open-ended waveguide probe at various separation distances to compute the received power at the port of the probe.

Free-space simulation of a 2x4 patch antenna array was performed in the absence of the waveguide probe and total power was computed over the probe aperture at various separation distances, i.e., integral of real part of normal component of Poynting vector over the aperture

area. At these separation distances, the second set of simulations were conducted by placing the waveguide probe to compute the total received power at the port of the waveguide. The total power over the aperture area at various separation distances with and without the WR-15 waveguide probe is plotted below in Figure G-2:

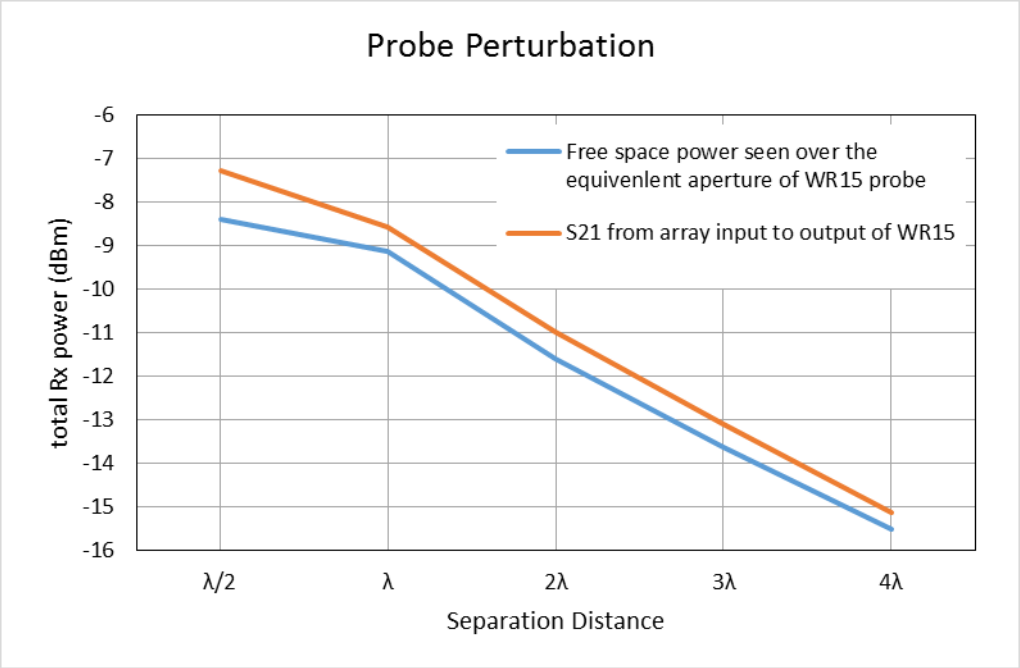

Figure G-2: Simulated total power incident on probe aperture with and without the WR-15 waveguide probe at various separation distances from a 2x4 patch antenna array.

S21 is defined from input of the patch array to the output of the waveguide probe. Since we are measuring at the port of waveguide probe (in actual measurements), it will give a direct comparison on power incident in no-probe condition to power received by waveguide probe (S21) for a normalized input power at the patch array (0 dBm).

From Figure G-2, the WR-15 waveguide probe will measure power density significantly different from incident power density at separation distances <λ and at distances >λ, the probe measures within 0.6 dB of incident power density. This 0.6 dB has been accounted for in the measurement uncertainty budget in Appendix B. As expected, the WR-15 probe perturbation decreases with increasing separation distances.

G.2 Accuracy of absolute amplitude measurement validation

The accuracy of measurement and simulation setups for known sources was verified in this section. Near-fields were measured for a standard horn antenna and a 2x4 patch array at 2λ distance (10 mm @ 60 GHz) away. The horn antenna is a known source having a gain of 25.1 dBi, and the 2x4 patch array was measured using the substitution method with the horn antenna resulting in a measured gain of 14.0 dBi. Both these sources were also simulated using Ansys Electromagnetics Suite 17.0.0. The simulated gain of the horn and 2x4 patch array were 25.4 dBi and 14.1 dBi, respectively. This correlation validates the modeling aspects of simulation approach.

Furthermore, good agreement was found in measured and simulated power density at 2λ distance away from the aperture of the source.

Table G-1 shows the comparison of peak power density in a plane parallel to the aperture and 2λ away.

Table G-1: Peak power comparison

Source/input power	Peak PD measured at 2λ (W/m^2)	Peak PD simulated at 2λ (W/m^2)	Delta (dB)
Horn antenna/2 dBm	2.97	3.14	-0.27
2x4 patch antenna/1.4 dBm	17.43	15.9	0.40

Figure G-3 and Figure G-4 show the measurement and simulation setups along with power density distributions.

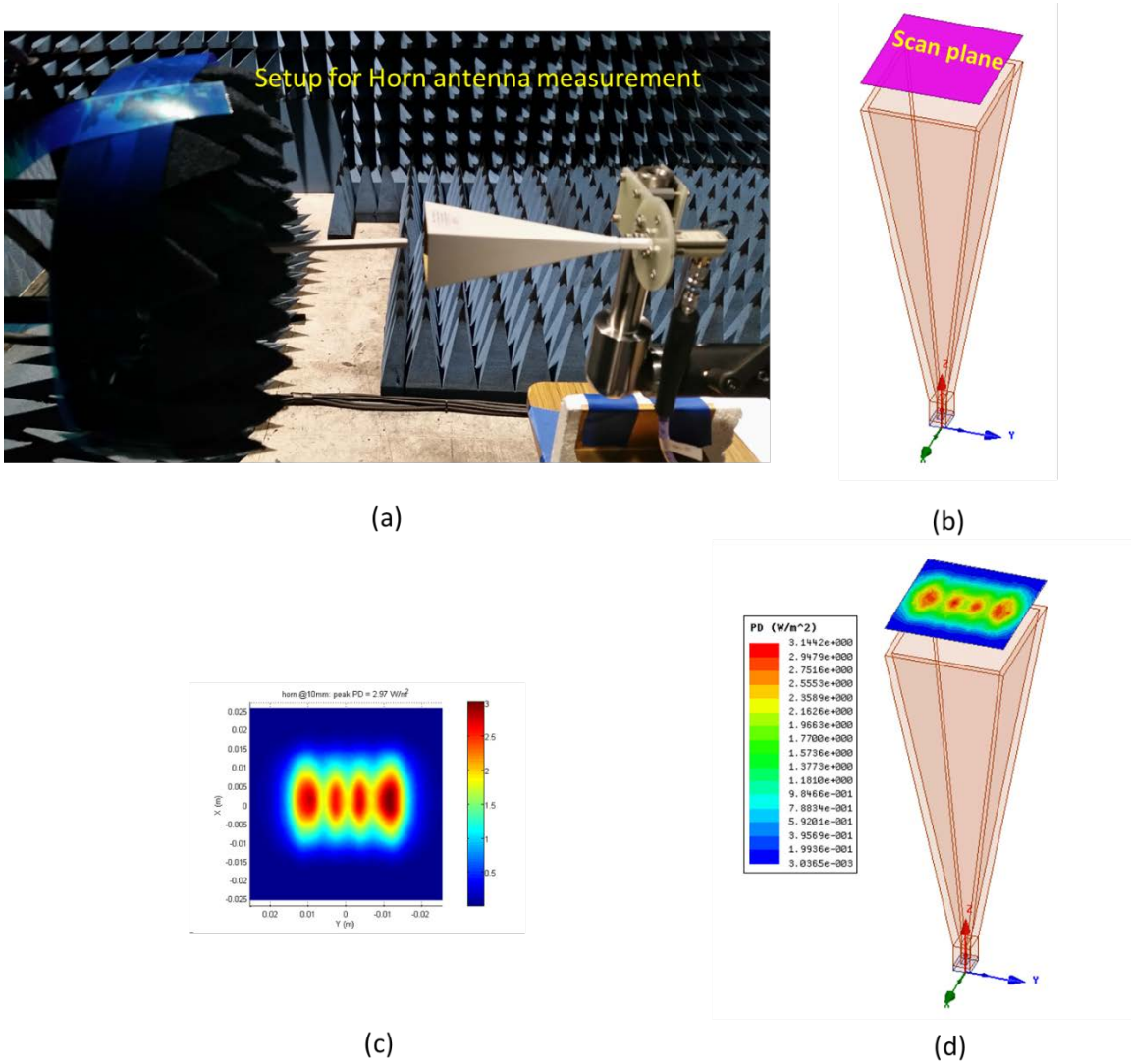

Figure G-3: Horn antenna: (a) measurement setup, (b) simulation setup, (c) measured power density, (d) simulated power density

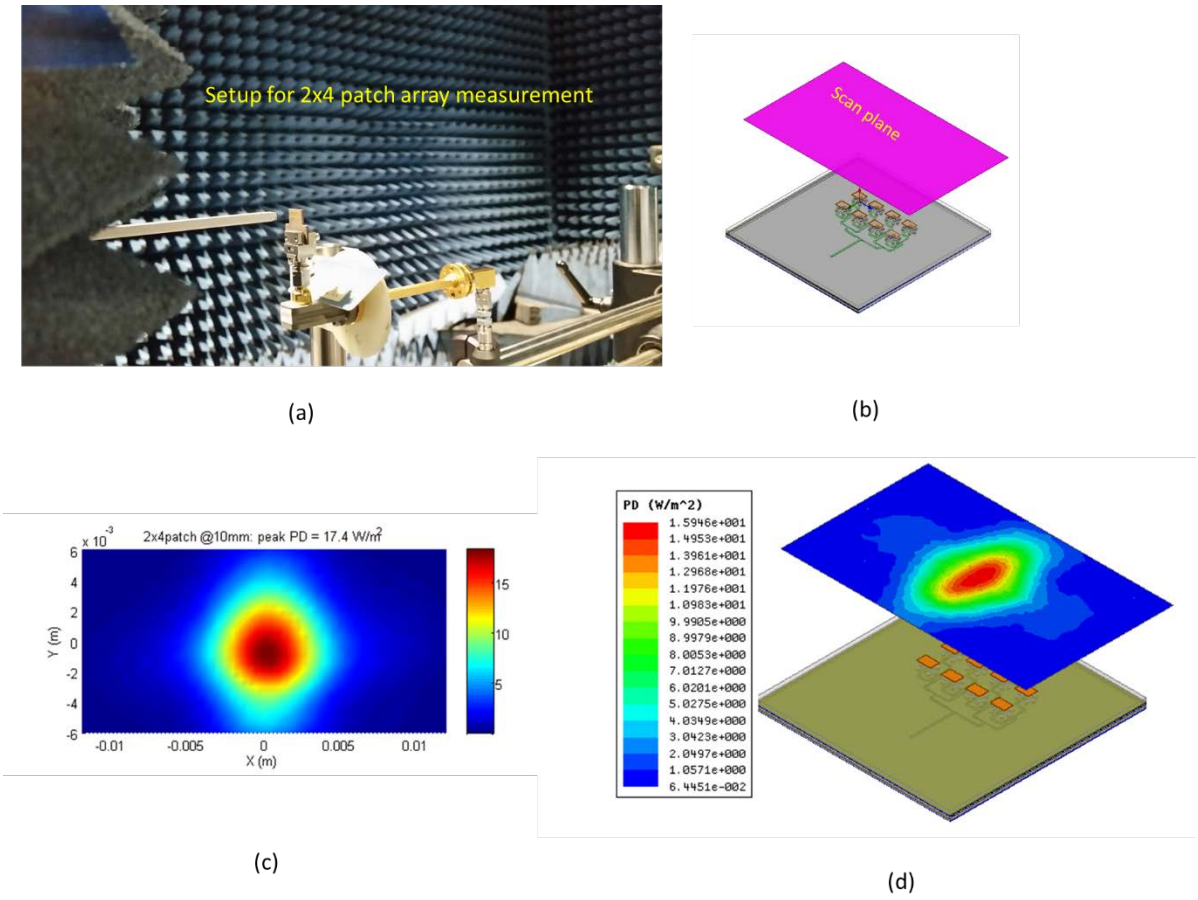

Figure G-4: 2x4 patch array: (a) measurement setup, (b) simulation setup, (c) measured power density, (d) simulated power density

Since the measurement and simulation are two independent approaches, those two methods can validate each other, i.e. one method compliments the other. The good agreement between the measurement and simulation shown in this section validates the measurement setup for absolute amplitude measurement.

H KDB 865664 D02 Reporting Considerations

In this report, guidelines in KDB 865664 D02 were followed.

Table H-1 provides a summary of KDB 865664 D02 reporting considerations for RF exposure compliance versus what we reported.

Table H-1: KDB 865664 D02 reporting considerations

#	KDB 865664 D02 (all reports)	Comments (this report only)
2.1a	Device operating configurations and exposure conditions	See Appendix A
2.1b	Statement of compliance	See Chapter 0
2.1c	Information and test results for compliance	See Chapter 4
2.1d.1	Operating modes, nominal and maximum output power, frequency bands, etc.	See Chapter 2 and Appendix A
2.1d.2	Antenna illustrations and separation distances	See Appendix A
2.1d.3	Voice and data mode transmission requirements	Not applicable
2.1d.4	Duty factor and power reduction requirements	Not applicable
2.1e	Various wireless modes	Not applicable
2.1f	Details on test equipment, calibration, numerical simulation tools	See Chapters 3 and 4, Appendix E and G
#	**KDB 865664 D02 (MPE reports)**	
2.2a	Test setup details	See Section 4.2
2.2b	Max output power delivered to antenna. Cable losses must be accounted.	See Appendix A
2.2c	Measurement points and separation distances from antenna. Spatially averaged results.	See Section 4.3
2.2d	Simultaneous transmission	Not applicable
2.2e	Occupational exposure limits	Not applicable
#	**KDB 865664 D02 (analysis reports)**	
2.4a	Device operating configurations, exposure conditions, max output power, duty factor and test exclusion.	▪ See Chapter 3 and Appendix A ▪ Used numerical simulations for test exclusion/worst-case determination in Section 3.3
2.4b	SAR test exclusion	Not applicable
2.4c	Mobile exposure<300kHz, SAR meas.<100MHz	Not applicable

#	KDB 865664 D02 (numerical SAR sim report)	
2.5a	Computational resources	Ansys Electromagnetics Suit 17.0.0 on a server with at least 96 GB RAM, 1TB hard drive.
2.5b	Numerical modeling implementation and validation	Used standard sources such as horn antenna to validate through measurements in Appendix G. PWS Implementation in Appendix D
2.5c	Computational parameters	See Sections 3.1 and 3.2
2.5d	Phantom model implementation and validation	Not applicable
2.5e	Tissue dielectric parameters	Not applicable
2.5f	Transmitter model implementation and validation	Validated single active antenna element case through measurement in Section 5.1
2.5g	Test device positioning (description and illustration)	See Sections 3.1 and 3.2
2.5h	Steady state termination procedures (convergence)	Ensured (see Section 3.2)
2.5i	Computing peak SAR from field components	Extracted power flowing through the exposure plane (see Section 3.3), and Appendix C
2.5j	1-g averaged SAR procedures	Performed 1cm^2-spatial averaging on power density (see Section 3.3)
2.5k	Total computational uncertainty	See Appendix B
2.5l	Test results for determining SAR compliance	▪ Identified worst-antenna configurations through simulation (see Section 3.3) and Appendix C ▪ Performed measurements for compliance demonstration (see Section 4.3)